SECOND EDITION

11 Volume Set

TREATISE ON GEOPHYSICS

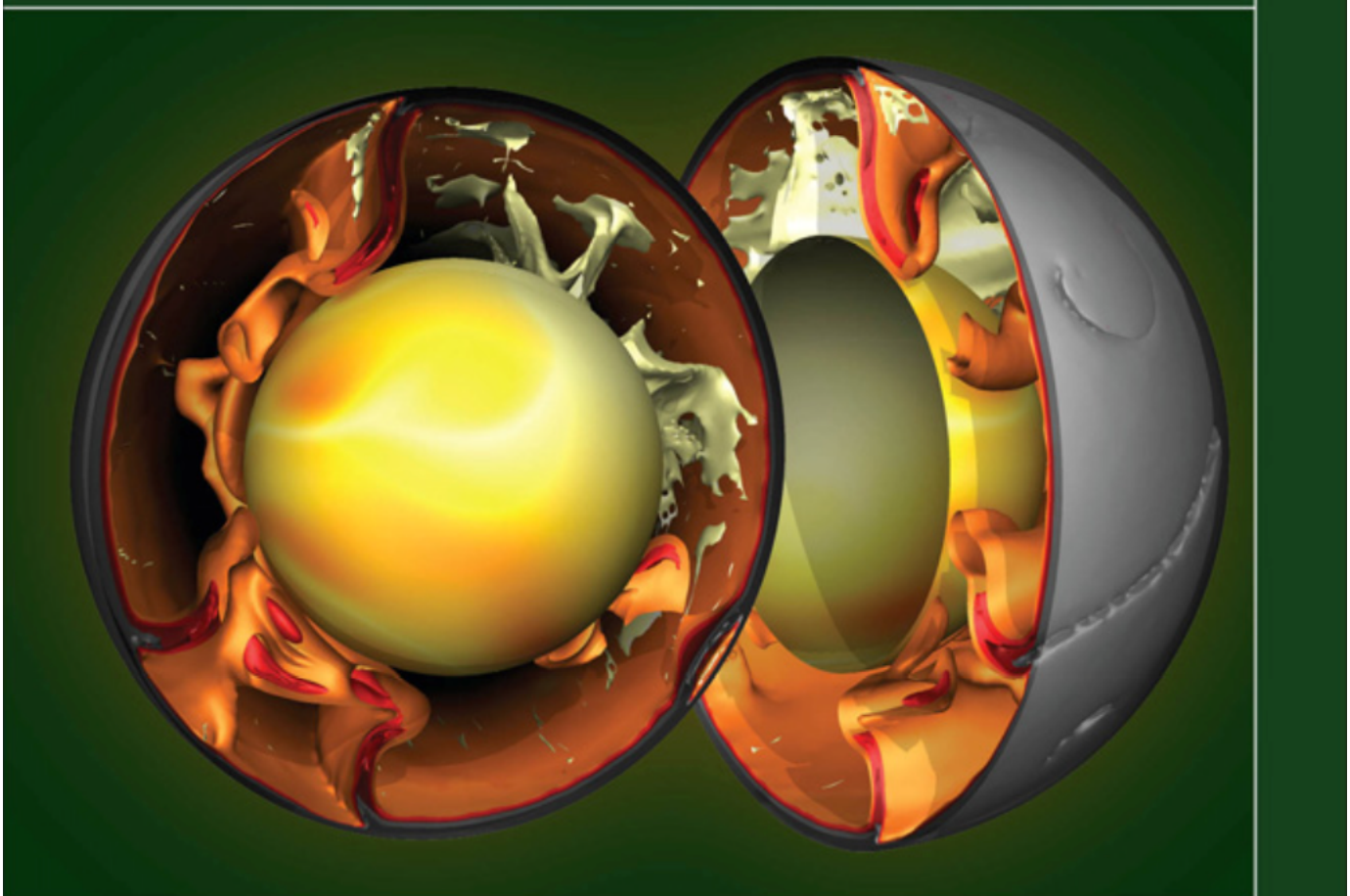

EDITOR-IN-CHIEF: GERALD SCHUBERT

6.02 Plate Tectonics

P Wessel, University of Hawaii at Mānoa, Honolulu, HI, USA
RD Müller, University of Sydney, Sydney, NSW, Australia

Glossary

Hot-spotting A technique by Wessel and Kroenke (1997) that uses seafloor flow lines to infer hot spot locations.
OMS Modeling technique of O'Neill et al. (2005).
PFRM Polygonal finite rotation method of Harada and Hamano (2000).
WHK Hybrid modeling technique of Wessel et al. (2006).
WK97 An APM model proposed by Wessel and Kroenke (1997).

*Treatise on Geophysics, 2nd edition, (*2015), vol. 6, pp. 45-93

Abbreviations

APM	Absolute plate motion
APW	Apparent polar wander
GPS	Global Positioning System
PURs	Partial uncertainty rotations
RPM	Relative plate motion
TPW	True polar wander
VLBI	Very long baseline interferometry

6.02.1 Introduction

In geologic terms, a plate is defined based on mechanical and rheological arguments. The plate is that part of the outer shell of the Earth that moves coherently as a rigid body without significant internal deformation over geologic timescales. The word tectonics comes from the Greek root 'to build.' By combining these two words, we get the term plate tectonics, which refers to how the Earth's surface is composed of rigid plates that are moving relative to one another on top of hotter, more mobile mantle material. The idea of a lithosphere, representing a strong, outer layer of the Earth overlying a weak asthenosphere, was first introduced by Barrell (1914), long before the realization that the outer shell of the Earth forms a thermal boundary layer of a convecting system. The rise of the plate tectonic hypothesis led to the view that mid-ocean ridges may be associated with a cold, strong boundary layer and that trenches were sites where boundary layers became detached from the surface, being recycled back into the Earth's mantle (e.g., McKenzie, 1969). This approach led to some of the first successful attempts to create relatively simplistic, linear models for mantle convection (e.g., McKenzie et al., 1973), which agreed remarkably well with observations of bathymetry and heat flow from the ocean basins (Sclater and Francheteau, 1970; Sclater et al., 1971).

The concept of seafloor spreading was originally proposed by Hess (1962) and Dietz (1961) who suggested that new seafloor is created at mid-ocean ridges, spreads away from them as it ages, and is subducted at trenches. This idea borrowed some concepts from the much earlier (and in hindsight prescient) model suggested by Arthur Holmes (1944). Building on Hess and Dietz's contributions to understanding seafloor spreading and subduction, a major contribution came from Wilson (1965), who developed the concept of plates and transform faults. He suggested that the active mobile belts on the surface of the Earth are not isolated but continuous and that these mobile belts, marked by active seismicity, separate the Earth into a rigid set of plates. These active mobile belts consist of ridges where plates are created, trenches where plates are destroyed, and transform faults, which connect the other two belts to each other. **Figures 1** and **2** show bathymetry, modern ship track coverage, and gridded magnetic anomalies in two areas that served as keys for developing the seafloor spreading hypothesis in the North Atlantic (Heirtzler et al., 1968) and the East Pacific (Menard, 1964) oceans.

Central to the theory of plate tectonics is the concept of internal rigidity of tectonic plates together with Euler's theorem, which allows us to model the relative motion of plates quantitatively. All plates can be viewed as rigid caps on the surface of a sphere. The motion of a plate can be described by a rotation about a virtual axis that passes through the center of the sphere (Euler's theorem). In terms of the Earth, this implies that an angular velocity vector originating at the center of the globe can describe motions of plates. The most widespread parameterization of such a vector is using latitude and longitude to describe the location where the rotation axis cuts the surface of the Earth and a rotation rate that corresponds to the magnitude of the angular velocity (in degrees per million years or microradians per year). The latitude and longitude of the angular velocity vector constitute 'Euler's pole.'

The formal hypothesis of plate tectonics states that the Earth is envisioned as an interlocking internally rigid set of plates in constant motion. These plates are rigid except at plate boundaries, which are lines between contiguous plates. The relative motion between plates gives rise to earthquakes; these earthquakes in turn define the plate boundaries. There are three types of plate boundaries: (1) divergent boundaries, where new crust is generated as the plates diverge; (2) convergent boundaries, where crust is destroyed as one plate dives beneath another; and (3) transform boundaries, where crust is neither produced nor destroyed as the plates slide horizontally past each other. Not all plate boundaries are as simple as the main types discussed earlier. In some regions, the boundaries are not well defined because the deformation there extends over a broad belt, a plate-boundary zone (Gordon, 2000). Because plate-boundary zones involve at least two large plates and one or more microplates caught up between them, they tend to have complicated geologic structures and earthquake patterns.

6.02.2 Studies of Relative Plate Motions

6.02.2.1 Determination of the Present-Day Plate Motions

There are a number of different methods that can be used to determine instantaneous rotations for relative plate motions at the present. Such rotations can be described by angular velocity vectors and obey standard vector algebra, that is, the angular velocity vectors ${}_{A}\boldsymbol{\omega}_{B}$ and ${}_{B}\boldsymbol{\omega}_{C}$ describing the rotations of plate B relative to plate A and plate C relative to plate B can simply be added vectorially to obtain ${}_{A}\boldsymbol{\omega}_{C}$, the rotation of plate C relative to plate A. The present-day plate motions can now be measured in real time using satellite technology; hence, they are much better constrained than plate models for the geologic past. The methods used include the following:

1. The orientation of active transform faults between two plates can be used to compute their direction of relative motion. The relative motion of two plates sharing a mid-ocean ridge is assumed to be parallel to the transform faults, because the arcs of the faults are expected to be small circles. This would imply that the rotation pole must lie somewhere on the great circle perpendicular to the small circles defined by the transform faults. Hence, if two or more transform faults between a plate pair are used, the

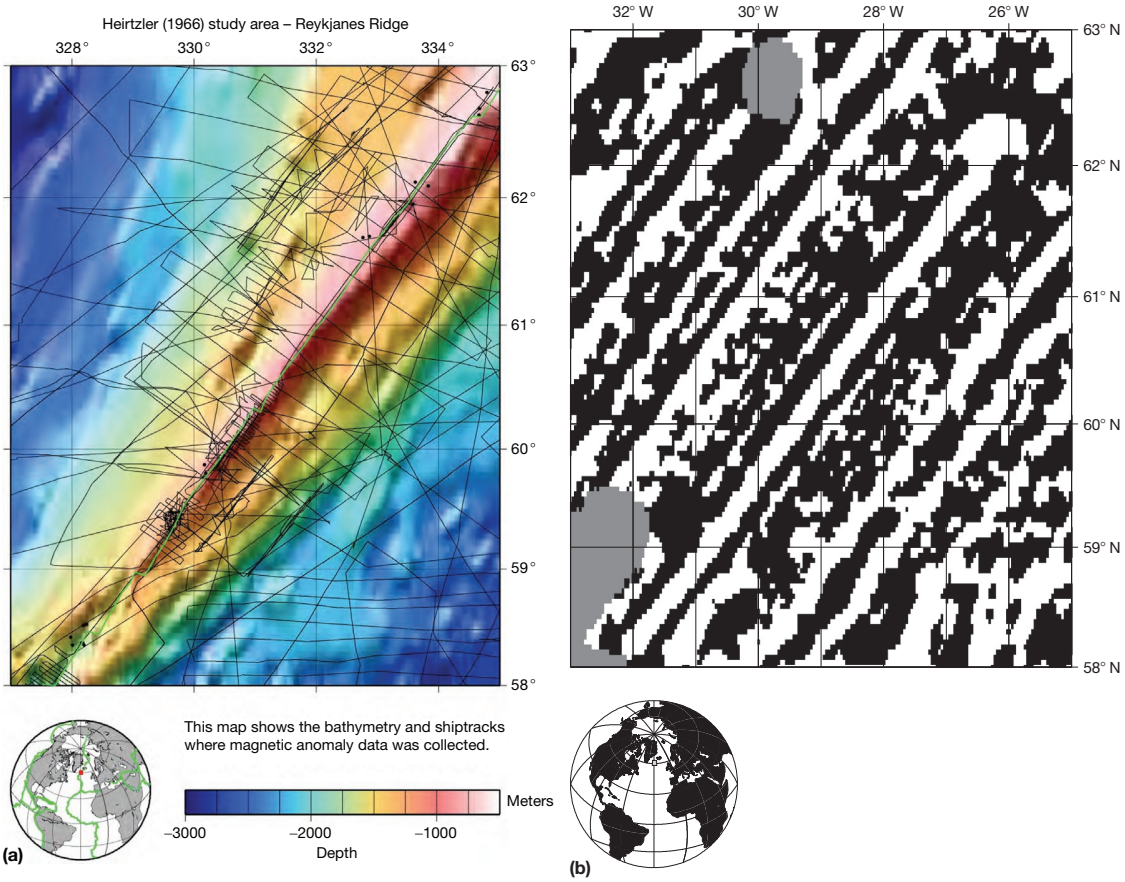

Figure 1 Gridded magnetic anomalies (b) based on magnetic anomaly ship track coverage in the National Geophysical Data Center (NGDC) database south of Iceland (a), a key area for plate tectonic theory development (Heirtzler et al., 1968). Black corresponds to magnetic anomalies due to a normal and white to a reversely polarized field (b).

intersection of the great circles approximates the position of the rotation pole (e.g., Morgan, 1968).

However, the reality of how well transform faults represent small circles about rotation poles has been found to deviate from plate tectonic theory for a number of reasons. For example, Müller and Roest (1992) investigated the North Atlantic Ocean to determine how well the azimuths of mapped ridge offsets correlate with small circles of synthetic fracture zone flow lines. They used gravity anomaly profiles obtained from satellite altimetry data to locate a large number of fracture zones as well as extinct spreading ridges and V-shaped structures and evaluated the agreement between the mapped fracture zones and synthetic flow lines as predicted from plate models for the opening of the North, central North, and South Atlantic. The geometry of many small- and medium-offset fracture zones indicates that the ridge axis discontinuities that produce them can migrate along the ridge, causing off-axis traces that deviate from tectonic flow lines. Recently, a global digital community dataset of oceanic fracture zones and other seafloor discontinuities was published by Matthews et al. (2011).

2. The spreading rates along a mid-ocean ridge as determined from magnetic anomaly patterns can be used to compute a rotation pole, since the spreading rate varies as the sine of the colatitude (i.e., angular distance) from the rotation pole. **Figure 3** illustrates a revised digital isochron chart of the ocean floor, based on Müller et al. (2008).
3. Fault plane solutions (focal mechanisms) of earthquakes at plate boundaries can be utilized to compute the direction of relative motion between plates. Only the location of the pole, but not the spreading rate, can be determined this way. A global model for current plate motions based on data of types (1)–(3) has been constructed and reviewed by DeMets et al. (2010).
4. Geologic markers are used along plate boundaries on land, in particular along strike-slip faults, to determine the neotectonic local relative motion. Markers used include streambed channels, roads, and field boundaries that have been offset by strike-slip motion.
5. A method that has been in use for quite a while is called very long baseline interferometry (VLBI). In this method, quasars are used for the signal source and terrestrial radio telescopes as the receivers. The difference in distance between two telescopes is measured over a period of years.
6. Satellites have made it possible to measure the present-day plate motions in real time at many more stations than

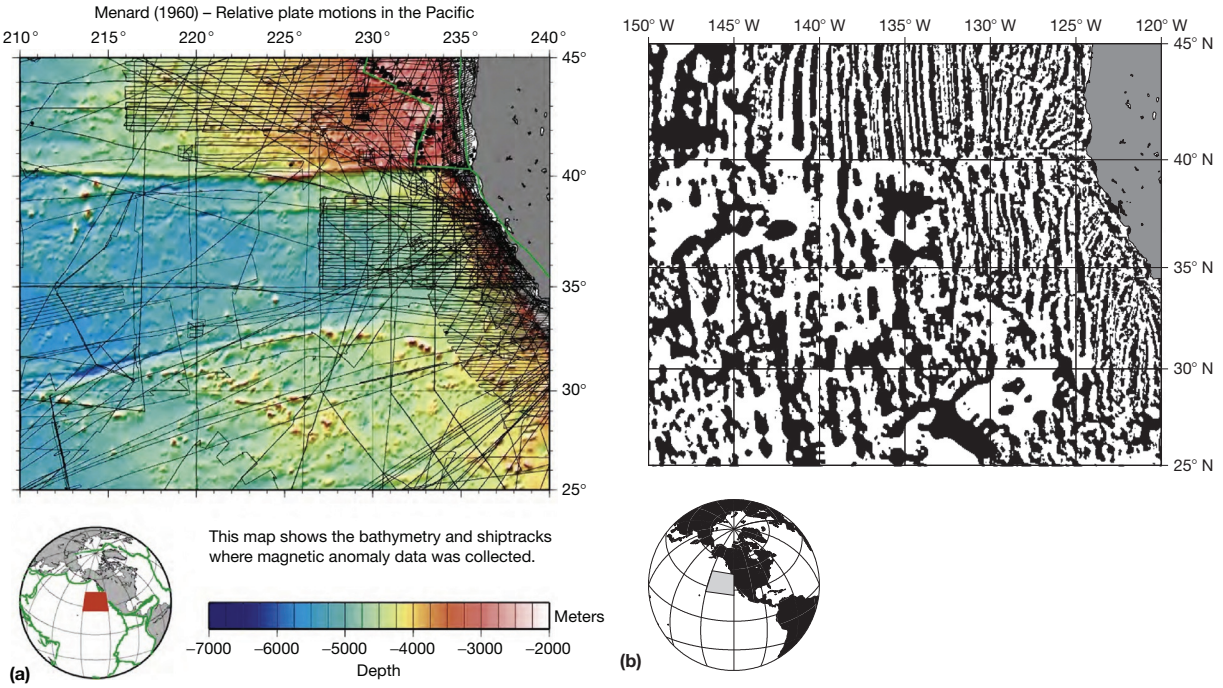

Figure 2 Gridded magnetic anomalies (b) based on magnetic anomaly ship track coverage in the NGDC database in the northeast Pacific, another key area for plate tectonic theory development (Menard, 1964) (a). Black corresponds to magnetic anomalies due to a normal and white to a reversely polarized field (b).

possible using the VLBI technique, which depends on permanent radio telescopes as the receivers. Satellite laser ranging techniques using the Global Positioning System (GPS) have been used very successfully recently to measure plate motions all over the world, especially in areas that are subject to earthquake hazards (see **Chapter 3.11**). GPS measurements are based on 24 satellites, resulting in full GPS coverage for navigation purposes anywhere in the oceans and providing opportunities better than ever before to monitor plate motions in real time with high-precision receivers. A survey time of about 1–2 years is sufficient to obtain a value outside of the error range. Using VLBI and GPS data jointly together with data such as SLR and DORIS (Argus et al., 2010) offers the possibility for rigorous kinematic analysis of regional deformation and strain accumulation along faults – however, this type of model derived from space-geodetic data over a few decades and differs significantly from the corresponding angular velocities averaged over several millions of years. A current plate motion model based solely on GPS data was constructed by Kogan and Steblov (2008); based on just a few decades of data, it differs significantly from the corresponding angular velocity averaged over the past 3.2 Myr, such as those of the MORVEL model (DeMets et al., 2010).

6.02.2.2 Techniques Used in Relative Plate Motion Studies

Unlike recent (instantaneous) plate motion, past plate motions require the use of finite rotations whose manipulation is considerably more complex. Some of the earliest quantitative efforts to model plate kinematics involved the fitting of coastlines on either side of the Atlantic by Bullard et al. (1965), who proposed a computer-generated prebreakup fit of the continents. Their fitting technique was based on the minimization of gaps and overlaps of isobaths that were assumed to be representative of the boundaries between continental crust and oceanic crust. A more advanced method is the Hellinger (1981) method that is based on fitting magnetic anomaly and fracture zone data. In this method, combined magnetic and fracture zone data are regarded as points on conjugate isochrons, which are considered to be great-circle segments. Even though fracture zones should ideally be represented by small-circle segments, the difference between short small and great-circle segments is negligible, and great-circle segments are computationally easier to handle. The best-fit reconstruction is computed by minimizing the sum of the misfits of conjugate sets of magnetic anomaly and fracture zone data points with respect to individual great-circle segments. Using this method, both the resulting rotation pole and the sum of the misfits depend critically on correctly identifying conjugate data points that belong to a common isochron segment. This represents a certain disadvantage compared with the method suggested by McKenzie and Sclater (1971), which minimizes the misfit area between two isochrons. In practice, the application of the Hellinger criterion of fit poses no problem, as observational errors are associated with individual data points, thus covering the relative differences in uncertainty between different groups of observations, for instance, magnetic crossings based on older, badly navigated cruises as compared with recent GPS-navigated cruises. Also, rotation poles have been published for most plates describing their late Cretaceous/Tertiary history of motion; therefore, an estimate for an initial rotation is always available.

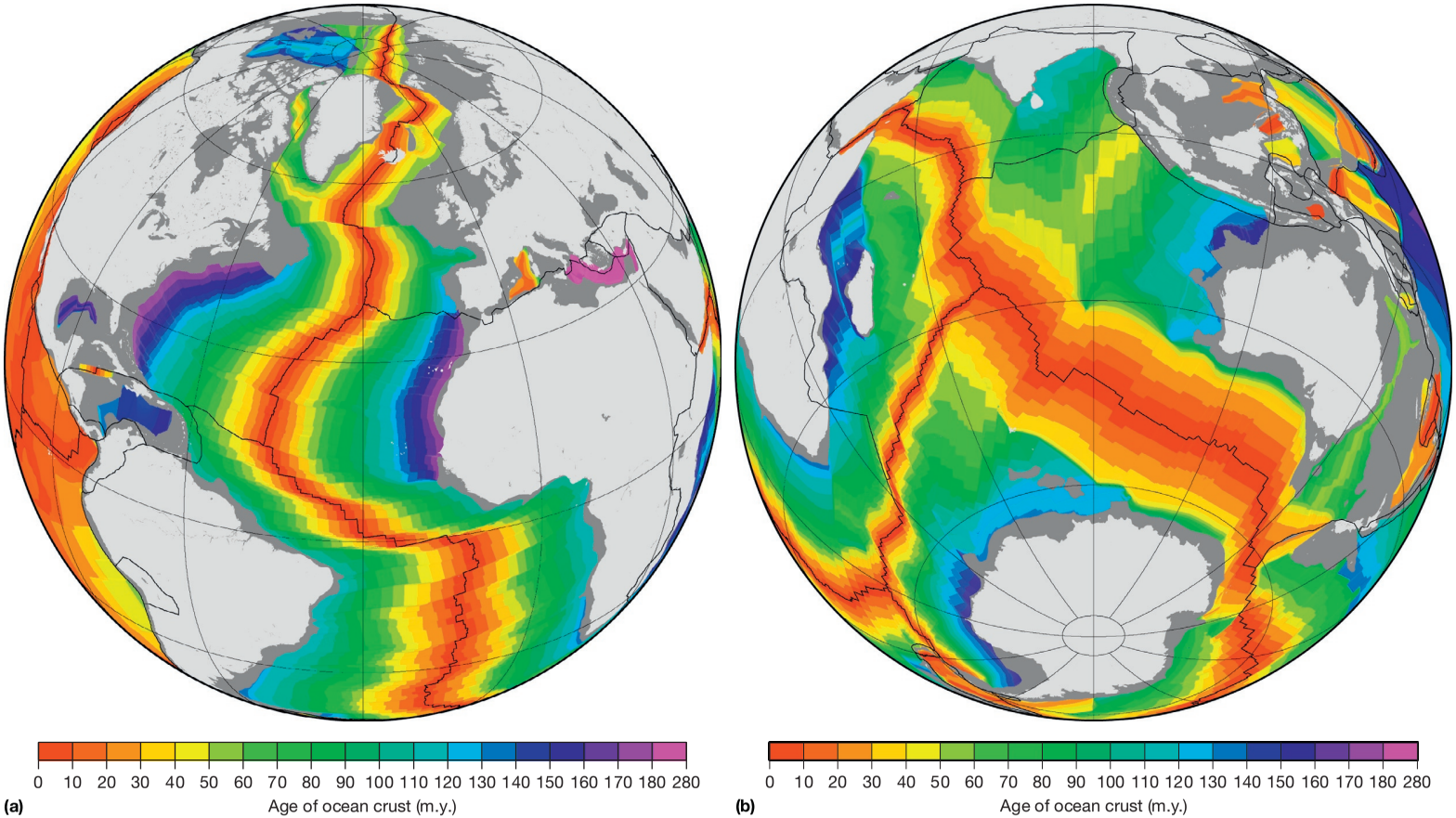

Figure 3 (Continued)

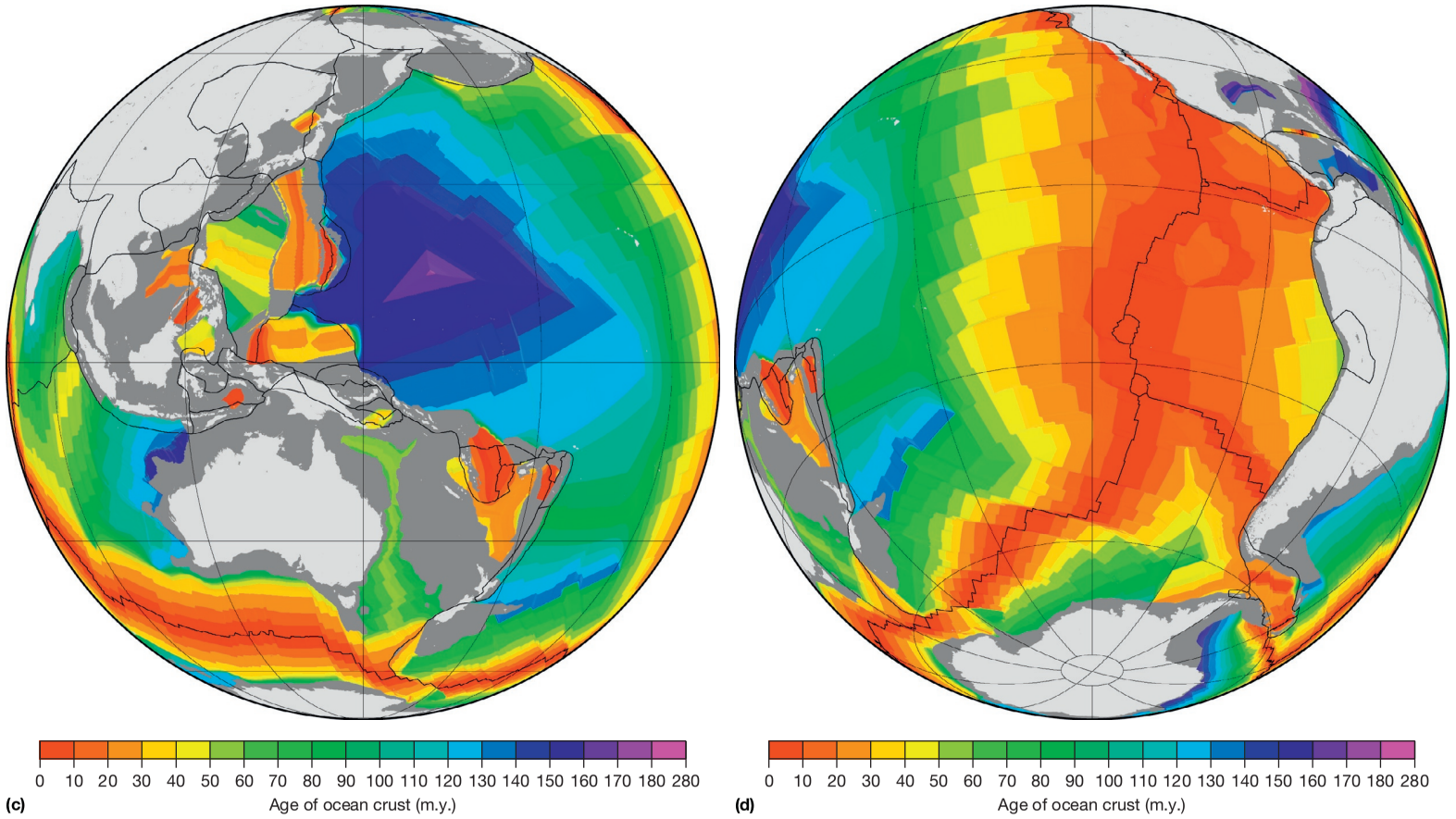

Figure 3 Revised age of the global ocean floor from Müller et al. (2008) with plate boundaries from Bird (2003) overlain. (a) Atlantic Ocean view, (b) Indian Ocean view, (c) West Pacific view, (d) East Pacific view.

Data from one plate (plate 2) are rotated to fit the data on another plate (plate 1) using the rotation $\hat{\mathbf{A}}$, an estimate of the true rotation $\mathbf{A}$ (Figure 4). This rotation is determined by minimizing the sum of the data misfits to great-circle segments.

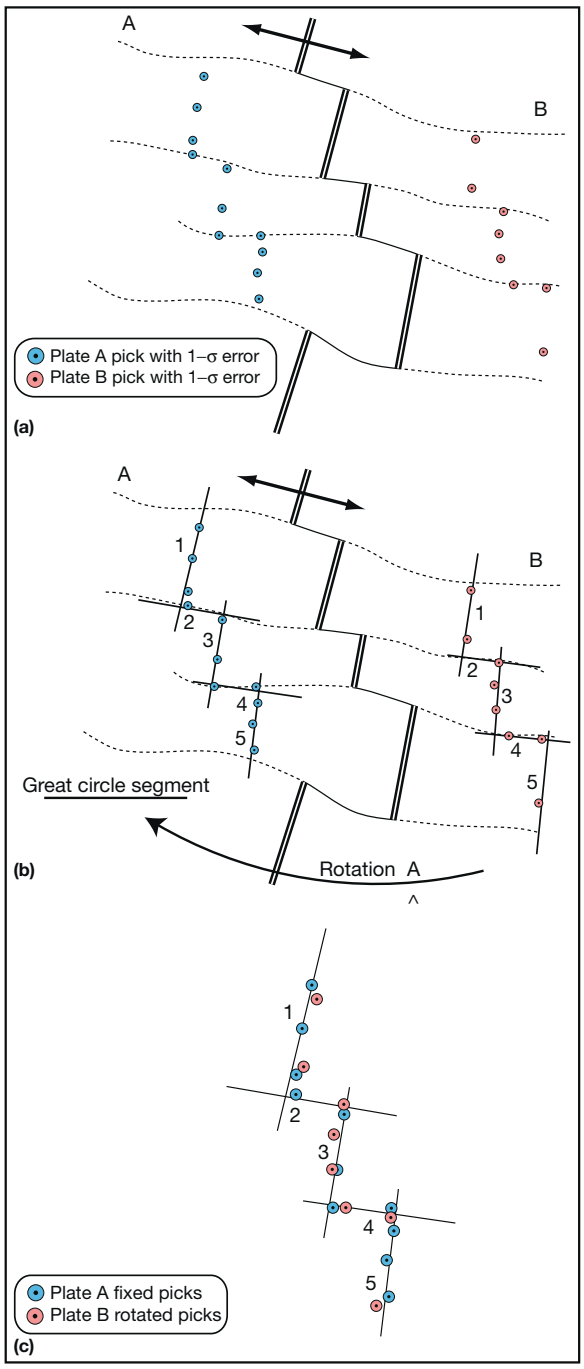

Figure 4 The Hellinger criterion of fit: (a) magnetic picks from two plates are identified, (b) conjugate picks are grouped, (c) data from one plate. Data from one plate (plate 2) are rotated to fit the data on another plate (plate 1) using the rotation $\hat{\mathbf{A}}$, an estimate of the true rotation $\mathbf{A}$. This rotation is determined by minimizing the sum of the data misfits to great-circle segments.

For a more comprehensive overview of fitting methodologies for tectonic reconstructions, see Matias et al. (2005). In terms of determining relative plate motions based on oceanic data, magnetic anomalies and fracture zones are critical.

6.02.2.2.1 Uncertainties in relative plate rotations

Plate kinematicists try to establish a relationship between their model parameters and the goodness of fit of the model with respect to the data. In the case of plate rotations, the model is given by a rotation, which may be represented by a three-dimensional (3-D) Cartesian unit vector (x, y, z), describing the location, and an angle (ω), corresponding to the length of this vector. In turn, the misfits of the data can be described by small Cartesian vectors, which correspond to an uncertainty ellipse about the rotation pole. Hence, the model is described by four parameters (x, y, z, ω) and the misfit in the data by three parameters (x, y, z).

This problem is conceptually similar to projecting the 3-D surface of the Earth onto a 2-D flat map surface. In the case of maps, the projection is not linear, that is, the projection cannot be accomplished without distortions unless one takes an area so small that the curvature of the Earth is negligible. Equivalently, the relationship between a rotation pole and the misfit of the data from two tectonic plates is only approximately linear for very small rotation angles. The reason is that rotations do not comprise a linear subspace in any Euclidean space. This causes a problem for calculating uncertainties of rotations, since the concepts of expected value and statistical parameters such as mean and variance require the fitted parameter to vary over some linear subspace.

Therefore, it would be impossible to establish a direct relationship between finite total reconstruction poles and misfits in the data, because this relationship is highly nonlinear with increasing rotation angles. This problem was first recognized by Stock and Molnar (1983), who proposed a recipe for calculating uncertainties in plate rotations in two steps:

1. Reconstruct the data by finding the best-fit reconstruction.
2. Estimate the uncertainties by the so-called partial uncertainty rotations.

Uncertainties of finite plate rotations are assumed to correspond to misfits in the reconstructed data points in terms of small rotations about three different rotation poles, which either misfit fracture zones and magnetic anomalies or skew the fit of all data (Stock and Molnar, 1983). Figure 5 shows reconstructed magnetic anomaly and fracture zone identifications (crosses and dots represent identifications from two conjugate plates), and large bold dots show the locations of three rotation poles, which are used to express the misfit of the data with respect to isochron segments (ridge and transform segments approximated by great-circle segments).

Molnar and Stock (1985) noted that a measure of the uncertainty of a rotation is how much a small deviatoric rotation, when added to the best-fit rotation, affects the fit of the data. If a small deviatoric rotation significantly degrades the fit of the data, the uncertainty in the rotation is small. Conversely, if a small deviatoric rotation to the best-fit rotation does not significantly degrade the fit, the uncertainty in the rotation is larger. Molnar and Stock (1985) suggested that the best way to

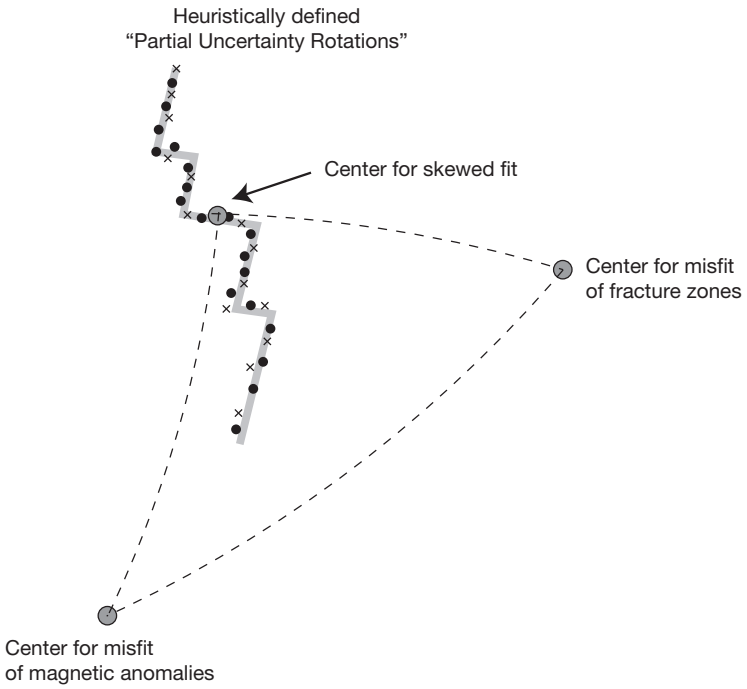

Figure 5 Partial uncertainty rotations. Reconstructed magnetic anomaly and fracture zone identifications (crosses and dots represent identifications from two conjugate plates) and large bold dots show the locations of three rotation poles, which are used to express the misfit of the data with respect to isochron segments (ridge and transform segments approximated by great-circle segments).

parameterize uncertainties in a rotation is by defining a group of small rotations $\Delta\mathbf{A}$, which can be added to the estimated rotation $\hat{\mathbf{A}}$ without significantly degrading the fit. They named the resulting rotations partial uncertainty rotations (PURs; see Figure 5). This eliminates the problem with parameterizing the rotation itself (any parameterization will do), and the problem becomes choosing a parameterization for the group of small rotations $\Delta\mathbf{A}$ that distorts it the least. This formulation is known as a moving parameterization, since rotations close to $\hat{\mathbf{A}}$ are parameterized by their differences from $\hat{\mathbf{A}}$.

6.02.2.2.2 Quantitative implementation of PURs

The method mentioned earlier is heuristic, and it is left to the scientist to decide which misfit is 'acceptable' and which one is 'unacceptable.' Hence, there is a need for an algorithm to rigorously compute uncertainties in plate rotations based on the misfit of the data, the geometry of the plate boundary, and the number of data points. This goal was accomplished by Ted Chang and coworkers (Chang, 1987, 1988; Chang et al., 1990; Kirkwood et al., 1999). In a nutshell, their approach is as follows:

1. Estimate the unknown rotation by minimizing a least squares criterion due to Hellinger (1981). The estimate for the unknown rotation is denoted by $\hat{\mathbf{A}}$.
2. Using a Taylor series centered at $\hat{\mathbf{A}}$, approximate the Hellinger criterion by the error sum squares of a suitable linear regression. As noted earlier, neither the data space, the surface of a sphere, nor the space of rotations is a Euclidean space, and hence, the problem of plate reconstruction is intrinsically nonlinear.
3. Let $\mathbf{A}$ denote the unknown true rotation, and write both $\mathbf{A}$ and $\hat{\mathbf{A}}$ as 3×3 matrices. Hopefully, $\hat{\mathbf{A}}$ is close to $\mathbf{A}$, and $\mathbf{A}^t\hat{\mathbf{A}}$ will be a small rotation. Let $\mathbf{u}$ be a 3 vector such that the direction of $\mathbf{u}$ gives the axis of $\mathbf{A}^t\hat{\mathbf{A}}$ and the length of $\mathbf{u}$ gives the angle of rotation of $\mathbf{A}^t\hat{\mathbf{A}}$. An approximate covariance matrix for $\mathbf{u}$ can be determined by applying standard least squares theory to the approximating linear regression found in step (2). This covariance matrix can be used, using standard statistical approaches, to express the uncertainties in $\mathbf{A}$.

This approach focuses on the deviation $\mathbf{A}^t\hat{\mathbf{A}}$ of the true rotation from the estimate $\hat{\mathbf{A}}$. Since the approximating linear regression is derived using a Taylor series centered at $\hat{\mathbf{A}}$, this approximating regression is naturally expressed in terms of deviations from $\hat{\mathbf{A}}$. This results in a covariance matrix for $\mathbf{u}$, a 3-component vector, which is determined by $\mathbf{A}^t\hat{\mathbf{A}}$, visualized as an ellipsoid (Figure 6). The fundamental insight gained from these concepts and approaches is that the uncertainties in a rotation are best expressed in terms of the deviations of the rotation from the best-fit rotation, not in terms of the error in the best-fit rotation itself.

The choice of parameterization of Chang (1988) is the moving exponential parameterization, based on the three-component vector $\mathbf{u}$. The advantage of the exponential parameterization is that it represents small rotations near the origin with minimal distortion. Parameterizations such as spherical coordinates (λ, θ, ρ) or Euler's angles (α, β, γ) have singularities near the origin and are not suitable for describing small

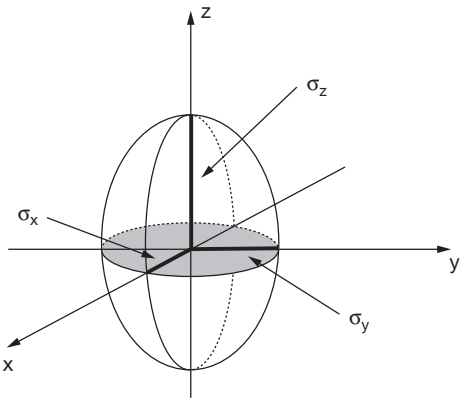

Figure 6 This ellipsoid reflects a fitted rotation uncertainty region expressed by a three-component vector **u** based on a 3×3 covariance matrix (see text for details).

rotations (Chang et al., 1990). The uncertainty of our estimated best-fit rotation is given by the covariance matrix cov (**u**). However, we also have uncertainties associated with our observations, that is, the errors in picking magnetic anomaly and fracture zone locations. The quality factor κ relates the uncertainties assigned to the data ($\hat{\sigma}$) to their true estimates (σ). The estimated factor $\hat{\kappa}$ is related to the uncertainties in the data by $\hat{\kappa} = (\hat{\sigma}/\sigma)^2$. Here, κ is unknown, but a method developed by Royer and Chang (1991) allows us to calculate $\hat{\kappa}$ from the misfit, the geometry of the plate boundary, and the number of data as

$$\hat{\kappa} = \frac{N - 2s - 3}{r}$$

where $N - 2s - 3$ represents the number of degrees of freedom, N is the number of points, s is the number of great-circle segments, and r is the total misfit (sum of squares of the weighted distances). The parameter $\hat{\kappa}$ indicates whether the assigned uncertainties are correct ($\hat{\kappa} \approx 1$), underestimated ($\hat{\kappa} \ll 1$), or overestimated ($\hat{\kappa} \gg 1$).

The confidence region of an estimated best-fit rotation $\hat{\mathbf{A}}$ is a three-dimensional ellipsoid (i.e., the axes are latitude, longitude, and angle). This ellipsoid can be projected onto a latitude–longitude plane using an algorithm described in Hanna and Chang (1990).

Chang (1988) observed that if one considers the eigenvectors of $(\text{cov}(\mathbf{u}))^{-1}$, these describe three axes at 90° to each other. Their respective eigenvalues constrain the maximum permissible rotation θ about these axes that will degrade the fit of the data to a specified limit. These rotations are roughly equivalent to the PURs described by Molnar and Stock (1985) (Figure 5). This analogy is useful for understanding what the matrix cov(**u**) actually represents.

6.02.2.3 Example: Central North and South Atlantic Reconstructions

The following example is taken from Müller et al. (1999), who combined magnetic anomaly data in the central North and South Atlantic Oceans with *Seasat* and *Geosat* satellite altimetry data to create a self-consistent dataset of magnetic and fracture zone identifications for the two ocean basins. This work builds on several decades of marine geophysical data collection and related papers in the central North and South Atlantic Oceans (e.g., Cande et al., 1988; Collette et al., 1984; Klitgord and Schouten, 1986; Roest, 1987; Roest et al., 1992; Shaw and Cande, 1990). The finite motion poles and their uncertainties were estimated for 15 times from chron 34 to the present using Chang's inversion method (Chang, 1987, 1988; Chang et al., 1990), allowing a simple parameterization of the rotation uncertainties along a plate circuit path. The rotations and their uncertainties were then combined to model the North–South American history of relative motion, and its effect on Caribbean tectonic history (Müller et al., 1999). The magnetic and fracture zone picks used in this model are shown in Figures 7 and 8.

A critical aspect in the reconstruction method is the correct assessment of the uncertainties in the location of the data that will propagate into the uncertainties of the rotation parameters (location of the rotation pole and rotation angle). Following a detailed analysis of the dispersion of magnetic anomaly C5 crossings in the Indian Ocean by Royer et al. (1997) and Müller et al. (1999) assigned $1-\sigma$ nominal uncertainties of 4 km to the magnetic anomaly crossings and of 5 km to fracture zone crossings following the Müller et al. (1991) analysis of depth to basement and geoid data along the Kane Fracture Zone.

Finite rotations for North American–African and South American–African plate motions were computed for 12 times from chron 34 to the present (Figure 9). The 95% confidence regions are three-dimensional ellipsoids in latitude, longitude, and rotation angle space. In order to represent them on a map, the ellipsoids are projected onto the latitude–longitude sphere. The projected uncertainty ellipses include uncertainties in latitude, longitude, and angle, but one must keep in mind that the true size of the rotation uncertainties (i.e., ellipsoids), which are described by the covariance matrices, might not be reflected well by their 2-D projection onto the sphere. For instance, in the case of the South Atlantic, the 2-D uncertainty in the location of the chron 5 best-fitting pole appears to be at least 10 times larger than the 2-D uncertainty in the location of the chron 21 rotation pole, whereas the volume of the 95% confidence region for chron 5 rotation is only about three times larger than for the chron 21 rotation (7838 vs. 2773 km^3, respectively). Conversely, the 95% uncertainty volume for chron 8 (19 705 km^3) is 2.5 larger than for chron 5, whereas its 2-D projection is about three times smaller than for chron 5.

The projected rotation confidence regions show a trend from larger uncertainties for younger chrons to more tightly constrained older reconstructions. This simply reflects the fact that when the rotation angle is small, changes in the position of the rotation pole only have small effects on the fit of the data, whereas the converse is true for large rotation angles. Somewhat ironically, older reconstructions are generally better constrained than younger reconstructions, even though this effect can be somewhat offset by relatively larger datasets for younger chrons.

The central North Atlantic and South Atlantic rotations can then be added, one with its angle reversed, to compute North–South American rotations (Figure 10). The resulting

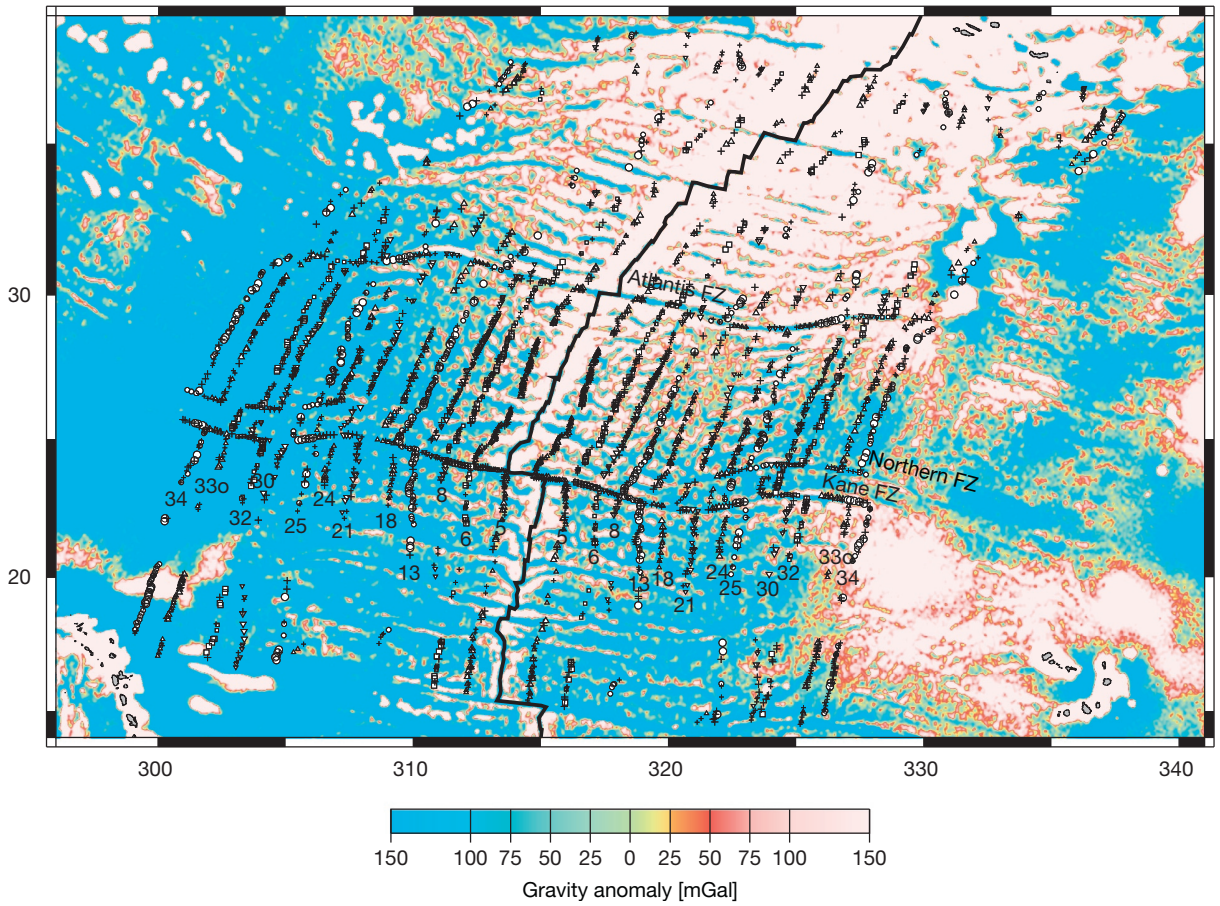

Figure 7 Gravity anomalies from satellite altimetry from Sandwell and Smith's (1997) grid, downward continued to the seafloor (Walter Smith, personal communications, 2006) and interpreted and rotated magnetic anomaly and fracture zone identifications in the central North Atlantic. The unrotated magnetic and fracture zone identifications are identified by the following symbols: triangle (C5, 9.74 Ma; C18, 38.43 Ma; C30, 65.58 Ma), square (C6, 19.05 Ma; C21, 46.26 Ma; C32, 71.59 Ma), upside down triangle (C8, 19.05 Ma; C24, 52.36 Ma; C33o, 79.08 Ma), and circle (C13, 33.06 Ma; C25, 55.90 Ma; C34, 83 Ma). All rotated data points are marked by crosses. Paleoridge or transform segments as defined by magnetic anomaly or fracture zone identifications, approximated as great circles in the inversion method used here, are denoted by alternating small and large symbols.

pole path shows (1) very stable poles of motion from chron 25 to 21 and from chron 18 to 8; (2) an important northward migration of the rotation poles from chron 34 to chron 18; and (3) a southward migration until chron 6. The North American–South American rotation stage poles always lie outside the Caribbean Plate; for the ages younger than chron 25 (55.9 Ma), they lie within or in the vicinity of the North American–South American plate boundary, implying a different sense of motion along strike of this plate boundary.

Figure 11 shows North American–South American plate motion through time, illustrated by the successive motion of three points attached to the North American Plate with respect to the South America Plate for 11 stages from chron 34 (83 Ma) to the present, including uncertainties of the location of rotated points. For each stage rotation vector, a simultaneous 95% confidence region is plotted about the young ends of the relative motion vectors, that is, the ellipse about points at chron 33o reflects the uncertainty for the chron 34–33o stage rotation. A simultaneous confidence region represents the area (on the surface of the Earth) in which a point on a given plate may have been located with equal likelihood for a particular reconstruction time, with 95% confidence. This means that with 95% confidence, there is an equal likelihood that a rotated point may end up anywhere within the 95% confidence region. The simultaneous 95% confidence regions increase in size with increasing distance from the stage pole of motion; in the Caribbean area, they increase in size correspondingly from east to west (Figure 11).

Even though the projected confidence ellipsoids of the finite rotation poles for North American–South American plate motion for chrons 18–6 show large overlaps (Figure 11), the simultaneous 95% confidence regions for the three rotated points shown indicate only little overlap. This may appear puzzling but only reflects the imperfect nature of the 3-D finite rotation pole error ellipsoid projections onto a spherical surface in Figure 10, as discussed before. In other words, this result shows that the covariance matrices and uncertainty ellipsoids for these reconstructions are different enough to distinguish different phases of convergence in the late Tertiary outside of the 95% error bounds. Combined

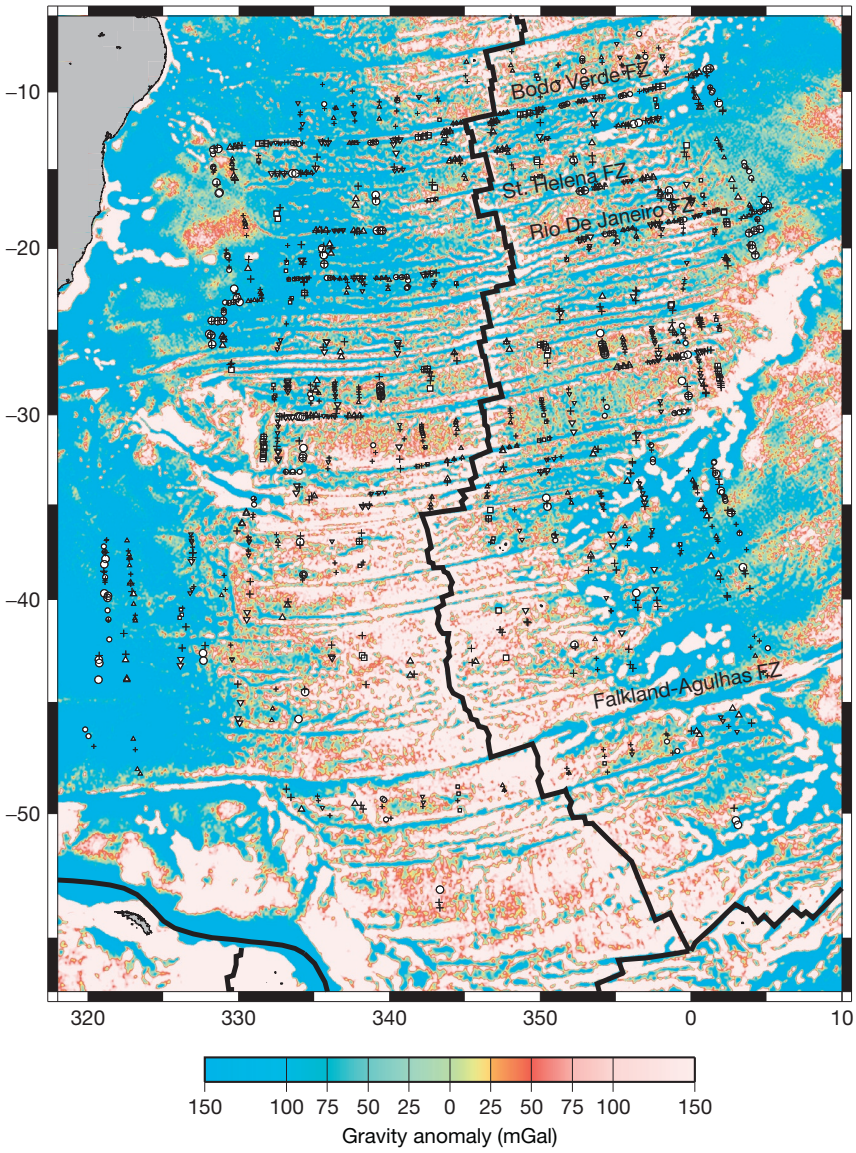

Figure 8 Gravity anomalies from satellite altimetry, downward continued to the seafloor as in Figure 7 and interpreted and rotated magnetic anomaly and fracture zone identifications in the South Atlantic. The symbols used for plotting magnetic and fracture zone identifications follow the same convention as in Figure 7.

magnetic and fracture zone identifications and a rotation model can then be used to construct seafloor isochrons, which in turn can be gridded to produce a continuous map of seafloor ages (Figure 3) (Müller et al., 2008).

6.02.2.4 The Emergence of Reconstruction Tools

Traditionally the domain of specialists, the calculation of plate tectonic reconstructions has in recent years become much more accessible to a broad range of Earth scientists, students, and others. A key development is GPlates (www.gplates.org), an open-source paleogeographic information system running on Windows, Linux, and Mac OSX (Boyden et al., 2011; Qin et al., 2012; Williams et al., 2012). It enables the interactive manipulation of plate tectonic reconstructions and the visualization of geodata through geologic time (Figure 12). Developed originally as a standalone software, GPlates has gradually grown into an open innovation platform by employing an open standards-based information model, by implementing extensive data import/export capabilities, developing an emerging Python plug-in framework, and establishing links to web services. This extensible platform allows users to explore the evolution of the entire Earth system in accordance with past tectonic plate configurations by combining GPlates with a variety of research tools, data, and workflows. GPlates applications include tectonics, geodynamics, basin evolution, orogenesis, deep Earth resource exploration, paleobiology, paleoceanography, and paleoclimate. We believe such free tools will ultimately lead to the democratization of plate reconstructions.

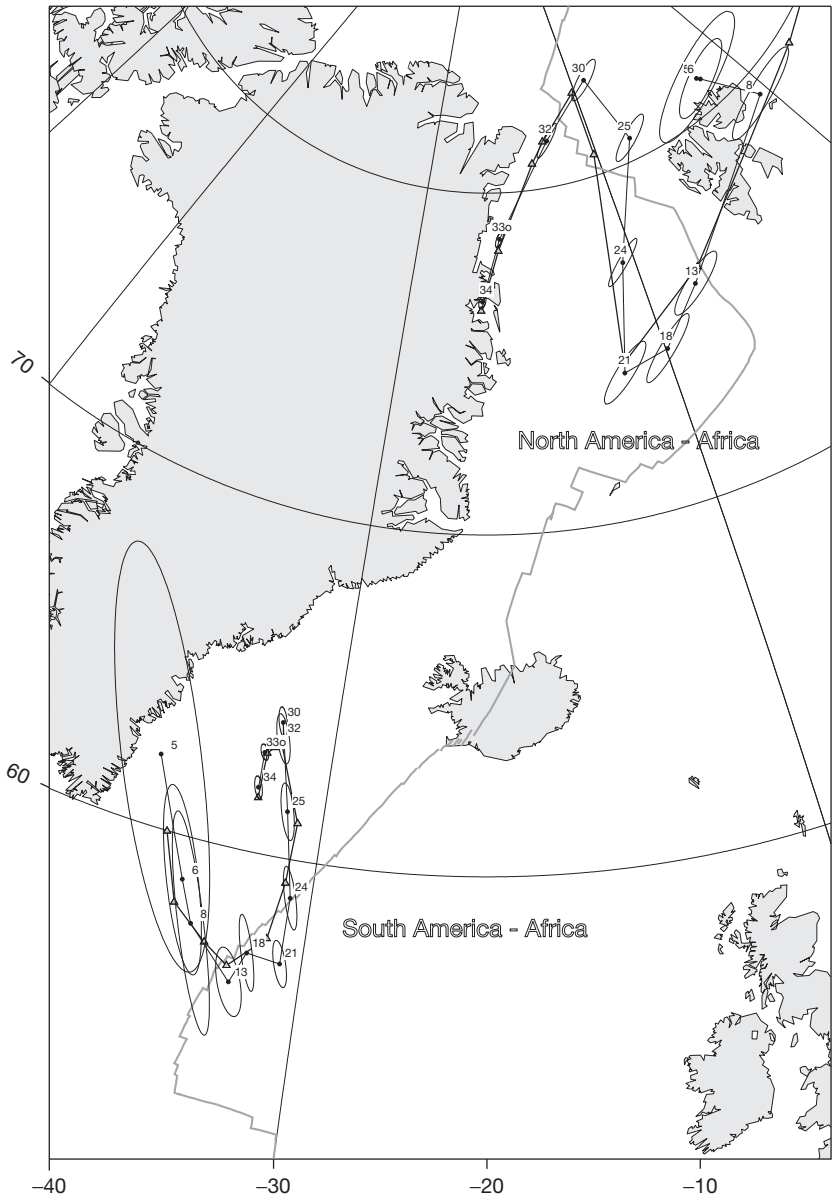

Figure 9 Total reconstruction poles and 95% confidence ellipses for North American–African (upper right) and South American–African (lower left) plate rotations for 12 reconstruction times from chron 34 (83 Ma) to the present. Note the sharp cusp in the North American–African pole path at chron 8 (25.8 Ma), marking a global plate reorganization, expressed, for example, also in the cessation of seafloor spreading in the Adare Trough between East Antarctica and West Antarctica.

6.02.2.5 Diffuse Plate Boundaries

As mentioned, the plate tectonic theory was developed using the approximation of rigid plates moving on a spherical Earth, separated by relatively narrow boundaries where much of the observable deformation is localized (e.g., McKenzie and Parker, 1967; Morgan, 1968; Wilson, 1965). The motions of plates were described with simple Euler's rotations on a sphere, and the motions were discontinuous only at the plate boundaries themselves. To a first approximation, this simplification has worked exceedingly well, particularly in the quest to understand the kinematic evolution of the ocean basins, but as both data and analyses have become more sophisticated, it is clear that there are departures from this simple, cartoonlike picture of how the Earth works. Early assessment of departures from the rigid plate model suggested that distributed deformation might be associated with zones of lithospheric weakness (such as fossil plate boundaries, fracture zones, and other scars in the oceanic lithosphere) (e.g., Bergman and Solomon, 1980; Sager and Keating, 1984; Stein, 1979; Sykes, 1978). However, as data of higher resolution have become available, a more complicated picture has emerged. For instance, the Indo-Australian Plate, once considered to have some weak zones associated with the Ninetyeast Ridge, has been shown to be better

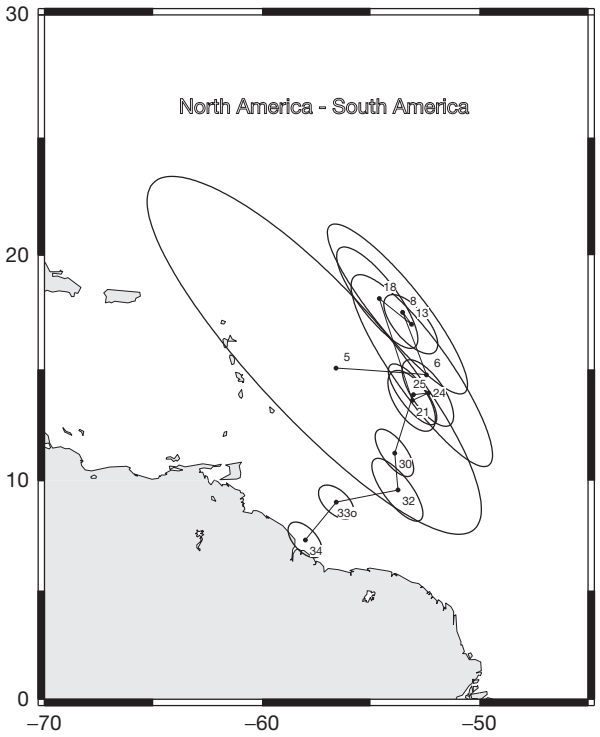

Figure 10 Total reconstruction poles for 12 reconstruction times for North American–South American relative plate motions since chron 34 (83 Ma). These rotations have been computed by combining the finite rotations and their 95% confidence regions shown in **Figure 9**. After Müller RD, Royer JY, Cande SC, Roest WR, and Maschenkov S (1999) New constraints on Carribean plate tectonic evolution. In: Mann P (ed.) *Caribbean Basins*. Amsterdam: Elsevier.

described as a composite plate made up of three-component plates (the Indian, Capricorn, and Australian Plates) separated by diffuse boundaries. Royer and Gordon (1997) coined the terms 'component' and 'composite' plates in order to allow a better description of the actual situation found in the oceans. When compared to predictions of stress modeling, it is seen that areas of high deviatoric compression roughly correspond with regions of observed crustal contraction, whereas areas predicted to have high deviatoric extension correspond to regions where stretching seems to be occurring. In detail, however, much of the deformation within these regions is accommodated by older weaknesses in the crust such as preexisting and reactivated faults (see **Chapter 6.04**) (Gordon, 2000).

The predicament of the Indo-Australian Plate is not unique. Africa, with its well-developed extensional activity in the Great Rift Valley, is now considered a composite plate made up of the two rigid component plates (Nubia and Somalia) (Chu and Gordon, 1999; Gordon, 1998), whereas North and South America can be considered component plates in the large American composite plate. It seems clear that diffuse plate boundaries are sites of strong plate coupling compared with narrow plate boundaries where the decoupling of mechanical properties is more complete; this is reflected in strain rates that are much higher across narrow plate boundaries (Gordon, 2000). **Figure 13** illustrates the distribution of diffuse plate boundaries. Indeed, the lowest strain rates at narrow plate boundaries exceed the upper strain rates from diffuse boundaries by two orders of magnitude. Such partitioning of strain may be a strong argument for describing plate evolution in terms of a non-Newtonian, self-lubricating rheology (e.g., Bercovici, 1993). It is interesting to note that the pole of rotation describing the relative motion between two component plates tends to lie within the diffuse boundary, and Gordon (2000) proposed the term 'convergent–divergent pivot' for such rotations that describes the change from extensional to compressional deformation within the short distance of the diffuse boundary. Work by Zatman et al. (2001, 2005) indicates that the location of such rotation poles within the diffuse boundary is favored by both geometric and rheological arguments.

6.02.3 Intraplate Volcanism

6.02.3.1 The Morphology of the Ocean Floor

In 1963, Tuzo Wilson noted that in certain locations around the world, such as Hawaii, volcanism has been active for very long periods of time (Wilson, 1963). This seemed to indicate that relatively small, long-lasting, and anomalously hot regions – called hot spots by Wilson – existed below the plates in the mantle that would provide localized sources of high heat energy (thermal plumes) to sustain volcanism (see **Chapter 7.10**). Specifically, Wilson hypothesized that the distinctive linear shape of the Hawaiian Island–Emperor seamount chain resulted from the Pacific Plate moving over a deep, stationary hot spot in the mantle, located beneath the present-day position of the Hawaiian Island. More than a hundred hot spots beneath the Earth's crust have been active during the past 10 Myr. Most of these are located under plate interiors (e.g., the African Plate), but some occur near diverging plate boundaries. Some are concentrated near the mid-oceanic ridge system, such as beneath Iceland, the Azores, and the Galápagos Islands. A widely used method of reconstructing plates relative to a fixed mesosphere utilizes linear chains of volcanoes that display age progression and are thought to be caused by focused spots of melting in the upper mantle. We will return to this topic shortly.

While it was the larger seamount chains that caught Wilson's eye, it had been known for some time that the oceans were littered with underwater volcanoes known as seamounts. Following the end of World War II, the rapid expansion of ocean-going expeditions with echo-sounding instruments promoted a major advance in the understanding of seafloor morphology, leading to the realization that the oceans had mountain chains of extraordinary length; this discovery was popularized by the early maps of Lamont Heezen and Tharp (1961, 1964). Also on those maps were the renditions of numerous seamounts. During World War II, Princeton geologist Harry Hess discovered and mapped several flat-topped seamounts that he named guyots; these were apparently former islands that had been eroded down to sea level and later drowned (Hess, 1946). Menard had surveyed many seamounts in the Pacific and suggested that there might be as many as 100 000 seamounts exceeding a height of 1 km in the Pacific

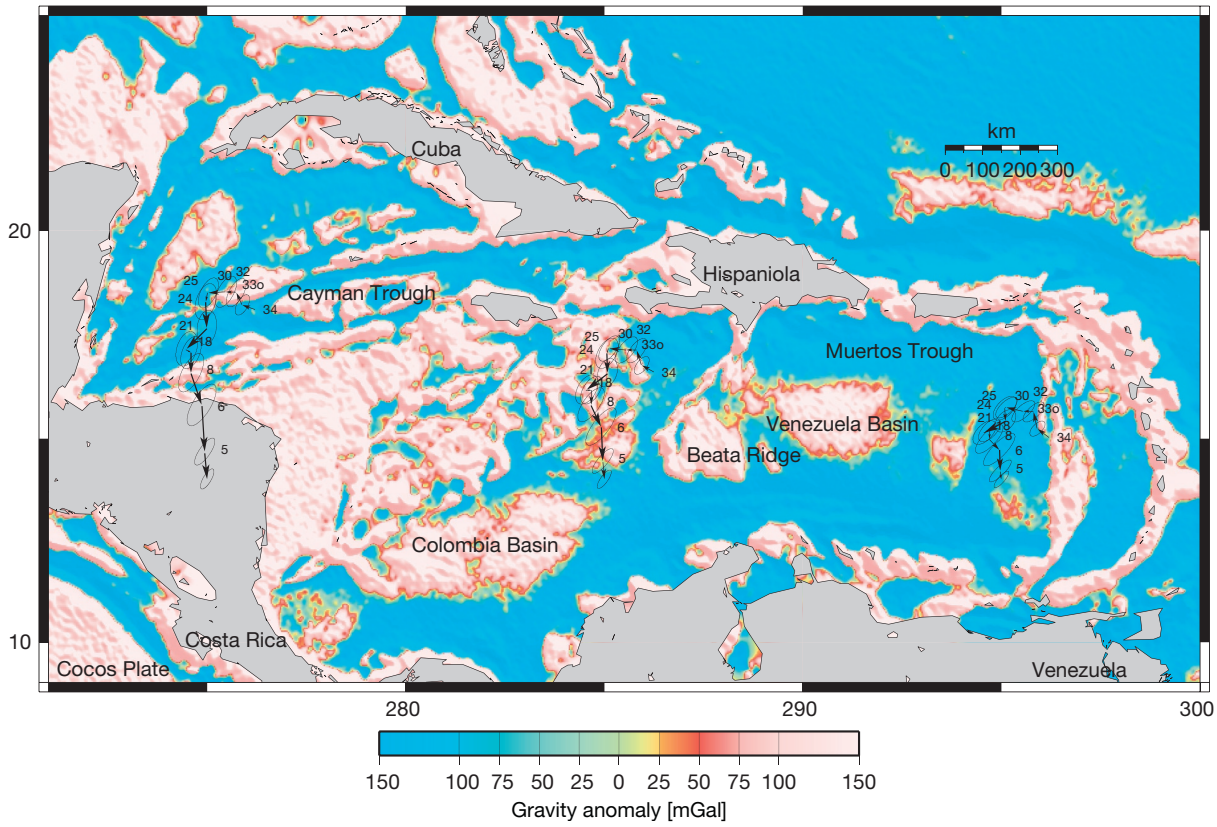

Figure 11 North American–South American plate motion through time of 3 points attached to the North American Plate with respect to the South American Plate for 11 stages from chron 34 (83 Ma) to the present. The simultaneous 95% confidence regions for each stage rotation vector are plotted about the young ends of the relative motion vectors, that is, the ellipse about points at chron 33o reflects the uncertainty for the chron 34–33o stage rotation. This figure demonstrates that this model cannot resolve very slow relative motions between chrons 25 and 24; some overlap between the confidence regions for chrons 32 and 30 and 18 and 13 is also observed. However, all other stage vectors are well resolved.

alone (Menard, 1964). However, because of the vastness of the oceans and the sparse sampling provided by surface ships, the majority of seamounts went uncharted. Most statistical treatments of seamount populations relied on extrapolations from smaller, well-surveyed areas by dense, single-beam echo-sounding tracks or by the improved coverage of the newer multibeam systems. With the advent of satellite altimetry, a new technique became available for the study of seamounts. Figure 14 illustrates the leaps in resolution afforded by the new space-based techniques. The global gravity maps derived from the *Seasat* altimeter mission by Bill Haxby clearly depicted an impressive richness of seafloor fabric, in particular a plethora of underwater volcanoes (Haxby, 1987; Haxby et al., 1983). Using *Seasat* along-track profiles of sea surface heights, Craig and Sandwell (1988) were the first to undertake a truly global investigation of the seamount distribution, finding around 8500 individual edifices distributed throughout the world's oceans. They were able to confirm that the Pacific Ocean basin hosts the majority of the seamounts and that the western Pacific displays an unusual high density of large seamounts. However, due to the large track spacing (~100 km), many seamounts were only partially surveyed and many more fell within the gaps between tracks. The newer *Geosat*/*ERS-1* data vastly improved the coverage by having much closer track spacing, and by 1997, a new global gravity grid superior to the *Seasat* grids had been provided (Sandwell and Smith, 1997). Using this data, Wessel and Lyons (1997) were able to characterize almost 8900 seamounts in the Pacific Ocean alone, with most of the increase in population coming from smaller, hitherto uncharted seamounts. Wessel (2001) extended this analysis to all oceans, counting a total of almost 14 700 seamounts, later revised to 11 882 (Wessel et al., 2010) due to duplicates (Figure 15). Statistical treatment of the observed population suggests that the sizes of seamounts approximately follow a power-law relationship that, when extrapolated below the size of the smallest seamounts that are reliably identified by altimetry, matches Menard's earlier prediction of 100 000 seamounts of at least 1 km in height (Figure 16). Marine geologists now routinely study seamounts of much shorter stature (down to a few tens of meters), and if the inferred frequency–size relationship holds for even these smaller seamounts, one would predict a global total of more than one million seamounts, making these morphological features second in ubiquity only to the abyssal hills. Recent work, however, has suggested that the log–log relationship may not hold for smaller sizes, thus reducing the census downward to perhaps just 40–50 000 for seamounts whose heights exceed 100 m (Kim and Wessel, 2011).

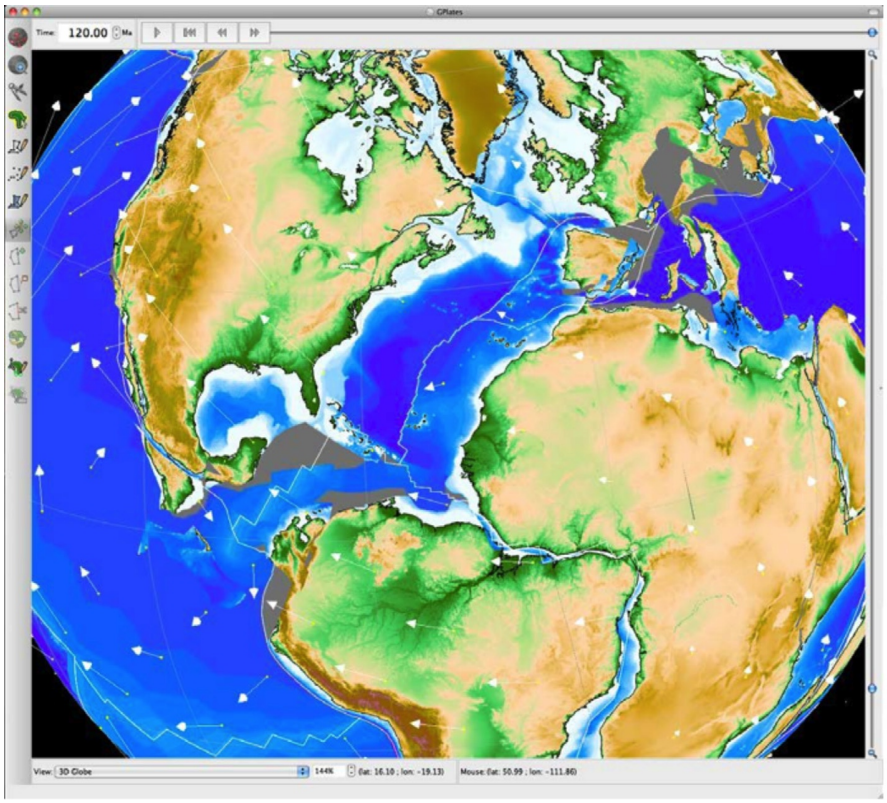

Figure 12 Interactive plate reconstructions. Snapshot at 120 Ma in GPlates showing the opening of the North Atlantic. Continents are shown with the present-day elevations, and the ocean depths are depicted in shades of blue (deep, dark blue; shallow, light blue). White arrows indicate predicted plate motion vectors.

6.02.3.2 Seamount Provinces

A closer examination of the spatial distribution of seamounts shows that there are at least three superimposed populations. The most numerous group is the smaller seamounts. Studies have indicated that the majority of these smaller seamounts were formed in close proximity to a spreading ridge, often right on the ridge flank and sometimes very close to transform offsets. Here, excess amounts of melt ascend through thin and fractured crust, forming small, subcircular seamounts – often just a few tens to hundreds of meters in elevation (e.g., Smith and Cann, 1990). Occasionally, somewhat larger seamounts can be formed. It is likely that most, if not all, smaller seamounts formed in this near-ridge tectonic environment since the rapid increase in lithospheric thickness away from the ridge would make the penetration of small amounts of melt from an increasingly deeper source less likely. Consequently, observed seamount production rates decrease with increasing crustal age and lithospheric thickness, being highest close to the ridge axis (e.g., Batiza, 1982). At fast-spreading ridges, such as the East Pacific Rise, small seamounts form on the flanks of the ridge where the crust is just 0.2–0.3 Myr old, and their abundance correlates with spreading rate (e.g., White et al., 1998). In contrast, at slow-spreading ridges such as the Mid-Atlantic Ridge, small seamounts appear to be produced almost exclusively within the median valley (e.g., Smith and Cann, 1990). Studies have shown that many of these new seamounts undergo extensive tectonic deformation by normal faulting that reduces their original heights considerably (Jaroslow et al., 2000). It is also evident that the increased sediment coverage on older seafloor (e.g., Ludwig and Houtz, 1979) is likely to bury the smallest and most numerous seamounts with height less than 100 m after a few tens of millions of years.

It seems to be a fact that the majority of larger seamounts found in the ocean basins were formed in an intraplate setting, far from the presence of active plate boundaries. Because of their frequent alignment into linear, subparallel chains that appear to correlate with the direction of current or past plate motions (e.g., Duncan and Clague, 1985; Koppers et al., 2001; O'Neill et al., 2005; Wessel and Kroenke, 1997), the most widely accepted origin of such seamounts remains that of the hot spot hypothesis, as mentioned earlier. The relative motion between plates and plumes leads to the formation of lines of extinct volcanoes; these exhibit monotonic age progressions, reflecting the history of past plate motions. Since the early formulation of the hot spot hypothesis, numerous hot spots have been proposed for sites of unusual volcanic activity (e.g., Burke and Wilson, 1976; Clouard and Bonneville, 2001; Sleep, 1990). Yet, conclusive imaging of the underlying mantle plumes using seismic tomography remains elusive (Nataf, 2000), despite tantalizing results from Iceland (Wolfe et al., 1997). For instance, the archetypal strong

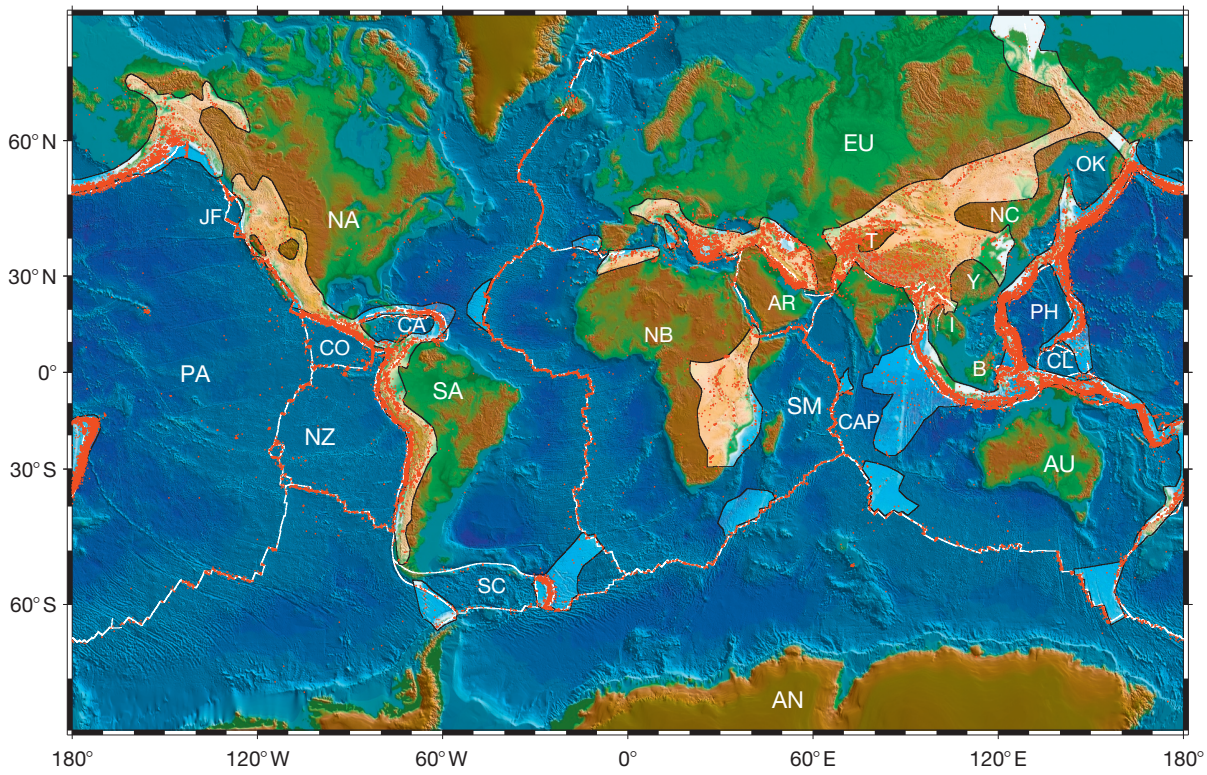

Figure 13 Map showing idealized narrow plate boundaries (Coffin et al., 1997), shallow (0–70 km depth) seismicity (red dots) (Engdahl et al., 1998), and regions of diffuse plate boundaries (areas of lighter illumination) based on Figure 1 of Gordon (2000) who inferred deformation from seismicity, topography, other evidence of faulting and nonclosure of plate motion circuits. These deforming regions, which constitute diffuse plate boundaries, cover ~15% of the Earth's surface. Plate abbreviations: B, Borneo; AN, Antarctica; AR, Arabia; AU, Australia; CA, Caribbean; CAP, Capricorn; CL, Caroline; CO, Cocos; EU, Eurasia; I, Indo-China; IN, India; JF, Juan de Fuca; NA, North America; NB, Nubia; NC, North China; NZ, Nazca; OK, Okhotsk; PA, Pacific; SA, South America; SC, Scotia Sea; SM, Somalia; Y, Yangtze; T, Tarim Basin; PH, Philippine.

plume that many believe has formed the Hawaiian–Emperor seamount chain and currently is assumed to underlie the Hawaiian hot spot at the southeast end of the Hawaiian Island is not well resolved (Cao et al., 2011; Wolfe et al., 2009), whereas other, less productive hot spots (e.g., Easter, Ascension, and Azores) appear more strongly manifested in the tomographic images (Montelli et al., 2004). Although the simple age progressions predicted by the hot spot hypothesis are reflected in the observations for several seamount chains (such as the Hawaiian–Emperor and Louisville chains), others exhibit a more complex age pattern that casts some doubt on the hot spot theory being the only explanation for such volcanism (e.g., Anderson et al., 1992; Dickinson, 1998; McNutt et al., 1997).

With some exceptions, the seamounts formed by hot spot volcanism tend to grow into the largest seamounts found in the oceans (Figure 17). In particular, intraplate seamounts formed on old (and hence thicker and thus stronger) oceanic lithosphere can in some cases reach almost 10 km (measured from the base on the seafloor to the tallest peak on an island). A case in point is Mauna Kea, one of five volcanoes that form the Hawaiian Island, which is the tallest mountain on Earth. Given the smallest features (~100 m) considered to be seamounts by most geologists, the sizes of observed seamounts span almost three orders of magnitude.

A few isolated, large intraplate seamounts are apparently not associated with any plume or hot spot seamount chain, such as Shimada Seamount in the Pacific (Gardner et al., 1984) and Vesteris Seamount in the North Atlantic (Haase and Devey, 1994). Because of their large sizes, they most likely formed on relatively thick and strong crust; this makes it likely that the available melt took advantage of preexisting zones of weakness in the lithosphere, probably made more vulnerable by extensional stresses related to plate motion changes (e.g., Sager and Keating, 1984).

The third group of seamounts is composed of those making up island arcs. Distinctly different from the two other classes of seamounts, the island arc seamounts form at subduction zones where one oceanic plate is being forced to subduct beneath the other. As subducting plates descend into the mantle, the higher pressure and increasing temperatures eventually cause decompressional melting of the old seafloor crust, the blanket of wet sediments (if any), and any preexisting seamounts to produce an ascending basaltic melt of a different magmatic composition than is available at spreading centers. In particular, the magma may be more volatile, increasing the chance of explosive eruptions. Geometrically, the distribution of these island arc seamounts and islands reflects the trend of the convergent plate boundaries, and the overall plate tectonic geometry places strong constraints on the evolution of such seamounts (e.g., Fryer, 1996).

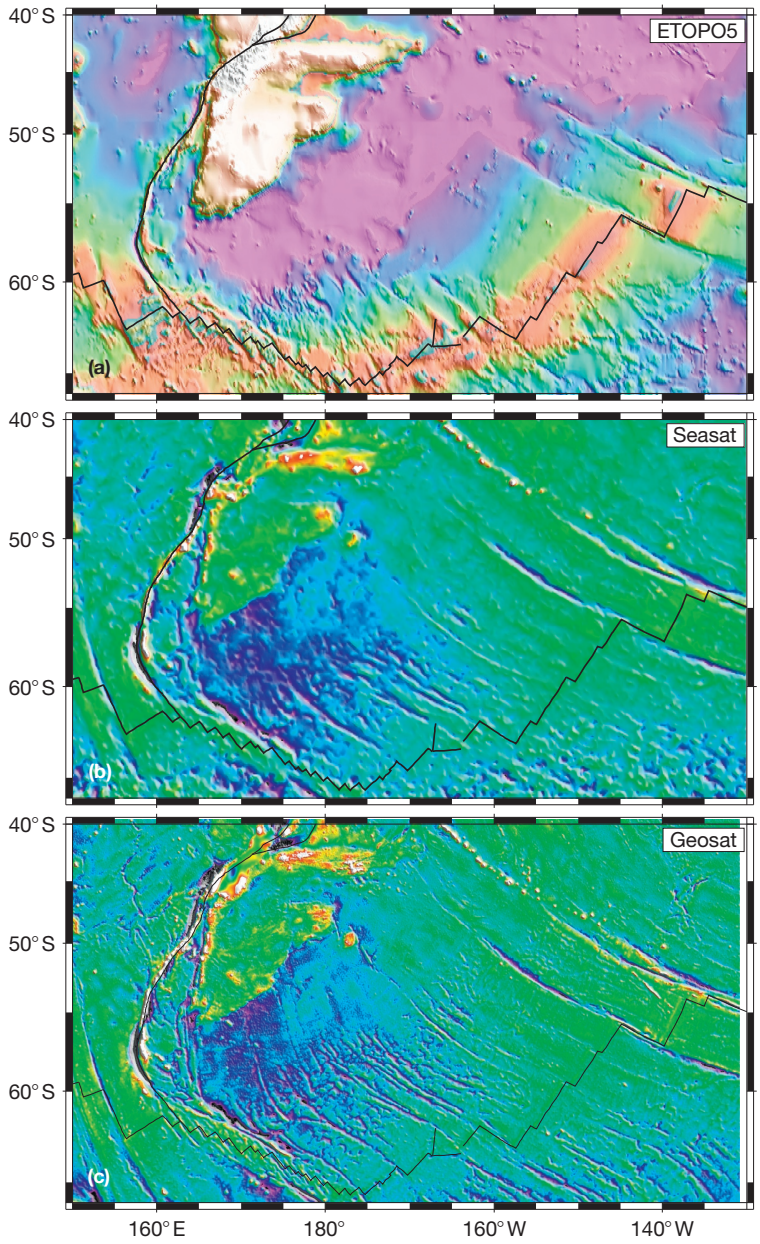

Figure 14 Improvements in mapping the large-scale morphology of the seafloor. (a) The ETOPO5 global 5 × 5 minute bathymetry grid, based largely on SYNBAPS (Van Wyckhouse, 1973), was derived from contour maps and yielded a coarse view of the seafloor, in particular in the remote southern oceans. However, it was a quantitative improvement from the more artistic map renditions of Heezen and Tharp (e.g., Heezen and Tharp, 1961). (b) The first global gravity field derived from *Seasat* altimetry was published by Haxby (1987) using the methodology of Haxby et al. (1983). In his map, fracture zones and seamounts were much better resolved. (c) The most recent version of *Geosat/ERS-1* altimetry-derived free-air anomalies (Sandwell and Smith, 1997) shows an order of magnitude more details, resolving morphological fabric hitherto only seen in dense ship surveys. The mapping of tectonic fabric such as fracture zones has allowed a marked improvement in plate tectonic modeling (e.g., Cande et al., 1995).

Geographically, these island arc seamounts are found in the relatively narrow collision zones between the converging tectonic plates, thus occupying a small area of the total seafloor. Like hot spot-produced seamounts, the island arc seamounts can reach considerable height and often form islands (hence the term island arcs). However, unlike the situation at hot spot-produced seamounts and oceanic islands, the volcanic activity along an active arc is essentially simultaneous, geologically speaking, with older seamounts constantly being overprinted by younger ones.

6.02.3.3 Significance of Seamounts

Seamounts present windows into the mantle, allowing scientists to examine in detail the nature of the magma that is

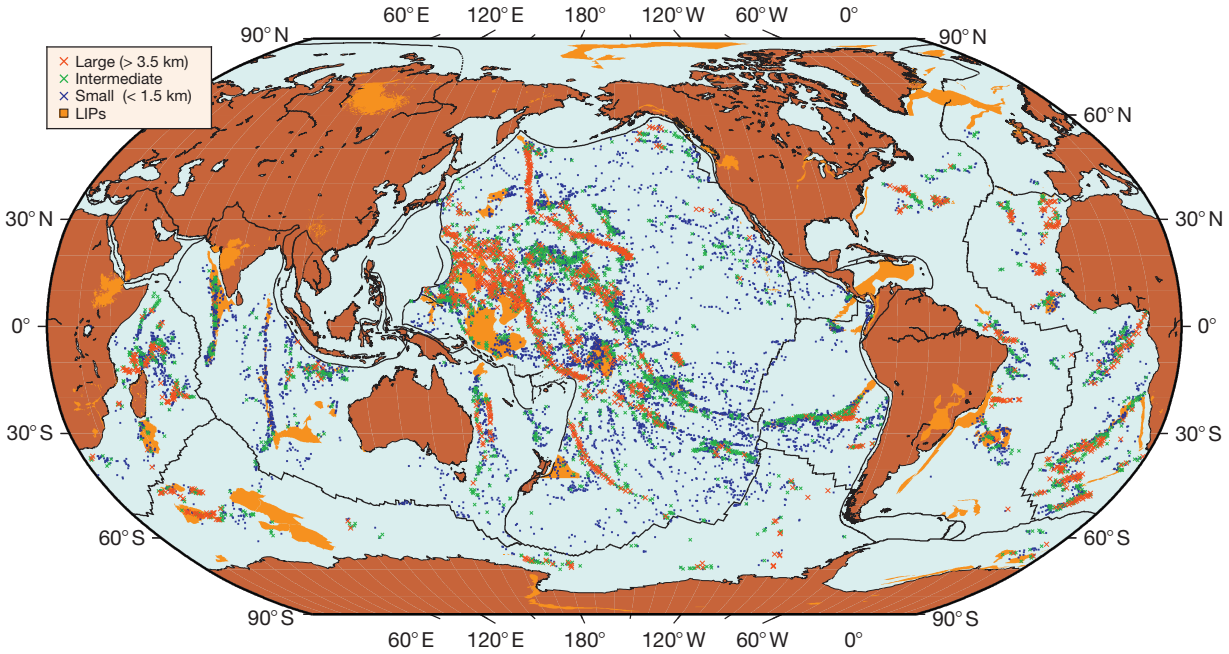

Figure 15 Global distribution of seamounts as identified by Wessel (2001) in a vertical gravity gradient grid (in units of mGal m^{-1} or Eötvös) derived from the *Geosat/ERS-1* satellite altimetry (Sandwell and Smith, 1997). Red crosses are large seamounts (>120 Eötvös, generally >3.5 km tall), blue are small seamounts (<60 Eötvös, generally <2.5 km tall), whereas green crosses are of intermediate size. The majority of seamounts can be found in the Pacific basin, with the remainder divided between the Atlantic and the Indian Oceans. Large igneous provinces are outlined in dark orange (e.g., Coffin and Eldholm, 1992); these are often associated with seamount provinces.

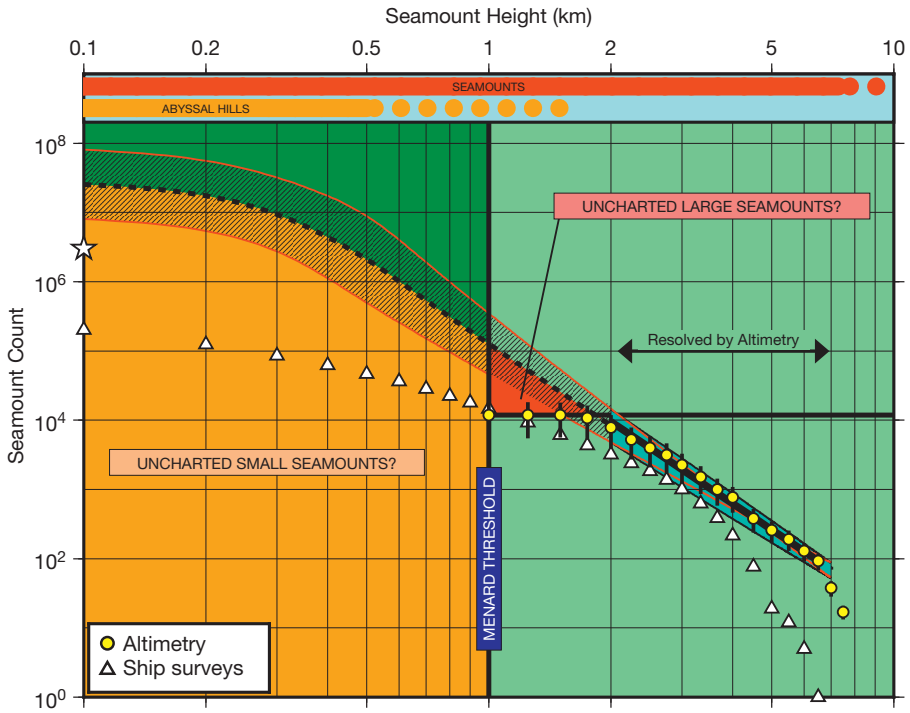

Figure 16 Global seamount size–frequency distribution. Height–frequency distributions of seamounts based on satellite altimetry (yellow circles) and single-beam bathymetry profiles (white triangles). Cyan band represents ±30% uncertainty in counts, yielding upper/lower extrapolations to smaller sizes (red lines with hachured uncertainty). The flattening of predictions for heights <500 m is due to sedimentation and area considerations (see text). There could be approximately 125 000 seamounts taller than 1 km and as many as 25 million taller than 100 m, but the uncertainties are considerable. White star (3 million) is adjusted prediction by Hillier and Watts (2007). Redrawn from Wessel et al. (2010).

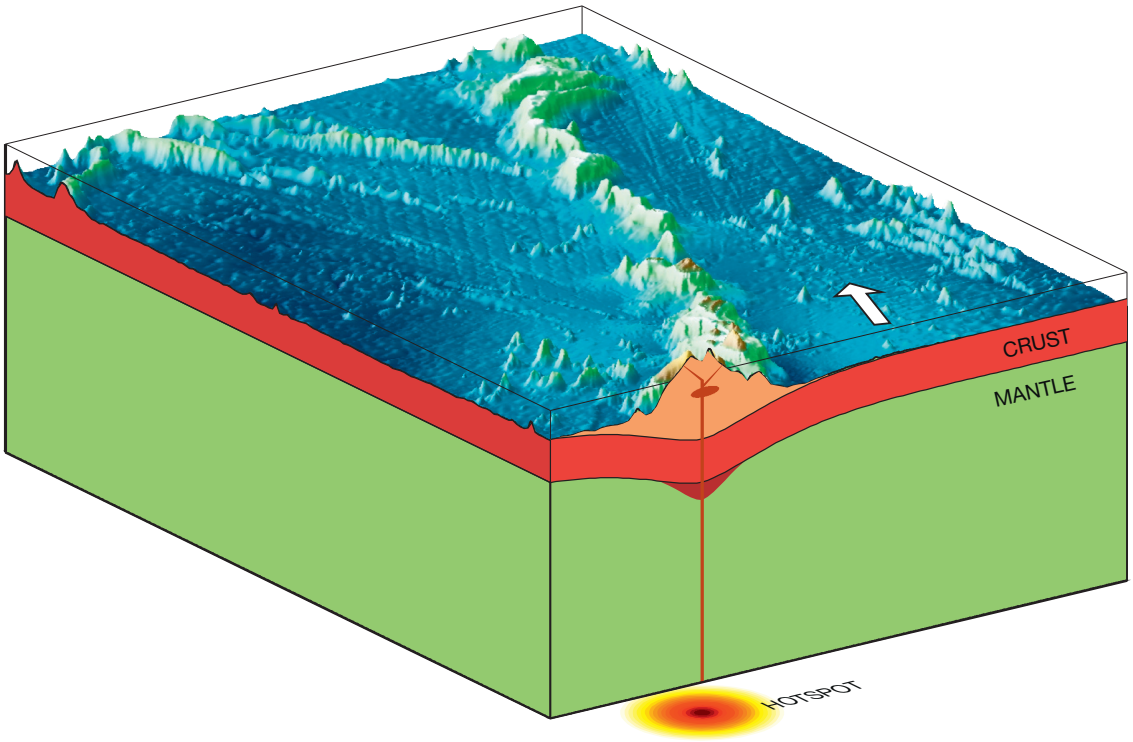

Figure 17 Sketch illustrating intraplate seamount (and island) formation over the Hawaiian hot spot. Given a thick and strong lithosphere (~90 Myr old), intraplate seamounts can grow very tall and even breach sea level to form oceanic islands. The large volcanic piles deform the lithosphere, which responds by flexure. The plume beneath the plate feeds the active volcanoes by a network of feeder dikes; some magma may pond beneath the crust as well (Watts and ten Brink, 1989). As the plate motion carries the volcanoes away from the hot spot (arrow indicates current direction of motion), they cease to be active and form a linear seamount or island chain.

erupting. While overwhelmingly basaltic, minor changes in the chemical and isotopic composition of lavas can be mapped and such patterns can be used to make inferences about the source, such as the depth of the magma and its ultimate composition (e.g., Janney et al., 2000). The extrusive volume represented by seamounts is a significant fraction of the entire crustal production, perhaps as much as 10% (Batiza, 1982), and both spatial and temporal variations in this intraplate volcanic budget shed light on the plate tectonic evolution of the ocean basins and the mechanisms by which the Earth gets rid of its excess heat. Furthermore, the alignment of seamounts into chains provides a means to decipher the motion of the tectonic plates over long geologic intervals, enabling a better understanding of the climatic changes experienced at islands that simply follow from latitudinal migration of plates carrying seamount provinces on their backs (e.g., Kroenke, 1996). Many seamounts have active hydrothermal convection systems that may have a significant effect on element cycles involving seawater (Batiza, 2001), and they also participate in the dissipation of residual heat from the formation of both seamount and seafloor (e.g., Harris et al., 2004). Finally, seamounts and islands act as measuring sticks for relative sea level variations, which can have both eustatic and tectonic components (Douglas, 1991; Tushingham and Peltier, 1992).

The bathymetry of the ocean floor influences the ocean circulation in several ways. Most importantly, the first-order bathymetric features such as ridges and plateaus steer the currents and in places provide barriers that prevent deep waters from mixing with warmer, shallower waters. However, there is a growing awareness that smaller-scale bathymetry, such as seamounts, may play a largely overlooked role in the turbulent mixing of the oceans (e.g., Kunze and Llewellyn Smith, 2004). In fact, measurements suggest that mixing around a shallow seamount is many orders of magnitude more vigorous than in areas far from seamounts (Lueck and Mudge, 1997). The precise understanding of how the Earth's climate will evolve depends on how quickly heat and carbon dioxide can penetrate into the deep oceans, and assumed rates of vertical mixing can affect model predictions considerably. Further mapping of seamounts and the inclusion of an accurate representation of the seafloor into models of global ocean circulation will be necessary in order to improve predictions of climate (e.g., Jayne et al., 2004).

Representing obstacles to flow, seamounts induce local currents, which can enhance the upwelling around the seamount. As this may bring up nutrient from the deeper ocean, primary productivity is enhanced, supporting a wide variety of life (Rogers, 1994). The importance of seamounts as habitats for ecological communities and in particular fish is being increasingly recognized, and a better understanding of the complex relationships between several parameters is required to develop well-founded policies on fisheries and conservation. Islands, as subset of seamounts that currently exceed sea level, also sustain unique flora and fauna and provide natural

laboratories for ecology, evolution, and cultural diversification (e.g., Price and Clague, 2002).

6.02.3.4 The Ages of Seamounts and Oceanic Islands

A key prediction of the hot spot hypothesis is that there should be a clear monotonic age progression along the seamount and island chains produced by hot spot volcanism. Consequently, the determination of actual ages from rock samples collected at these sites became of paramount importance early in the study of hot spot chains. Pioneering efforts by Turner, Duncan, McDougal, and others provided a valuable dataset whose importance cannot be overestimated (Duncan, 1981; Duncan and Clague, 1985; McDougall, 1971; Turner and Jarrard, 1982; Turner et al., 1980). A 2005 review by Clouard and Bonneville (2005) discusses a Pacific compilation of more than 1500 individual age determinations derived from almost 300 different volcanoes; since then, both Louisville (Koppers et al., 2011a) and Samoa (Koppers et al., 2011b) trails have seen renewed sampling. The picture that emerges from analyzing all the available data seems to be that, to first order, monotonic age progressions are observed at many of the Pacific chains, but for some, there is no clear pattern. Studies of age-progressive volcanism remain hampered by a lack of available samples; the realization that the field of radiochronology has made considerable advances since some of the earliest published dates, and hence, reanalysis is strongly recommended; and the discovery that volcanism at a given site can have an extended period of activity, making it difficult to say with certainty that the observed age is representative for the feature as a whole. In areas where new samples have been obtained and new, more sophisticated techniques have been applied to obtain the most accurate ages, significant discrepancies between the new and old dates are often found (e.g., Koppers et al., 2004). Such reanalysis not only is necessary but also suggests that caution must be used when combining old and new ages in age-progression studies. Some Pacific chains that geometrically seemed similar to the Hawaiian–Emperor bend (HEB) configuration have recently been dated, yielding ages that are difficult to understand in terms of hot spot volcanism (Koppers and Staudigel, 2005). It may be that volcanism caused by decompressional melting that rises up through new or existing cracks in the lithosphere, possibly helped by transient stresses during times of plate motion changes, is making studies of age-progressive volcanism more challenging.

The situation outside the Pacific is similar in the sense that tentative age progressions are often found for long seamount chains, but both the quality and the quantity of samples are much lower (e.g., Baksi, 1999). While new advances in dating technique promise to raise the quality of radiometrically determined ages to a higher level, the fact that reanalysis is a time-consuming and costly endeavor and the acquisition of new samples, in particular for older chains, is a difficult and costly proposition means that progress will come slowly. Consequently, the study of absolute plate motions (APMs) is a field that is in perpetual need of better data. New radiometric age data of high quality and from locations that are underrepresented in the database will, if collected, place the strongest constraints on the hot spot hypothesis.

6.02.3.5 Hot Spot Swells

The hot spot hypothesis states that seamount chains and oceanic islands are the surface expression of impinging mantle plumes. Upwelling mantle plumes are thought to form at either the core–mantle boundary (2900 km depth) or the boundary between the lower mantle and the upper mantle (670 km depth). One theory suggests that a 'plume head' develops, above a 'plume stem' (Bercovici and Kelly, 1997; Campbell and Griffiths, 1990; Coffin and Eldholm, 1993; Richards et al., 1989), but other scenarios of plume development with double plume heads (Bercovici and Mahoney, 1994) and time-varying magma output (Coffin et al., 2002) have also been suggested.

While most of our focus will be on assessing how the observed geometry and age progressions at such chains can be used to infer plate tectonic motions, another consequence of the hot spot hypothesis is the formation of hot spot swells around and downstream from the location of active hot spots (e.g., Crough, 1983; McNutt, 1998). Whereas the seamount chains are confined within a relatively narrow width (typically 100–200 km), the broader effect of the plume on the lithosphere and upper mantle can extend over a width of 1000 km or more. The most spectacular example of a hot spot swell is again coming from the Hawaiian chain where we find the aforementioned seamount chain located on top of a broad swell more that 3000 km long and 1200 km wide (e.g., Davies, 1992; Vidal and Bonneville, 2004; Wessel, 1993), but it should be noted that such thermal swells are present in all the oceans and associated with most of the hot spot chains. Observations suggest that the amplitude and extent of such swells are strongly dependent on the age of the underlying lithosphere; hence, Hawaii (located on seafloor of around 100 Ma) is much more pronounced than, say, the swells in French Polynesia (situated on seafloor of half that age) (Cazenave et al., 1988; Ceuleneer et al., 1988). Pioneering analysis of hot spot swells suggested the shallow bathymetry was a direct consequence of reheating of the lithosphere (Detrick and Crough, 1978), although some pointed out the possible role of compositional buoyancy (e.g., Jordan, 1979; Phipps Morgan et al., 1995), as well as the dynamic uplift (e.g., Olson, 1990). Modeling of the dynamic origin of hot spot swells is nontrivial but considerable progress has been made. The consensus view is that hot spot swells are best explained by the presence of a deep-seated upwelling plume, which explains both the broad swell and the focused volcanism (e.g., Ribe and Christensen, 1999).

6.02.4 Studies of APMs

6.02.4.1 Plume Theory, Seamount Chains, and the Fixed Hot Spot Hypothesis

As mentioned, Wilson (1963) hypothesized that the distinctive linear shape of the Hawaiian Island–Emperor seamount chain resulted from the Pacific Plate moving over a deep, stationary hot spot in the mantle, located beneath the present-day position of the Hawaiian Island. Heat from this hot spot produced a persistent source of magma by partly melting the overriding Pacific Plate. The magma, which is lighter than the surrounding

solid rock, then rises through the mantle and crust to erupt onto the seafloor, forming an active seamount. Over time, countless eruptions cause the seamount to grow until it finally emerges above sea level to form an island volcano. Wilson (1963) suggested that continuing plate movement eventually carries the island beyond the hot spot, cutting it off from the magma source, and volcanism ceases.

As one island volcano becomes extinct, another develops over the hot spot, and the cycle is repeated. This process of volcano growth and death, over many millions of years, has left a long trail of volcanic islands and seamounts across the Pacific Ocean floor. According to Wilson's hot spot hypothesis, the volcanoes of the Hawaiian chain should get progressively older and become more eroded the farther they travel beyond the hot spot. The oldest volcanic rocks on Kauai, the northwesternmost inhabited Hawaiian Island, are about 5.5 Myr old and are deeply eroded (McDougall, 1979). By comparison, on the Hawaiian Island – southeasternmost in the chain and presumably still positioned over the hot spot – the oldest exposed rocks are less than 0.7 Myr old and new volcanic rock is continually being formed. However, it is the monotonic age progression exhibited by dated rock samples dredged from submarine volcanoes all along the Hawaiian–Emperor chain that has convinced scientists of the general validity of the hot spot hypothesis (e.g., Clague and Dalrymple, 1989).

During the past 20 years, our knowledge of the Mesozoic and Cenozoic relative motion between the major tectonic plates has increased substantially even though 'absolute' plate motions relative to a 'fixed' mesosphere are still controversial. Identified marine magnetic anomalies, some as old as 165 Myr, along with seafloor tectonic lineations based on bathymetric and satellite altimetry data accurately define relative plate motions for most of the major plates. Paleomagnetic data and hot spot traces are among the concepts that have been used to attempt to constrain the 'absolute' plate motions. Paleomagnetic data can be used to determine the paleomeridian orientation and the paleolatitude of a plate, which together can be considered the paleopole for a given plate. However, since the Earth's dipole field is radially symmetrical, no paleolongitudinal information can be deduced from paleomagnetic data.

Seamount chains with a linear age progression (i.e., a hot spot track) can be used to restore plates to their paleopositions with the assumption that hot spots are either fixed or nearly fixed relative to each other ('fixed hot spot hypothesis'). Molnar and Stock (1987) showed though that during the Tertiary, the Hawaiian hot spot moved with an average velocity of 10–20 mm per year relative to the Iceland hot spot and to hot spots beneath the African and Indian Plates.

Numerous paleomagnetic datasets and models for the 'absolute' motions of the North American, African, and Eurasian Plates during the Mesozoic and Cenozoic have been published. Unfortunately, there are inconsistencies between different apparent polar wander (APW) paths and hot spot models. Especially for times older than about 45 Ma, large discrepancies are observed between APM models based on hot spot tracks and those based on APW paths from paleomagnetic data.

6.02.4.2 Motion of the African Plate

A widely used APM model based on fixed hot spots was proposed by Müller et al. (1993) who used a refined model for global relative plate motions and a compilation of the bathymetry and radiometric age dates of major hot spot tracks to test the 'fixed hot spot hypothesis.' They combined major hot spot tracks with well-documented age progression from the Atlantic and Indian Oceans and used an interactive technique to derive a 'best-fit' model in a qualitative sense for motions of the major plates in the Atlantic–Indian domain relative to hot spot tracks with a clear age progression.

Even though this model is widely used, it has some well-recognized shortcomings. The late Tertiary portion of this model was not well constrained by radiometric ages, based on the lack of published age dates for the post-30 Ma portion of most hot spot tracks involved at that time. For reconstruction times predating 80 Ma, the only available hot spot tracks with age progression in the Atlantic–Indian Oceans are the New England Seamount chain (linked to the Great Meteor hot spot) and the Walvis Ridge/Rio Grande Rise (linked to the Tristan hot spot) in the Atlantic Ocean. Therefore, the absolute motion of the Indian, Australian, and Antarctic Plates relative to the mantle has to be computed by plate circuit closure for these times. However, when the Müller et al. (1993) model was constructed, pre-80 Ma relative plate motions in the Indian Ocean were poorly known, due to a lack of data in crucial areas, in particular offshore Antarctica in the Enderby Basin and south of the Kerguelen Plateau. Here, a sequence of Mesozoic magnetic anomalies was subsequently mapped and modeled, starting at about 130 Ma (Gaina et al., 2003, 2007). However, the Müller et al. (1993) model was (incorrectly) based on the assumption of post-120 Ma breakup between India and Madagascar. Disagreements between hot spot and published paleomagnetic reference frames have been documented for India (Müller et al., 1994) and for Australia (Idnurm, 1985), suggesting that the mantle underlying the Indian Ocean may not have provided a fixed reference frame. Paleopoles for India from the Rajmahal Traps (Das et al., 1996; Rao and Rao, 1996) result in a paleolatitude of the traps at their time of formation (~117 Ma, Baksi, 1995) at 47° S (±400 km), whereas the Müller et al. (1993) model places them at about 40° S (±400 km).

A comparison of mid-Cretaceous (122–80 Ma) paleolatitudes of North America and Africa from paleomagnetic data with those from hot spot tracks (Van Fossen and Kent, 1992) has provided evidence for an 11–13° discrepancy, providing evidence that Atlantic hot spots were not fixed relative to the Earth's spin axis before 80 Ma, but moved southward as much as 18° (Torsvik et al., 2002) between 100 and 130 Ma. Others argue that this apparent southward movement was caused by true polar wander (TPW) (Prevot et al., 2002).

The Müller et al. (1993) APM model results in a relatively sharp bend of plate motion directions (e.g., of Australia and Antarctica) relative to the mantle at about 80 Ma, which originates from the bend between the New England Seamount chain and the Corner Rise seamounts at roughly 80 Ma in the central North Atlantic. An equivalent bend in fracture zones is not found in either the Atlantic or the Indian Ocean.

6.02.4.3 Motion of the Pacific Plate

The Pacific Plate is by far the largest tectonic plate on Earth, and its APM relative to the underlying mantle is predominantly determined by negative buoyancy forces related to subduction (e.g., Chapple and Tullis, 1977; Conrad and Lithgow-Bertelloni, 2002; Forsyth and Uyeda, 1975; Hager and O'Connell, 1981; Lithgow-Bertelloni and Richards, 1998). To first order, this assessment is well reflected in the north–south alignment of westward-dipping subduction zones along the Pacific Plate's western boundary and the generally westward motion of the plate during the last ~50 Myr. The Pacific Plate's only eastward-dipping subduction zone is found along the short Queen Charlotte margin north of the Juan de Fuca Plate (**Figure 13**); the slab pull exerted at this margin is considered to be relatively minor (Hyndman and Hamilton, 1993). As changes in buoyancy forces are expected to develop slowly (e.g., Hall et al., 2003; Mueller and Phillips, 1991), APM should consequentially be steady and change slowly. However, other forces acting on the plates, such as resistive forces associated with collisions, can develop more rapidly and thus influence plate motions over shorter time spans (e.g., Cloos, 1993; Lithgow-Bertelloni and Richards, 1998). Consequently, various collisions have been given as reason for inferred short-term APM changes (e.g., Knesel et al., 2008; Wessel and Kroenke, 2007).

Because the Pacific Plate is entirely oceanic with no continents on which to establish a paleomagnetically determined plate motion history, APM models for the plate typically have been derived from the geometry and chronology of hot spot chains. The Hawaiian chain is clearly the most studied hot spot chain and has as its most characteristic feature the prominent bend near longitude 172° E, here called the HEB. It was also noted that the Louisville chain in the far South Pacific also had a bend, albeit much gentler and consistent with an ~25° local change in Pacific APM (Lonsdale, 1988). Since Wilson (1963) first suggested it, the HEB has been explained by a dramatic ~60° change in direction of Pacific Plate motion over a stationary hot spot in the mantle (Morgan, 1971). Consequently, the geometries of the Hawaiian–Emperor chain and other coeval chains (**Figure 15**) have been used to model the Pacific APM (e.g., Duncan and Clague, 1985; Koppers et al., 2001; Wessel and Kroenke, 2008; Wessel et al., 2006; Yan and Kroenke, 1993). All these APM models assumed hot spots with negligible motion.

The analysis of rock samples obtained from drilling the Emperor seamounts has revealed a frozen-in paleomagnetic field best explained if the seamounts were formed significantly further north (5–10°) of the present-day location of Hawaii (Kono, 1980; Tarduno and Cottrell, 1997). Efforts to project the APM of Africa, via the global plate circuit, into the Pacific failed to reproduce the shape of the HEB (Cande et al., 1995; Raymond et al., 2000). These inconsistencies lead to alternative models where the plume sustaining the volcanism was no longer stationary (Steinberger, 2000; Steinberger and O'Connell, 1998). Such models can potentially fit both the changing latitude of the hot spot (as suggested by paleomagnetics) and the geometry and age progression of the seamount chain. Some researchers concluded that no change in Pacific APM had taken place at all: Since the trail records the vector sum of plate and plume motion, it could be reconstructed by a rapid slowdown in the southward motion of the plume, while Pacific Plate motion remained unchanged in direction and magnitude (Tarduno et al., 2003, 2009).

To reconcile African and Pacific Plate APM models requires their propagation via the global plate circuit (Acton and Gordon, 1994). Because the history of all RPM changes between conjugate plate pairs is not known, the projection of the African APM into the Pacific is subject to uncertainties that cannot easily be quantified. For instance, by choosing a different plate circuit for connecting the Pacific to Australia via the Lord Howe Rise, Steinberger et al. (2004) showed that the HEB did seem to require a plate motion component and thus could not be caused by plume drift alone. However, Matthews et al. (2012) pointed out that subduction took place east of Australia during this time period, making such a direct circuit between Pacific and Australia tenuous. Preliminary paleolatitude information from the Louisville chain (Koppers et al., 2012) implies much less southward hot spot motion than determined for Hawaii from the Emperor seamounts, suggesting that the coeval Louisville bend is predominantly caused by a change in plate motion. The great-circle distances between same-age samples in the Hawaiian–Emperor and Louisville chains (Wessel and Kroenke, 2009) provide independent estimates of the separation of these two hot spots through time. Changes in this separation appear insignificant back to 55 Ma, but for the critical time period 80–55 Ma, this separation decreased by as much as 3–5° (**Figure 18**). Recently, Doubrovine et al. (2012) presented evidence for two equal and antipodal TPW episodes affecting the 90–60 and 60–40 Ma intervals, complicating matters further. Combined, this information suggests that the HEB is most likely a combination of change in plate motion, plume motion, and perhaps TPW, with individual contributions still to be properly determined.

6.02.4.4 Quantitative Methods for Reconstructing APMs

In considering seamounts and island chains as markers of past plate motion over stationary hot spots, Morgan (1971, 1972) realized that such trails should form sets of copolar small circles on the Earth surface as a consequence of Euler's theorem for plate motions on a sphere. Much early works were concerned with determining stage rotations that would describe the consecutive sets of small-circle motions. Traditionally, segments from different seamount chains thought to represent the same-age interval would be used to determine a single Euler's rotation pole by solving for a best-fit rotation pole (**Figure 19**). The opening angle would be assessed separately by trial and error since the lack of complete age coverage makes it difficult to determine the beginning and end of each segment uniquely. Given the age range of a particular set of copolar segments, opening 'rates' can be determined. This method is best suited to determine first-order trends in APM, but as more details are sought, the difficulty with identifying increasingly shorter small-circle segments and correlating these across several seamount chains becomes insurmountable. Nevertheless, because the data portray small circles, it was natural to define the model in terms of stage rotations and not total reconstruction rotations.

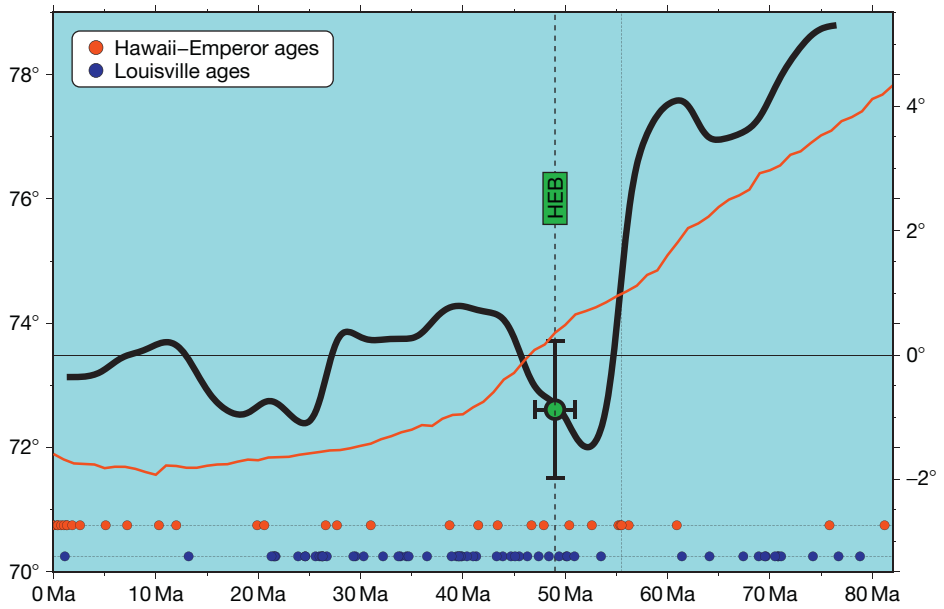

Figure 18 Variations in hot spot separation. Dated locations along the Hawaiian–Emperor and Louisville chains are used to infer the distance between these two hot spots as a function of time (heavy line). Circles show sample distribution, while green circle represents the $72.6 \pm 1.1^\circ$ separation between HEB and the Louisville bend (Wessel et al., 2006). At ~55 Ma, separation drops ~4° and remains stable until present day. Red line shows separation between moving hot spots in the Doubrovine et al. (2012) model.

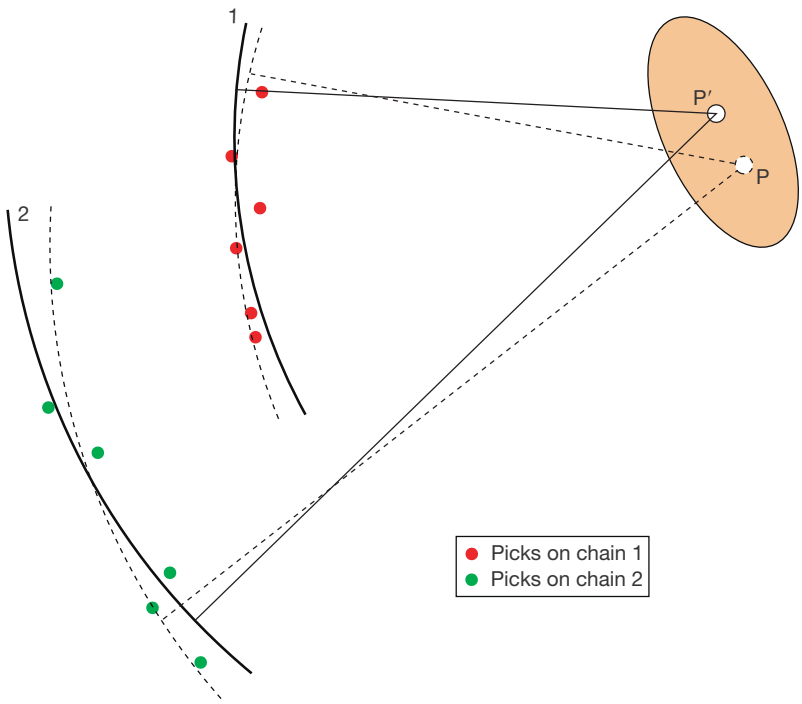

Figure 19 Traditional modeling of APM using stage rotations. Seamounts (red and green circles) are considered points that must approximately lie along small circles (heavy lines). Given a trial pole location (P′), a revised pole location P is found such that the misfit between seamounts and the local best-fitting small circle for each chain is minimized.

Although useful as an exploratory technique, the traditional APM modeling approach has many limitations: (1) short segments, possibly reflecting APM changes, are difficult to identify and correlate across several chains; (2) short small-circle segments become indistinguishable from great circles, and hence, angular distances to poles cannot be accurately determined; (3) without easily identifiable kinks that can be correlated between chain segments, ages are needed to define segments and make the correlation, and these are often lacking; (4) unlike RPM modeling, no rigorous approach for estimating APM uncertainties exists; (5) the method breaks down if hot spots are moving during a stage interval; and, finally, (6) no consistency check for hot spot locations is provided.

6.02.4.4.1 The hot-spotting technique

The last shortcoming was addressed by Wessel and Kroenke (1997) who discovered a simple geometric principle that allows researchers to assess the self-consistency of an APM model. Dubbed 'hot-spotting,' the technique accepts the APM model as correct and constructs seafloor flow lines backward in time from each location on the plate that has a seamount. Since seamounts are not singular points but rather have a finite size, Wessel and Kroenke (1997) convolved each seamount's shape with the corresponding flow line, resulting in a grid of values they called the cumulative volcano amplitude (CVA). The maximum CVA value is proportional to the amount of material produced by the hot spot. Because these flow lines illustrate the path of the seafloor over the mantle (and hence the hot spots, here assumed stationary), it follows that such flow lines must necessarily intersect at the locations of these hot spots (Figure 20). This is evidently true from geometric principles, but the application of the technique rests of several assumptions that must hold true for the result to be valid: (1) the hot spots must be fixed or moving very slowly, (2) the plate motion model must be approximately correct, (3) plates must be rigid over the time span represented by the hot spot volcanism, and (4) the seamounts considered must all have been produced over the hot spots in question. Departure from one or more of these assumptions will be highlighted by the hot-spotting calculations, such as mismatch between optimal and assumed hot spot locations; for a review of issues, see Wessel and Kroenke (1998a,b).

The hot-spotting technique has been identified with a particular plate motion model (called WK97) that was derived in the same article that introduced the geometric concept (Wessel and Kroenke, 1997). WK97 was based on the premise that Hollister Ridge, a site of ongoing eruptions, a site of acoustic noise, and the site of a geoid high, might possibly be the present-day location of the Louisville hot spot. From this assumption, one can derive a controversial plate motion model such as WK97, which added a new, 3 Ma rotation to an earlier APM model (Yan and Kroenke, 1993), which Wessel and Kroenke (2000) later revised to 6 Ma. The proposed 6 Ma change in Pacific APM coincided with numerous other pronounced changes along the plate's boundary (e.g., Krijgsman et al., 1999), including the development of microplates, extensional transform faults, and propagating ridges. While several earlier papers had proposed a late Neogene change in Pacific APM (e.g., Engebretson et al., 1985; Harbert and Cox, 1989; Pollitz, 1986), the WK97 model was much more radical,

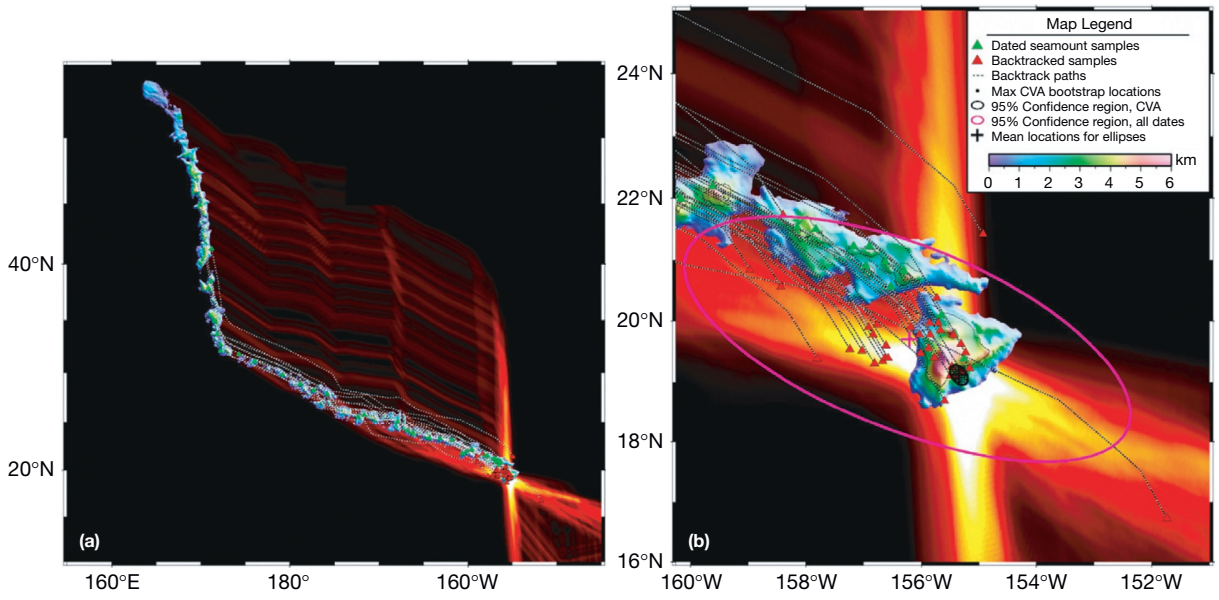

Figure 20 Hot-spotting is a geometric method that checks the self-consistency of an APM model (Wessel and Kroenke, 1997). By generating the flow lines of the seafloor back in time, it follows that seafloor with hot spot-produced seamounts has flow lines that must intersect at the hot spot location, provided hot spots are stationary and the plate is rigid. (a) Hot-spotting applied to all seamounts in the Hawaiian–Emperor chain (colored relief), resulting in a high density of flow line intersections just SE of the Hawaiian Island. Green triangles are dated seamounts, and red triangles are their reconstructed location based on their age. (b) Close-up of the hot spot region. Small black ellipse is the 95% confidence region (using a bootstrap approach) for the optional hot spot location based on the hot-spotting technique for this APM and the geometry of the chain. In contrast, the magenta ellipse is the 95% confidence ellipse for the relocated seamounts.

suggesting a low-latitude rotation pole to mimic the inferred pivoting of the Pacific Plate about the collision zone between the Ontong Java Plateau and the northern margin of the Australian Plate. As very recent changes in APM are subject to large uncertainties and much of the supporting evidence may also be explained in terms of RPM changes, their model remains speculative. Models of current APM are also sensitive to choice of seamount chains; if the recent change in the geometry of the Hawaiian chain is excluded, one will derive a model with a less pronounced change (e.g., Gripp and Gordon, 2002).

Hot-spotting is simply an application of Euler's theorem and is now understood to be related to the Hough transform used in pattern recognition (Wessel, 2008). As such, it takes the rotations of a plate motion model, constructs flow lines for all seamount locations, and lets their crossings reveal an optimal zero-age (hot spot) location. If given the WK97 rotations, it would find that the optimal hot spot location lies on Hollister Ridge since that is what the rotations were designed to do in the first place. Whereas hot-spotting is just a geometric test that can tell how *consistent* a plate motion model is given the data constraints, researchers that disagreed with the premise of WK97 tended to conclude that the hot-spotting technique itself was fundamentally flawed (Aslanian et al., 1998; Wessel and Kroenke, 1998c). A clearer presentation of what in hindsight is a simple procedure would have been preferable.

6.02.4.4.2 PFRM: the polygonal finite rotation method

Harada and Hamano (2000) made many of the other issues hampering traditional modeling irrelevant by introducing a new technique to determine total reconstruction rotations provided hot spot locations are known. Their polygonal finite rotation method (PFRM) was based on a simple geometric concept relating positions along the chains to the location of hot spots at the time the seamounts were formed (**Figure 21**). While their technique can be applied to the general case where hot spots are moving, their discussion and showcase of it were limited to the case of fixed hot spots. In that situation, the present location of N hot spots can be considered the vertices of an N-sided polygon. With hot spots fixed and plates rigid, there is a population of finite rotations that will rotate this polygon so that its vertices will each lie along the N seamount chains. Harada and Hamano (2000) found this population by a Monte Carlo approach, in which they assigned envelopes around the three seamount chains used in their analysis (Hawaiian–Emperor, Louisville, and Easter–Line Islands) and determined rotations by selecting points inside these envelopes and solving for rotations that reconstructed the selected points close to the corresponding hot spots. From this large set of rotations, one can determine representative rotations for a set of different opening angles. Unlike previous techniques, these rotations are purely geometric as no age constraints, other than the zero-age hot spot locations, went into their determination. Observed ages along the N seamount chains were then used to determine a smooth cubic spline function that relates opening angle to actual age. Their resulting APM model fits most chains in the Pacific fairly well, although the subjectively chosen width for the chain envelopes affected the smoothness and fit of the model. Since it was the envelopes and not the distribution of seamounts inside them that were used to derive rotations, the model was necessarily subjective.

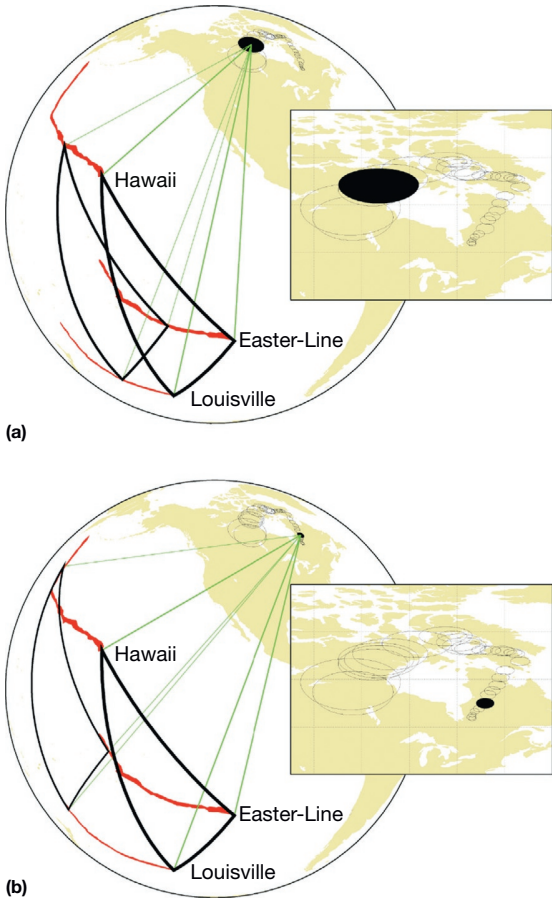

Figure 21 Almost continuous traces of poles for total rotation of the Pacific Plate can be calculated from more than two continuous hot spot tracks. By assuming fixed hot spots and a rigid plate, we know the spherical triangle whose vertices are the present hot spot locations can be recreated for earlier times. Using a Monte Carlo approach, Harada and Hamano (2000) were able to determine the locations of rotation poles for a swath of opening angles such that the shape of the spherical triangle would fit the chain. (a) For smaller opening angles, many rotation poles are found for each opening angle, resulting in larger uncertainties in the pole location. (b) For larger opening angles, the scatter in the locations of the rotation poles is much smaller. Redrawn from Harada and Hamano (2000).

6.02.4.4.3 Moving hot spots

Testing models for motions between individual and groups of hot spots requires mantle convection models, constrained by known plate motions. Steinberger and O'Connell (1997) were the first to develop models of hot spot motion and polar motion based on mantle flow models. Their novel model for the differential motion of individual hot spots is based on mantle density heterogeneities derived from seismic tomography and on known plate motions. Steinberger (2000) extended this type of modeling to a larger number of hot spots and flow models. These models combine large-scale mantle convection with smaller-scale features such as hot spots, whose

present-day locations are constrained by observations. This approach is most reliable in the Tertiary and has provided estimates for TPW, nondipole fields, and the motion of individual hot spots relative to each other for the last 68 Ma.

When these models are extended back to the Cretaceous, however, the advection of mantle density anomalies may result in runaway instabilities and other artifacts. Nevertheless, hot spot motion can still be computed prior to 68 Ma but with an additional uncertainty resulting from changes in mantle density structure and hence unaccounted mantle flow. Test runs for models from 120 Ma to the present, either including or excluding the advection of mantle density anomalies, have shown that there are many similarities between the two types of models. This indicates that meaningful predictions for relative hot spot motion can be made based on a simple mantle convection model constrained by time-dependent plate motions and constant mantle density heterogeneities. This strategy was used by O'Neill et al. (2003, 2005) to model the motion of plumes in a convecting mantle relative to each other, in the context of an 'interactive inversion' strategy. They explored the large parameter space inherent in these models to search for those mantle convection models that provide the best-fit to observed hot spot tracks and their age progression and minimize the disagreements between model-based paleolatitudes and paleolatitudes from paleomagnetic data. O'Neill et al. (2003, 2005) adopted the Hellinger criterion of fit (Hellinger, 1981) for deriving best-fit absolute plate rotations based on track geometries, radiometric ages, and the moving locations of plumes in a convecting mantle to derive covariance matrices for absolute rotations of plates in the Indo-Atlantic domain for the last 120 million years.

6.02.4.4.4 OMS: a modified Hellinger criterion for absolute plate rotations

The method proposed by O'Neill et al. (2005) for finding absolute plate rotations based on hot spot tracks with age progression is similar to that introduced by Hellinger (1981) for relative plate rotations; it is herein referred to as the OMS method. For relative plate rotations, the two datasets, isochrons and fracture zones, essentially describe two orthogonal types of data. Fracture zones are formed by the toroidal motion of two plates relative to one another; they effectively describe the flow lines of one plate relative to the other. Furthermore, they cut across isochrons; that is, many isochrons can be offset by the same amount by one fracture zone. Paleo-mid-ocean ridge segments of isochrons are reconstructed from the remanent magnetic signature of the ocean crust. Providing the reversal sequence has been identified correctly, the main sources of error are locations and the dates assigned by the reversal timescale.

However, there are important differences between data constraining the history of seafloor spreading and hot spot tracks. One problem with hot spot tracks is the relatively sparse temporal coverage of these tracks (e.g., Wessel and Kroenke, 1997). As a result, the focus of hot spot-based reconstructions has been the fitting of hot spot tracks to present inferred positions of these respective hot spots. These tracks essentially represent the flow lines of the plates relative to the position of the hot spots at the time of their formation. One the other hand, the dating of many hot spot tracks has reached a degree whereby the coverage rivals that of the magnetic anomaly sequence for some areas and times. The problem is that the dated tracks are not uniformly sampled; it is impossible to construct isochrons in the literal sense from sampled hot spot tracks. However, the age uncertainties can be considered along-track, based on the additional constraint that the tracks represent the flow lines. Conversely, assuming the profile normal to the hot spot track is made uniformly, we can say that the uncertainty in the position of the hot spot when it created a particular section is related to the geometry of the track cross section.

This provides us with two orthogonal datasets. We can date portions of hot spot tracks u_{ij} (green stars in Figure 22; i is the segment, j the point ($j = 1, \ldots, m_i$), and m_i the number of isochron points on the ith segment; in our case, 2). While the uncertainties for given 'isochrons' between tracks are likely to be extremely large, it is still possible to estimate the section of a track corresponding to a given time. We also have the track geometry itself (yellow stars in Figure 22), which represents the flow lines of plate motion relative to the underlying mantle, represented by the points v_{ik} ($k = 1, \ldots, n_i$, where n_i is the number of track points on segment i). The track sections are constrained in length, so that the track length considered is less than the converted 'length' of the along-track timing uncertainties. The best-fit rotation will be one that minimizes the misfit of these datasets and the present (or calculated) position of the hot spots responsible for them. The isochron segments are composed of data from two tracks, which must be fit to the two associated hot spot positions, while the track geometry dataset is uniquely fit to its associated hot spot. Thus, we have all the ingredients to estimate a rotation for a given time using the Hellinger criterion, which in modified form finds the rotation that minimizes

$$r(A,\eta) = \left[\sum_{i,j=1,2}^{\text{Hot spots}} \left(\frac{h^t_{i,j}\eta_i}{\sigma_{i,j}} \right)^2 + \sum_{i,j=1,2}^{\text{Isochrons}} \left(\frac{u^t_{i,j}A\eta_i}{\sigma_{i,j}} \right)^2 \right] + \left(\sum_{k}^{\text{Hot spots}} \left(\frac{h^t_k\eta_k}{\widetilde{\sigma}_k} \right)^2 + \sum_{k,h}^{\text{Track geometry}} \left(\frac{v^t_{k,h}A\eta_k}{\widetilde{\sigma}_{k,h}} \right)^2 \right)$$

Here, σ and $\widetilde{\sigma}$ are the uncertainties in the points interpolated from dated locations and digitized points along a track section. This assumes the data can be considered to approximate great-circle segments. This is obviously not true over the lifetime of a hot spot track; bends in the track, changes in rates of plate motion, and, most importantly, hot spot motion all introduce discrepancies into the great-circle approximation. However, if hot spots move an order of magnitude more slowly than their overriding plates, the deviations from the great-circle approximation for a given interval introduce errors much smaller than the errors inherent in the data.

6.02.4.4.5 Uncertainty in hot spot reconstructions using the OMS method

Hot spot reconstructions involve finding the best-fitting rotation that reconstructs volcanic chains to the present assumed position (or calculated past position) of the hot spot that formed them, for two or more hot spots. Thus, one can envisage two sources of error in such reconstructions – uncertainties

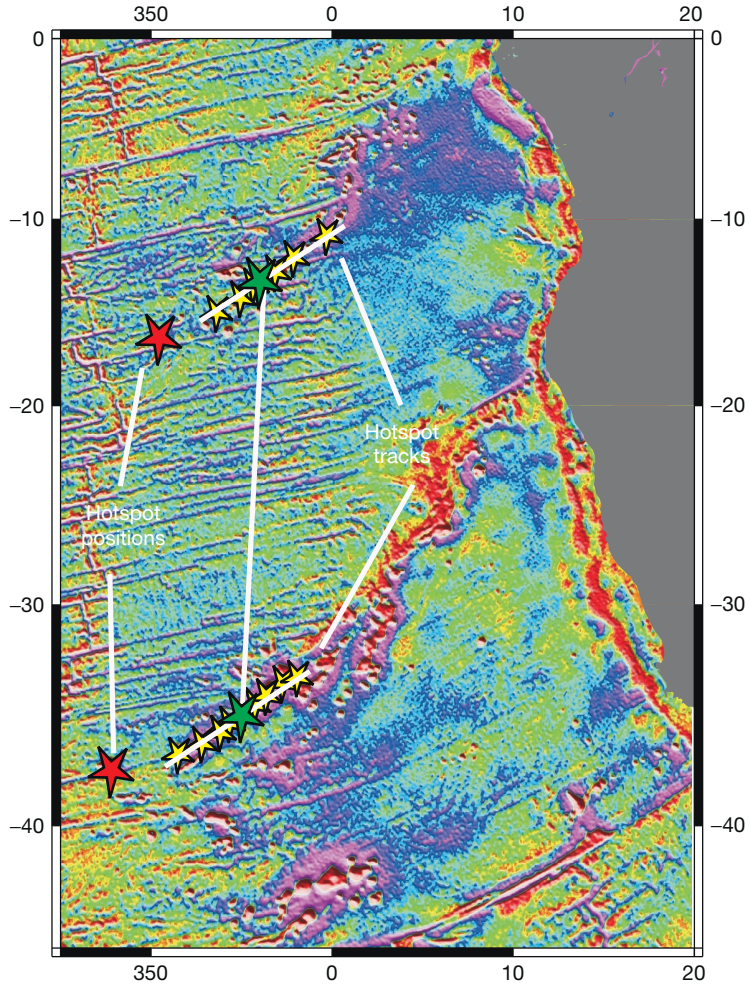

Figure 22 A modified Hellinger criterion of fit for hot spot track reconstructions (O'Neill et al., 2005). Red stars indicate the position of the hot spots, the digitized section of track within the uncertainties of the age we are interested in is shown as yellow stars, and best estimates of the position on the track of the age we want are shown as a green star. The track sections and age positions are considered conjugate datasets (hence, we have three sections here, black lines), and they are both reconstructed to the present position of the hot spot. Modified from O'Neill C, Müller D, and Steinberger B (2005) On the uncertainties in hot spot reconstructions and the significance of moving hot spot reference frames. *Geochemistry, Geophysics, Geosystems* 6: Q04003.

of the reconstructed sections of volcanic chains and uncertainties in the present-day or calculated past positions of the hot spots themselves.

In some cases, current volcanism has been used to infer the present-day position of a hot spot. For example, current volcanism on Réunion island has been inferred to represent the present surface expression of the Réunion plume (e.g., Müller et al., 1993). There are a number of possible departures from this simple plume–volcanism relationship that affect on our ability to constrain the position of mantle plumes. First is that melt produced by a plume may be advected laterally, either by asthenospheric conduits (Morgan, 1978; Müller et al., 1998) to active ridges or by sublithospheric topography (Ebinger and Sleep, 1998). This leads to the conclusion that volcanism can occur far from the actual position of a plume and that plumes can be responsible for volcanism over a wide area.

To give an example, the Walvis Ridge system is widely attributed to a plume located at Tristan da Cunha (Duncan, 1981; Morgan, 1971, 1972). However, present volcanism occurs on both Tristan da Cunha and Gough Islands (O'Connor and Le Roex, 1992), and both systems have left distinct lineations within Walvis Ridge, each with its own distinct age progression (see **Figure 23**). Which island better represents the position of the plume is unclear. Furthermore, O'Connor and le Roex (1992) suggested that the wide, distributed volcanism of the Tristan da Cunha and St. Helena hot spot systems may be due to the fact that the volcanic centers themselves are more spatially extensive, and more diffuse, than commonly assumed. One possible explanation of this is that plumes are larger than commonly assumed. Until recently, we have had no direct estimate of the diameter of plume conduits, only weak constraints based on their buoyancy flux and our inability to image them tomographically. Recently, Montelli et al. (2004) had presented tomographic images of upwelling plumes. Many of these plumes do not have resolvable features extending to the lower mantle. Others, for example,

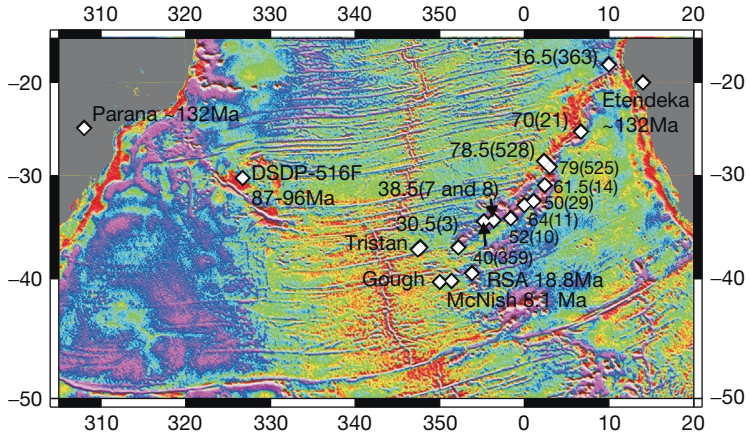

Figure 23 Gravity anomaly map of the South Atlantic, showing the Walvis Ridge and Rio Grande Rise hot spot system. Radiometric age for the ridge system is plotted based on a summary by O'Neill et al. (2003).

Kerguelen–Crozet, appear to have a common source in the lower mantle, suggesting that the initial conduit has split, similar to the suggestion of Coffin et al. (2002). The plume conduits themselves appear to be of the order ~200 km in the upper mantle, suggesting the volcanism we see is only the minor surface expression of fairly large mantle structures.

The uncertainty in the position of a hot spot is even greater for past times. O'Neill et al.'s (2003, 2005) mantle flow calculations and conduit modeling represent one attempt at constraining these past positions; however, the physical uncertainties in the input to these calculations, together with the uncertainties in modeling assumptions, make it difficult to constrain the uncertainties in these modeled positions in a meaningful way.

The uncertainties in reconstructing a volcanic chain can be divided into two groups: those related to the positional uncertainty of a hot spot at the time it created a specific portion of a ridge and those related to the age of that section. To use the Hellinger criterion, we require all the uncertainties in a spatial context, so we translate the age uncertainties into spatial uncertainties by combining them with the estimated angular velocities of the plates (and their uncertainties). Here, we make the assumption that the age uncertainties are larger than the inherent spatial uncertainties. This means that the positional errors need to be constrained by examining profiles across the hot spot chain and assume timing uncertainties, when converted to spatial uncertainties, fall along-track. The combined uncertainties for a given data point thus form an error ellipse centered on that point and elongate along the direction of the volcanic chain.

Figure 24 shows a gravity anomaly profile (Sandwell and Smith, 1997) across the Ninetyeast Ridge. This profile possesses a degree of uncertainty, in that we have inherent positional uncertainties of the satellite recording the data, and whatever geometric distortions are introduced by the gridding of the data. The highest peak of the ridge is assumed to represent the position of the plume at the time it formed this section. To find this, a one-dimensional low-pass filter is applied to the data, and a simple gradient algorithm is used to find the highest peak. For noncontinuous volcanic chains (e.g., seamount chains), this approach requires manual editing. To estimate the uncertainties in this position, we use the half-width of the profile. This is defined by the intersection of the profile with a point halfway between its maximum height and average background value (mean of the lower quartile).

The uncertainties of the ages of hot spot tracks stem first from the inherent uncertainties in radiometric ages. Given the great expense in obtaining oceanic samples, often, the quality of such samples is of small consequence in obtaining an age for them. The uncertainties in radiometric age are minor considering the systematic uncertainties in assigning an age to a particular portion of a volcanic chain.

A serious issue from a statistical point of view is due to the uneven sampling of volcanic chains and our inability to construct 'isochrons' in the standard sense. O'Neill et al. (2005) assumed a linear rate of spreading between dated points on hot spot tracks, to construct points for the times we are interested in. These points inherit uncertainties from the dates of the locations they are constrained from and from the assumption of spreading rate.

Finally, hot spot track age uncertainties must be converted into spatial uncertainties for use with the Hellinger criterion of fit. This involves combining the time error with the plate's angular velocity for that time, generally obtained from previous fixed hot spot reconstructions. This angular velocity has its own inherent uncertainty, and this must also be considered, and so the spatial uncertainty becomes

$$\Delta d = \Delta t \Omega + \Delta t \Delta \Omega$$

The error ellipses, for example, points along the Ninetyeast Ridge, at 10 Myr intervals, are shown in Figure 24. The elongate axis reflects the large time uncertainties of each point, expressed along the trend of the volcanic chain.

6.02.4.4.6 WHK: a hot-spotting–PFRM hybrid method

Wessel et al. (2006) extended the PFRM proposed by Harada and Hamano (2000) in several major ways, resulting in a hybrid method referred to as the WHK method. First, rather than relying on subjectively defined containment envelopes for each chain (since these become unconstrained where there are no significant surface expression of volcanism), they chose

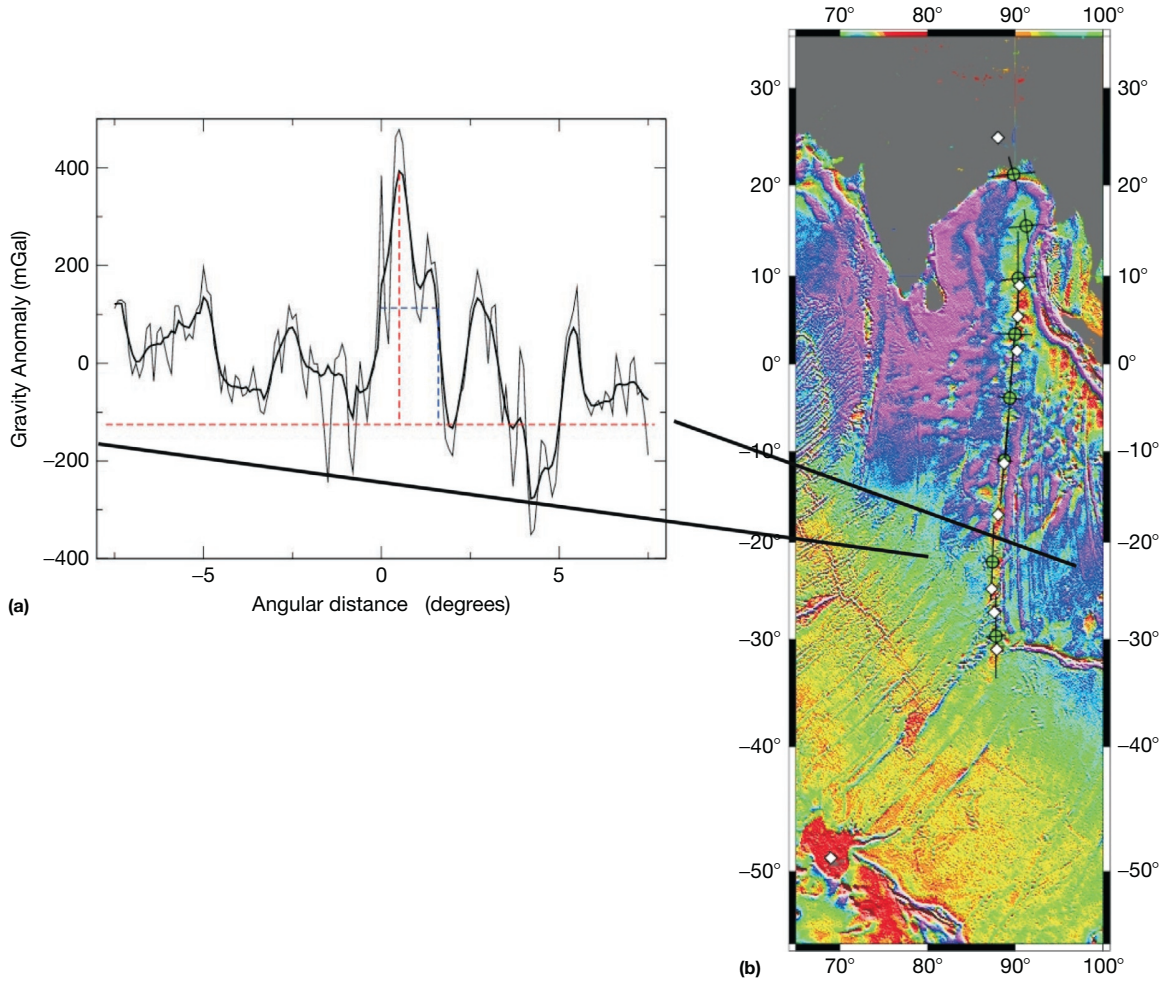

Figure 24 (a) Gravity anomaly cross section of the Ninetyeast Ridge, for the segment shown in (b). The highest point is defined by taking a 1-D filter of the data (thick line) and using a simple neighboring gradient method. The half-width of the profile is defined as the point where the profile crosses the average of the maximum and the average of the lower quartile (assumed base level of the profile). (b) Gravity anomaly map of the Ninetyeast Ridge, showing the profile half-widths as defined in (a) and the along-track errors, which are a combination of radiometric age errors, systematic time errors (see text), and plate velocities, together with their uncertainties, at 10 Myr intervals. The resulting error ellipses are extremely elongate along-track. Modified from O'Neill C, Müller D, and Steinberger B (2005) On the uncertainties in hot spot reconstructions and the significance of moving hot spot reference frames. *Geochemistry, Geophysics, Geosystems* 6: Q04003.

instead to use actual seamount signatures as expressed in high-resolution bathymetry grids to constrain the geometry. Specifically, the 2 min predicted bathymetry of Smith and Sandwell (1997) was high-pass-filtered to remove regional depth variations and isolate the seamount chains. Conservative envelopes were then used to exclude seamounts too far from any hot spot trail, resulting in their starting point for geometric modeling. This approach allows for gaps in coverage along trails. All grid nodes inside a seamount base contour were assigned unique chain identifiers so that overlapping trails could be handled (**Figure 25**). The number of chains that can be fitted for a given opening angle is thus variable. Rather than using a Monte Carlo inversion, they solved for all possible rotations using a grid search. The selected hot spot locations were rotated using the negative rotation so that the projected points would fall somewhere along the respective tails. Rotations that produced reconstructed points on or close to the trail (the cutoff depended on the uncertainty of the hot spot location) for two or more chains were kept; the remaining rotations were discarded. This procedure resulted in thousands of rotations for a wide range of opening angles.

Second, the population of rotations that were consistent with the given chain geometries was examined further in order to exclude rotations that were outliers with respect to the main trend. Because gaps along chains were explicitly treated, up to six chains could be included in the fitting, although the number varies with opening angle. Wessel and Kroenke (2008) extended this work to 12 chains, with a maximum of 6 chains fit simultaneously (**Figure 26**).

Third, they incorporated the hot-spotting principle to refine the locations of the starting points (hot spot locations) for each chain. This, of course, is only possible for long-lived chains reflecting significant changes in plate motion and furthermore is only valid for a situation in which the hot spots have not

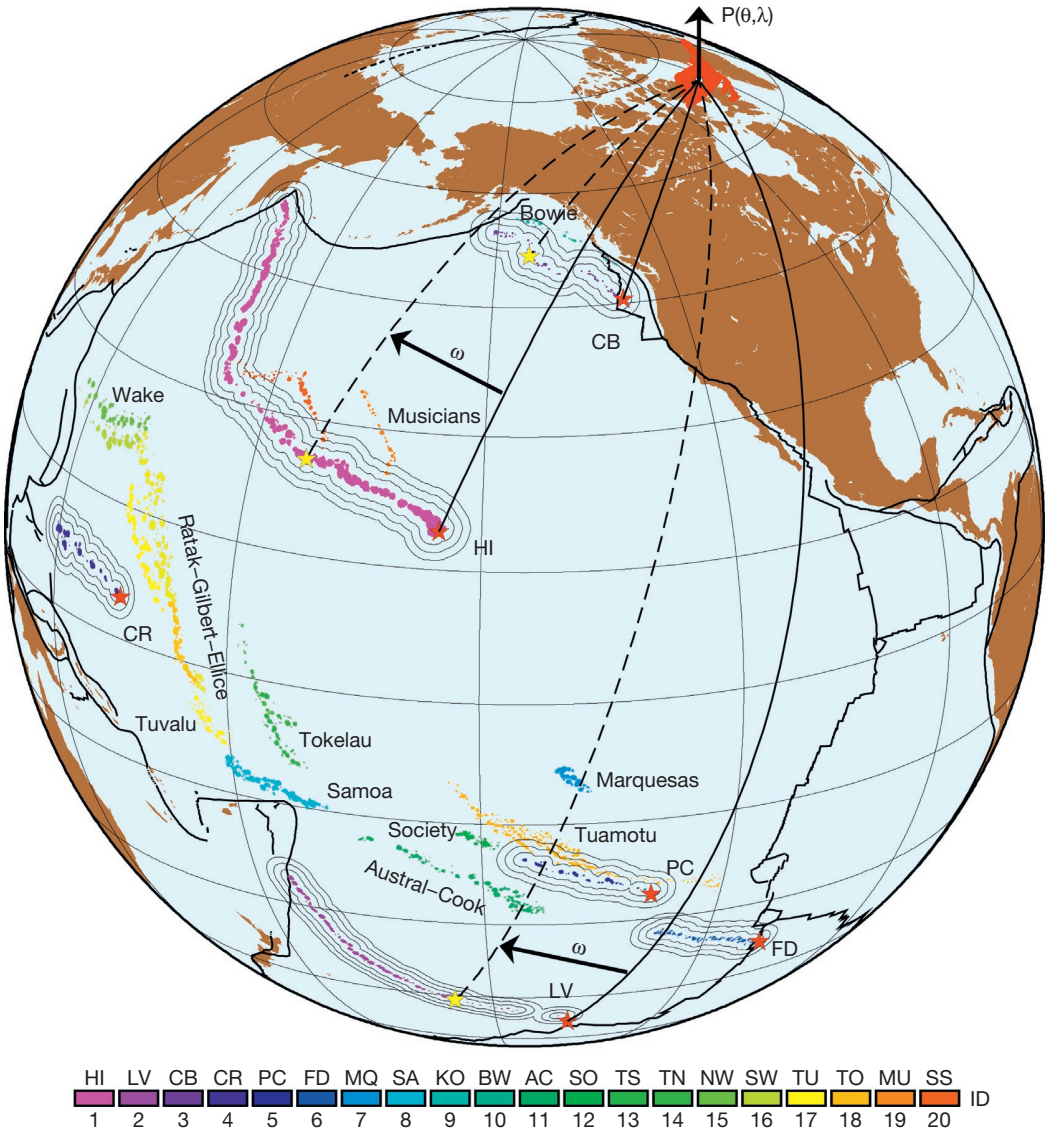

Figure 25 Seamount data constraints generated from the Wessel and Lyons (1997) seamount database. Unique chain ID numbers have been assigned to each seamount (as color-coded). The PFRM works by brute-force grid search of all possible rotations. For each trial rotation, here exemplified by the rotation pole P at (70° N, 66° W) with an opening angle of $\omega = 18°$, the M hot spot locations (red stars: HI, Hawaii; LV, Louisville; FD, Foundation; PC, Pitcairn; CR, Caroline; and CB, Cobb) are reconstructed (yellow stars). If two or more of these reconstructed points fall on or very close to their respective seamount chain, the rotation is included in the further analysis. The cluster of poles near P (red dots) represents all the rotations that passed the test for all opening angles in the $17° \leq \omega \leq 19°$ interval. Additional chains (shown but not used in the modeling) are Marquesas (MQ), Samoa (SA), Kodiak (KO), Bowie (BW), Austral–Cook (AC), Society Islands (SO), southern (TS) and northern (TN) Tokelau, southern (SW) and northern (NW) Wake, Tuvalu (TU), Tuamotu (TO), Musicians (MU), and Liliuokalani (SS). Figure redrawn from Wessel et al. (2006).

moved significantly. In essence, once a smooth geometric model of rotations was obtained, hot-spotting was applied to see if the optimal hot spot locations implied by the CVA maxima corresponded to the initial selection of hot spot locations. If a difference was discovered, the hot spot location would be moved accordingly and a new population of rotations was calculated using the modified hot spot locations. Several iterations were required before the process stabilized.

Finally, they improved the statistical treatment of the rotation population by determining representative average rotations for key isochron ages rather than for predetermined ranges of opening angles (as in Harada and Hamano, 2000). This was achieved by combining all age data (for all chains considered) on a single plot of age versus opening angle and then fitting a linear spline to represent the trend. Given the 95% confidence limits on the spline, they were able to project the age uncertainties into angle uncertainties and thus obtain the desired average rotations (**Figure 27**). Finally, their new technique included the construction of uncertainty covariance matrices for each total reconstruction rotation, allowing the uncertainty in the reconstruction to be quantified and displayed on maps. Their preliminary, high-resolution APM

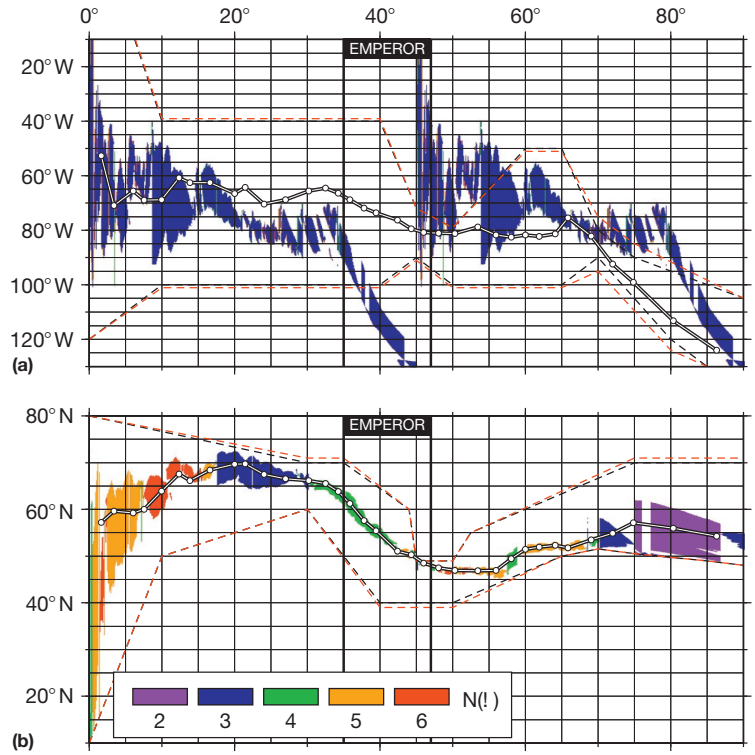

Figure 26 (a) All possible rotation pole coordinates as functions of opening angle (w), color-coded by how many chains were fitted simultaneously (black means rotations were deemed unsuitable on closer inspection). Trial rotations outside the dashed red lines were excluded as they always failed to fit the trails. (a) Longitude of rotation poles. Lines with white dots indicate smoothed model using the initial ~2° window for w. (b) Same for rotation pole latitudes. These estimates form the geometric part of the WK08-A model. Vertical lines delineate the range of angles corresponding to the 60–90 Ma Emperor stage. Figure redrawn from Wessel and Kroenke (2008).

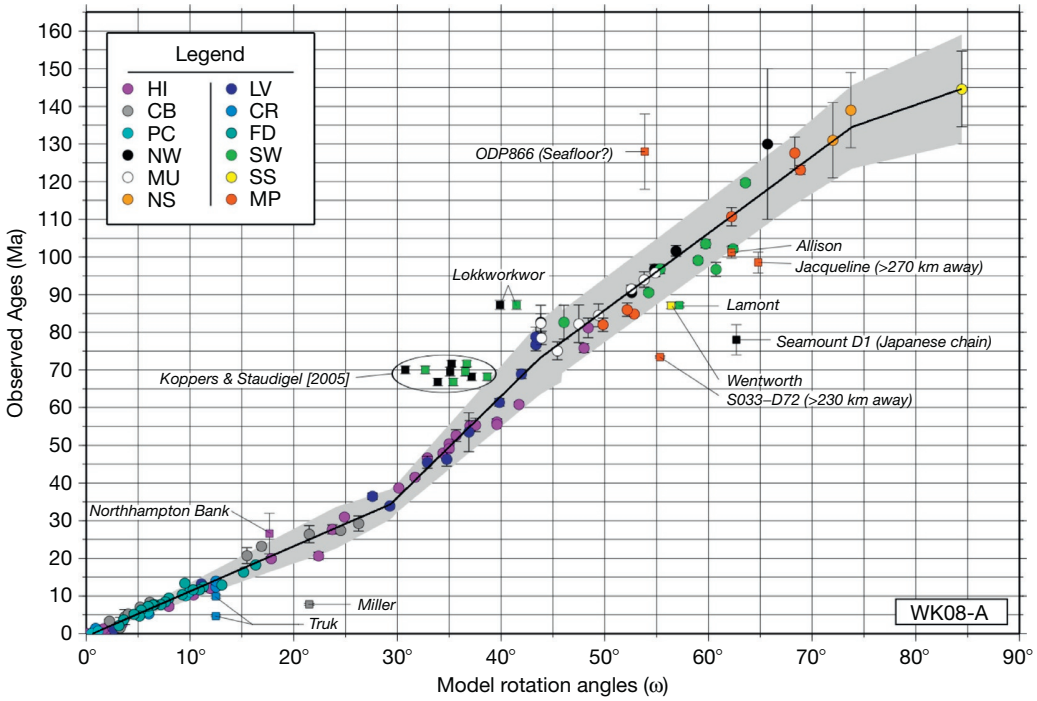

Figure 27 The $t(w)$ plot for the 12 Pacific chains used in the APM modeling with appropriate smoothing that reflects age uncertainties (WK08-A). The linear spline found four significant segments back to 144 Ma. Gray band represents a 95% confidence level for the spline. Given these uncertainties from ages, we project them onto the opening angle (w) axis to yield new w – windows to use for the smoothing of rotations (**Figure 26**). Circles represent samples used in the interpolation, whereas squares are samples rejected for reasons stated in the text. Some individual samples from the overlapping strands in the Ratak–Gilbert–Ellice chains appear twice (i.e., as both NW and SW with same age but different w) as they could belong to either chain. Figure redrawn from Wessel and Kroenke (2008).

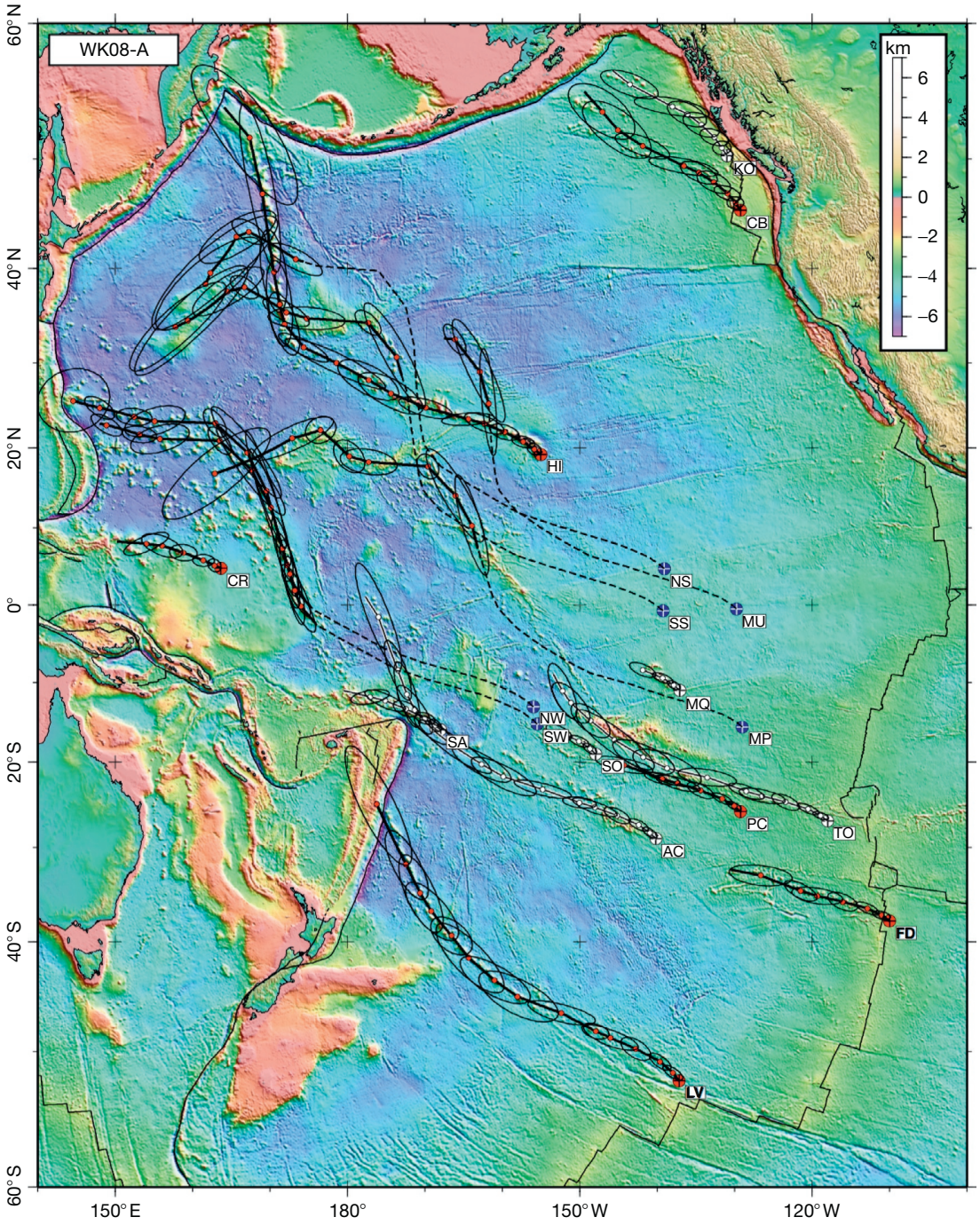

Figure 28 Pacific Plate with predicted tracks and 95% confidence ellipses on reconstructed points (red and white) along each trail for the WK08-A APM model. Solid black lines (and red points) are used for trails that constrained the model, with open lines (and white points) for prediction at other trails. Red (blue) circles indicate the model locations of active (extinct) hot spots; white circles show other hot spots not used in determining the APM. Long dashed lines connect extinct hot spots with assumed seamount chain. See caption of **Figure 25** for chain abbreviations. Figure redrawn from Wessel and Kroenke (2008).

model fits the data well, and its predictions for hot spot chains not used in the solution are satisfactory (Figure 28). Their findings suggest that the uncertainties or variability of radiometric ages makes it difficult to discern whether or not the Hawaiian or other Pacific hot spots have moved significantly with respect to each other based on geometry and age data alone. There is no age or geometry evidence that suggests significant motion of plumes since the formation of the HEB around chrons 21–22 (Sharp and Clague, 2006); this conclusion is corroborated by the paleolatitudes of Hawaiian

seamounts (Sager et al., 2005). However, prior to that time, the fewer seamount chain constraints and larger age scatter may suggest the need for additional model parameters (i.e., hot spot motion); the additional parameters would make it easier to reconcile the paleomagnetic data (Tarduno et al., 2003) and observed changes in the inter-hot spot separations (Wessel and Kroenke, 2009).

6.02.4.4.7 Comparison of the OMS and WHK modeling techniques

Since the OMS (O'Neill et al., 2005) and WHK (Wessel et al., 2006) techniques overlap in scope, we will compare them and discuss some of their similarities and differences. However, as both techniques have been introduced very recently, the approaches taken are somewhat different, and to date, they have been applied to different ocean basins; a direct comparison of model parameters is not yet possible.

Unlike classical APM modeling techniques, both techniques find total reconstruction rotations and provide rigorous covariance matrices that describe the uncertainties in the model rotations. The OMS method derives these from a modified Hellinger criterion, and thus, the parameterization of uncertainties is identical to that used in RPM studies; this is advantageous when combining APM and RPM rotations. The WHK technique, on the other hand, considers a different criterion of fit and hence is likely to yield a slightly different solution than OMS. Another advantage of the OMS method is that it works equally well with both fixed and moving hot spots (provided past hot spot locations are prescribed as functions of time), whereas the WHK method currently requires past hot spot locations as a function of opening angle; iterations will be required to extract a compatible angle–time relationship. The current locations of hot spots are input parameters for both methods. However, for fixed hot spots, the WHK method will adjust these locations for an optional fit using the hot-spotting test; this is not done in OMS. The OMS method needs to linearly interpolate between dated samples to determine points along the chain for the times of interest. The large uncertainties in ages therefore propagate directly into the locations chosen to determine the rotation. The WHK method does not need to use ages to determine points to be used in determining rotations; it first uses all points to determine an accurate motion path and only secondly analyzes the stacked ages to determine the history. The OMS technique must also make the approximation that the data can be considered great-circle segments; however, this is only likely to introduce minor errors. Finally, while the WHK method produces a smooth APM model by virtue of averaging thousands of rotations, the OMS technique has no mechanism for smoothing and consequently can generate a nonsmooth age progression along the hot spot track. Further development to address the shortcomings is likely to improve both techniques.

6.02.4.5 Global Ocean Basin Reconstructions

Because numerous plate pairs share divergent plate boundaries, it is possible to link plates not directly connected via intermediate plates that do share such boundaries, thus forming a plate circuit or plate chain (Cox and Hart, 1986). These relationships allow relative plate motions determined for one ocean to be propagated into other ocean basins. While limited versions of global models using plate circuits have been assembled since the beginning of plate tectonics (e.g., Le Pichon, 1968), more recent efforts have culminated in global models such as those presented by Torsvik et al. (2008) and Seton et al. (2012). In particular, Seton et al. (2012) constructed a new type of global plate motion model consisting of a set of continuously closing topological plate polygons with associated plate boundaries and plate velocities since the breakup of the supercontinent Pangaea. The uncertainties of reconstructing mid-ocean ridges and flanks in the Jurassic (~200–145 Ma) are substantial and arguably hard to quantify given that we depend on information preserved in the present-day ocean crust. However, even though the details of those mid-ocean ridge geometries are unknown, we can make reasonable estimates applying the principle of Occam's razor paired with the rules of plate tectonics as a guide to available geophysical and geologic data constraining mid-ocean ridge geometries through time.

Preserved magnetic lineations in the Pacific Ocean provide unequivocal evidence that a vast mid-ocean ridge system existed in the Pacific Ocean in the mid-Cretaceous/late Cretaceous, significantly longer than today's ridge system, and much of which is now subducted – this was first recognized by Larson and Chase (1972). Subsequent detailed mapping and compilation of magnetic M-sequence anomalies in the northwestern Pacific Ocean (Nakanishi et al., 1992) revealed the complete Mesozoic magnetic anomaly lineation pattern in this area. Nakanishi et al. (1992) wrote that "Reconstruction of the Late Jurassic lineations (e.g., in the East Mariana, Nauru and Central Pacific basins) reveals an exact shape of the Pacific plate in that period" – implying that the mid-ocean ridge system bounding the Pacific Plate can be reconstructed all the way back to the Jurassic. Their work also revealed the origin of the Pacific Plate as a triangularly shaped microplate at a triple junction in the Panthalassa Ocean basin, the predecessor of the Pacific Ocean. This forms the basis of Seton et al.'s (2012) Pacific Ocean reconstructions (**Figure 29**).

The longest now vanished mid-ocean ridge that once formed part of this ridge system is the Izanagi–Pacific ridge. Nakanishi et al. (1992) emphasized that the complete pattern of magnetic lineations preserved on the Pacific Plate reveals the configuration of the Pacific–Izanagi–Farallon triple junction, as the magnetic bight between the Japanese and the Hawaiian lineation sets is clearly identified. There are uncertainties associated with reconstructing the exact history of ridge subduction, asymmetries of spreading where we only have information on one plate preserved, and several other aspects of the exact mid-ocean ridge configuration in the Pacific Ocean in the Mesozoic. Seton et al. (2012) assumed that the triple junction between the Izanagi, Farallon, and Phoenix Plates that is known to have existed in the Late Jurassic based on magnetic lineations preserved in the West Pacific Ocean (Nakanishi et al., 1992), existed in similar form since the Early Jurassic at 200 Ma paired with an assumption of constant spreading rates between the Izanagi, Phoenix, and Farallon Plates between 200 and 170 Ma, corresponding to the time interval for which no magnetic lineations are preserved.

Seton et al.'s (2012) model includes recently proposed models for the opening of ocean basins between fragments of the Ontong Java–Manihiki–Hikurangi large igneous provinces

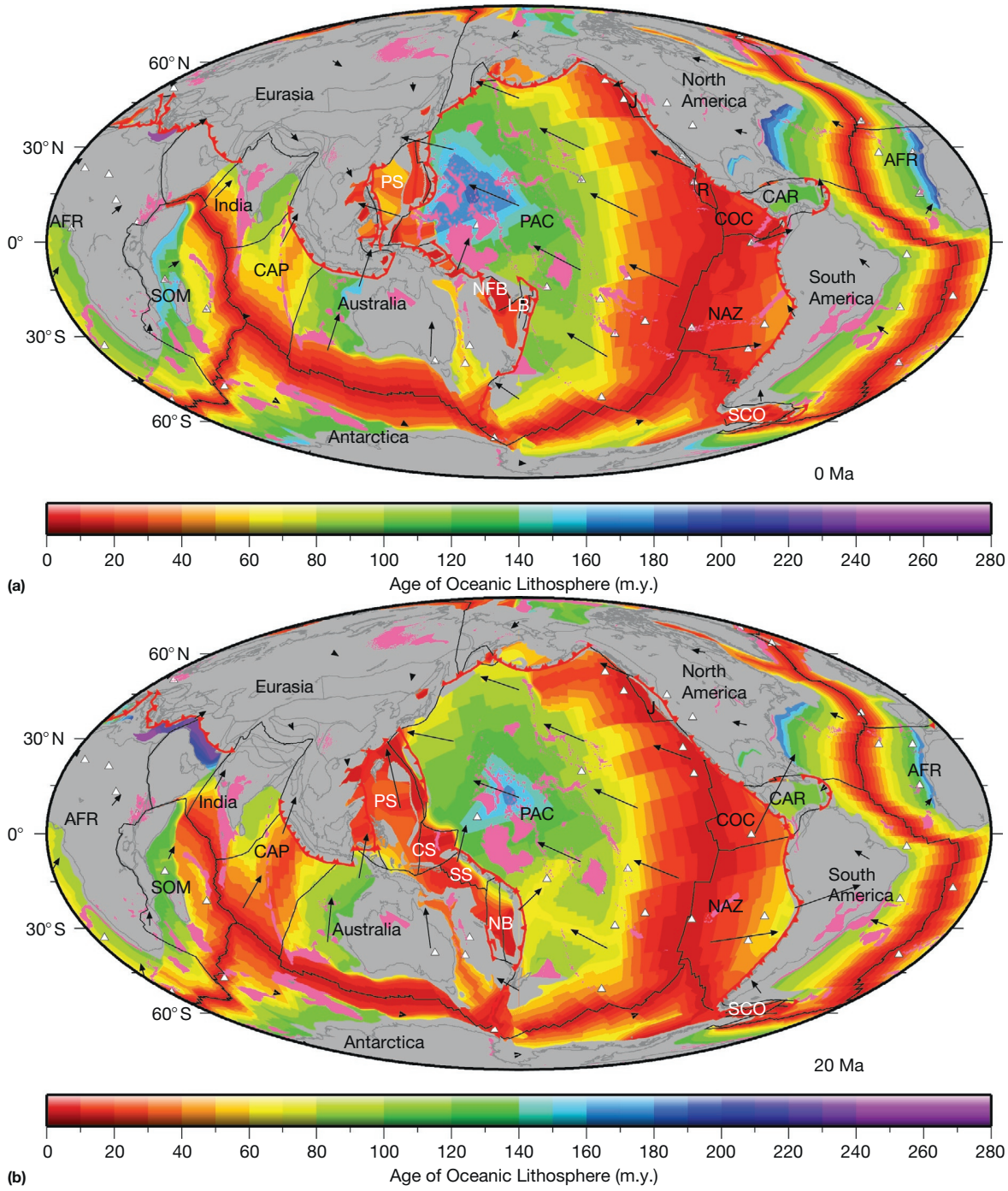

Figure 29 (Continued)

(Chandler et al., 2012; Taylor, 2006; Viso et al., 2005). In the Tethys, they follow the model by Stampfli and Borel (2002) and Golonka (2007), in which the Paleo-Tethys Ocean is closed in the Late Triassic/Early Jurassic, associated with the stepwise collision of a series of Gondwanaland ribbon continents with Eurasia. By using combined evidence from preserved magnetic lineations, and geologic data from accreted terranes such as 'Argo Land' and the rules of plate tectonics (Cox and Hart, 1986), it is possible to constrain the overall geometries of Tethys mid-ocean ridges quite well, as demonstrated by Heine et al. (2004). The closure of the Mongol–Okhotsk Ocean between 200 and 150 Ma is modeled after van der Voo et al. (1999). In their model, the breakup of the supercontinent Pangaea occurs in the central North Atlantic around 200 Ma (Labails et al., 2010) followed by the formation of the Pacific Plate about 190 Ma (Seton et al., 2012).

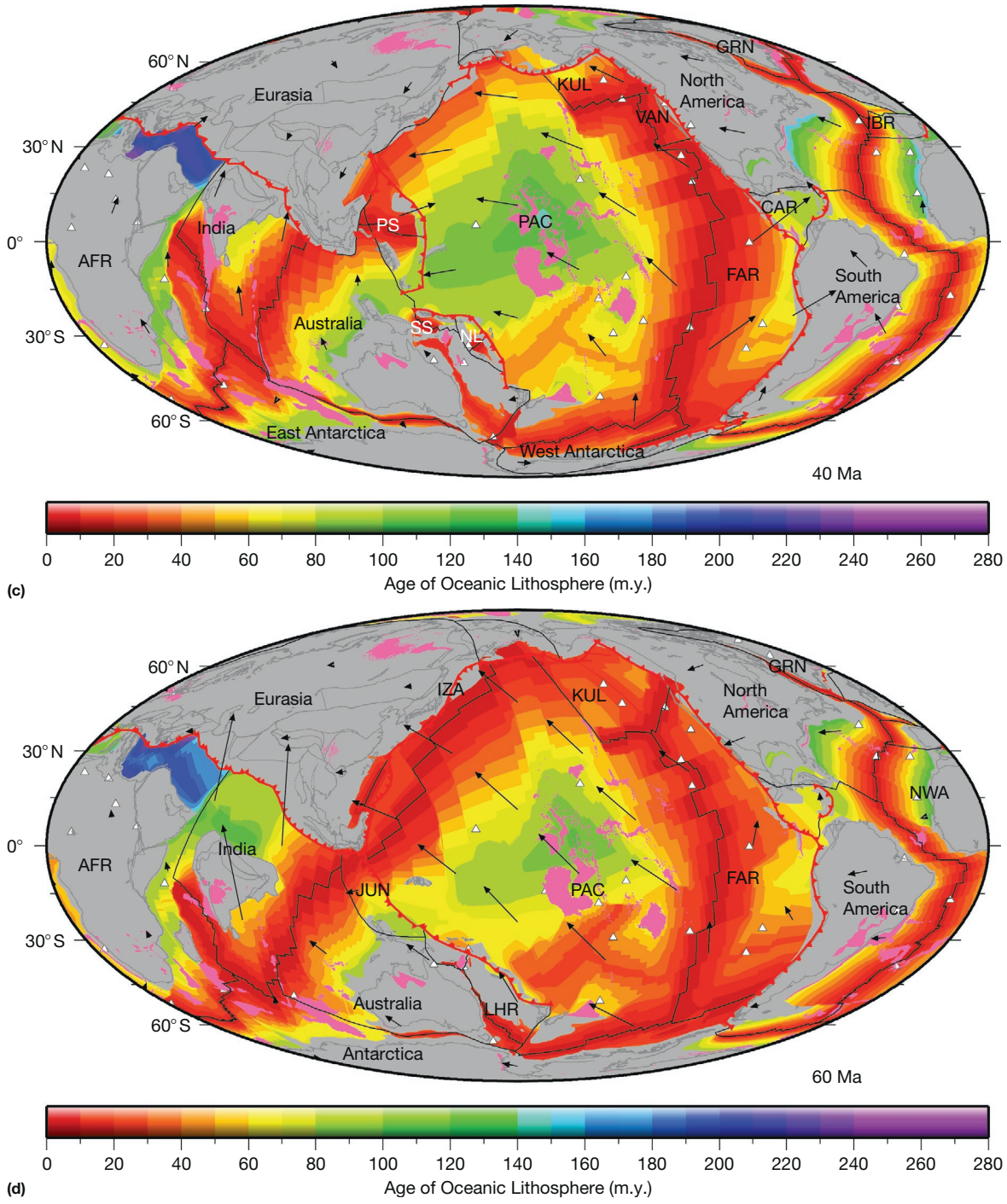

Figure 29 (Continued)

6.02.4.6 APM Models, Paleomagnetics, and TPW

APM models have traditionally been determined for a single plate (e.g., Pacific) or a set of plates connected by ridges (e.g., Africa and neighbor plates in the Indo-Atlantic). It is therefore of interest to propagate these predictions into other oceans using the plate circuits mentioned earlier so that APM models may be compared. As mentioned earlier, Molnar and Stock (1987) first showed that the hot spots in the Pacific appear to have moved relative to the set of hot spots used to determine Indo-Atlantic APM; however, Andrews et al. (2006) found that this relative motion is only significant prior to 68 Ma. There are two important issues that make these comparisons challenging. First, a key

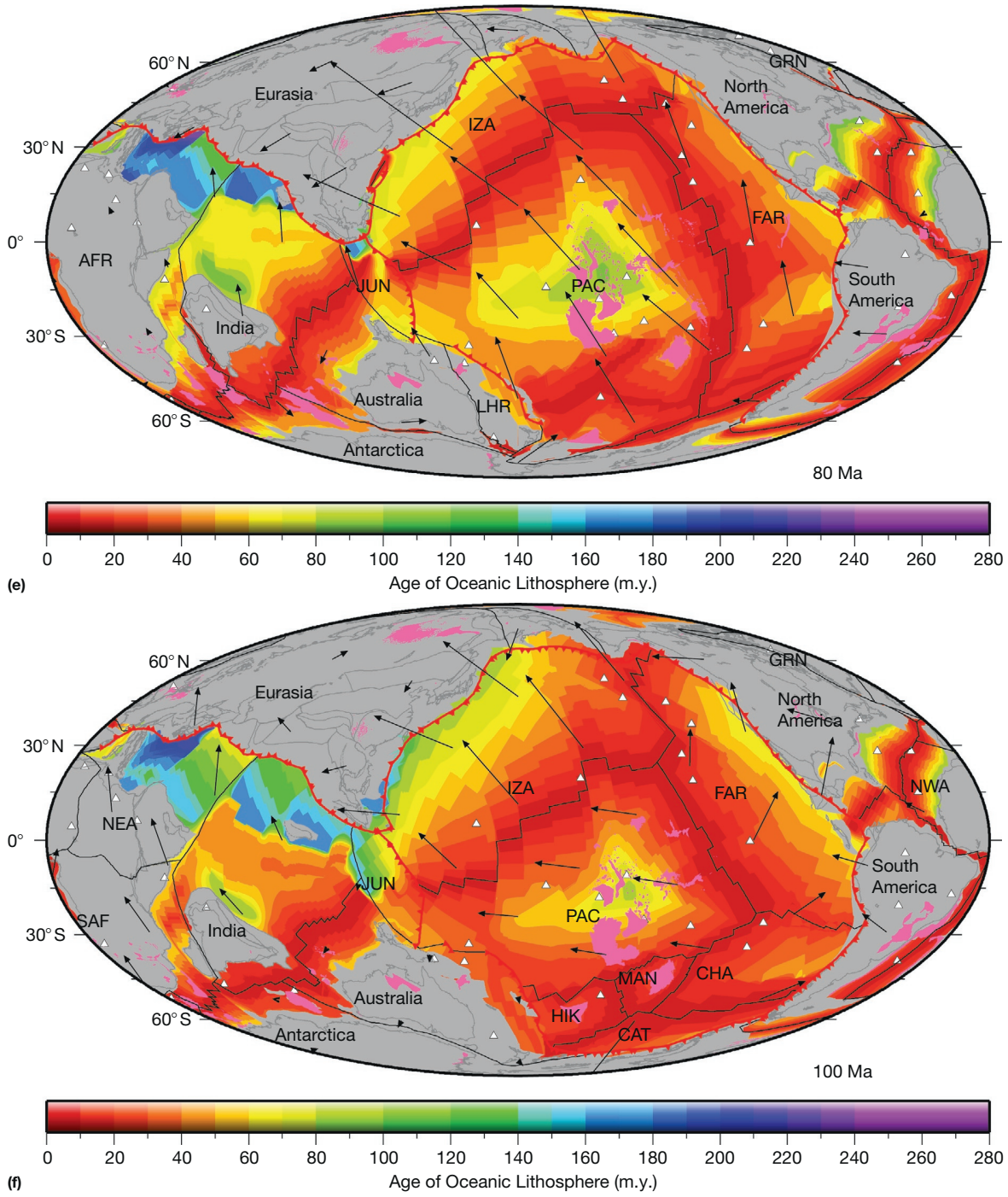

Figure 29 (Continued)

problem area in designing global plate circuits is the connection via West Antarctica. Because the boundary is located in the Ross Sea, the motion between East Antarctica and West Antarctica remains difficult to determine with precision. Seafloor spreading in the Adare Trough was first identified by Cande et al. (2000), but data remain sparse and relatively small changes in the RPM estimates propagate to give relative large changes elsewhere. In particular, continental deformation within the Transantarctic Mountains is difficult to reconstruct accurately, contributing to the total uncertainty. Second, relatively few hot spot chains have adequate (or any at all) sampling for paleomagnetic analysis, making the models incomplete.

A benchmark test for all global APM modeling has been how well an Africa-based APM, after projection via the plate

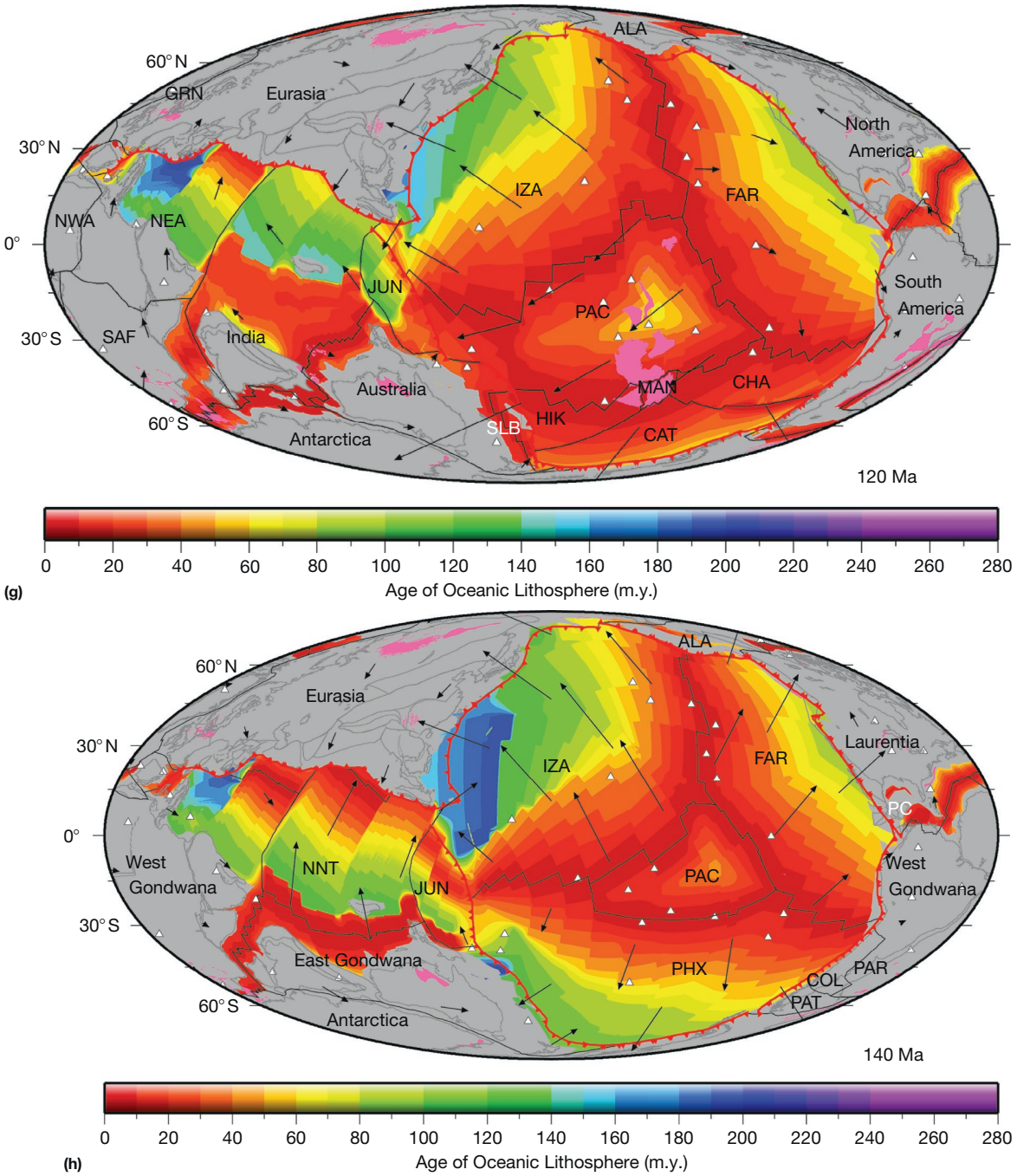

Figure 29 (Continued)

circuit, is able to reconstruct the trend of the Hawaiian–Emperor hot spot trail in the Pacific. Early efforts (Cande et al., 1995; Raymond et al., 2000) showed significant mismatch for reconstructions older than ~40 Ma and were unable to account for the geometry of the HEB. One approach to address this failure was to consider the effect of moving hot spots (Steinberger, 2000). The latitudinal component of such motions can be constrained by paleolatitudes, at least in the case of the Hawaiian plume (Tarduno et al., 2003). It is expected that recently published data from the Louisville chain (Koppers et al., 2012) will be used to constrain its hot spot motion as well. Steinberger et al. (2004) found that by using a moving hot spot APM model for Africa, the predictions in the Pacific depended on which plate circuit was used for the reconstruction. Using the East–West Antarctica circuit employed by Cande et al. (1995) again failed to match the

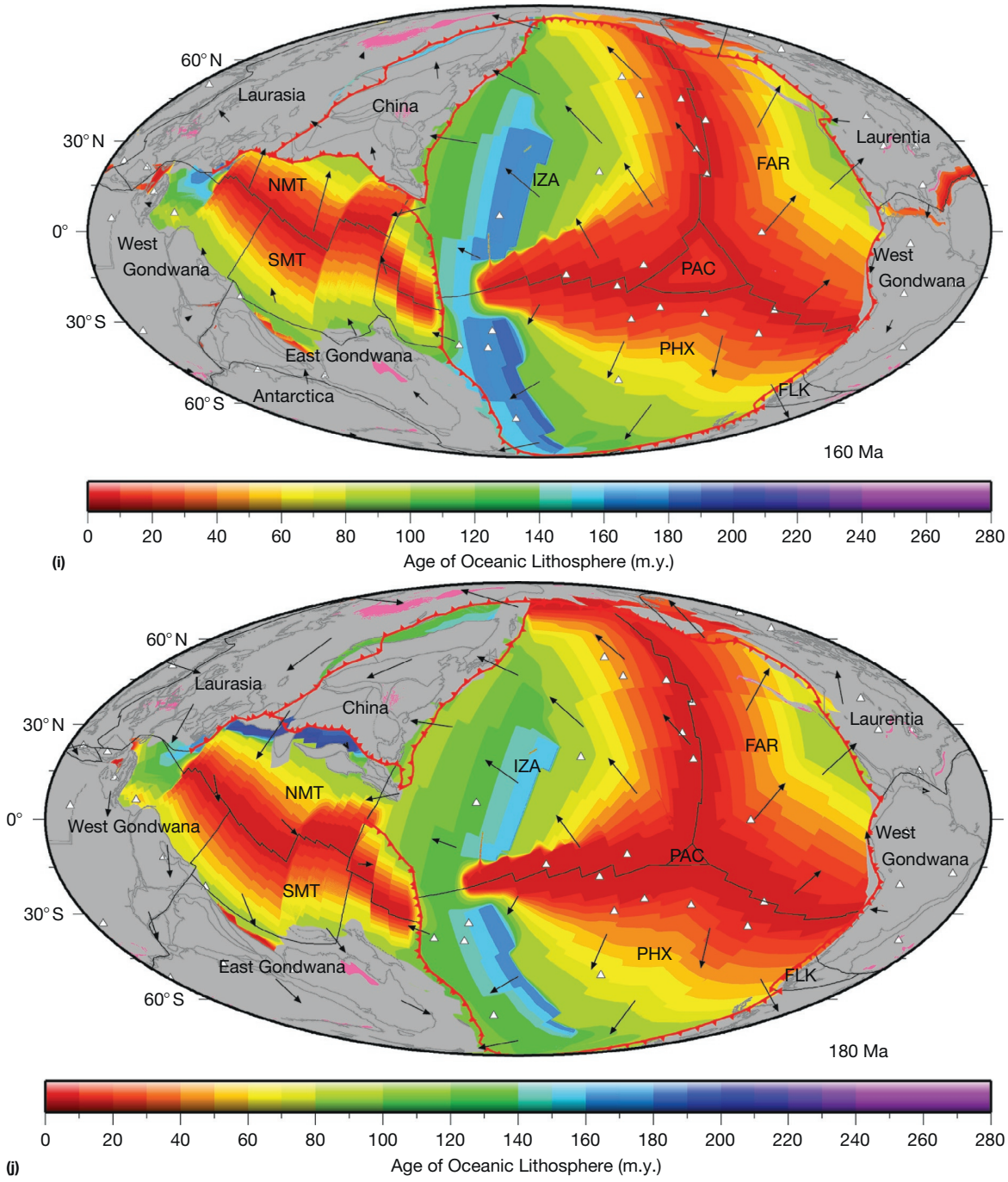

Figure 29 (Continued)

HEB geometry, but if a new circuit that connected Australia to the Pacific via Lord Howe Rise was used (thus bypassing West Antarctica entirely), the fit improved somewhat. This improvement led Doubrovine et al. (2012) to extend the approach of O'Neill et al. (2005) and determine a global APM that satisfied the geometry, age progression, and paleolatitude of five hot spot chains (Hawaii and Louisville on the Pacific Plate, Réunion and Tristan da Cunha on the African Plate, and the New England chain on the North American Plate). Their model championed the Lord Howe Rise circuit and represents a truly global moving hot spot APM model, despite some shortcomings in fitting the five individual hot spot trails. The Lord Howe Rise plate circuit is based on the assumption that there was no subduction east of the Lord

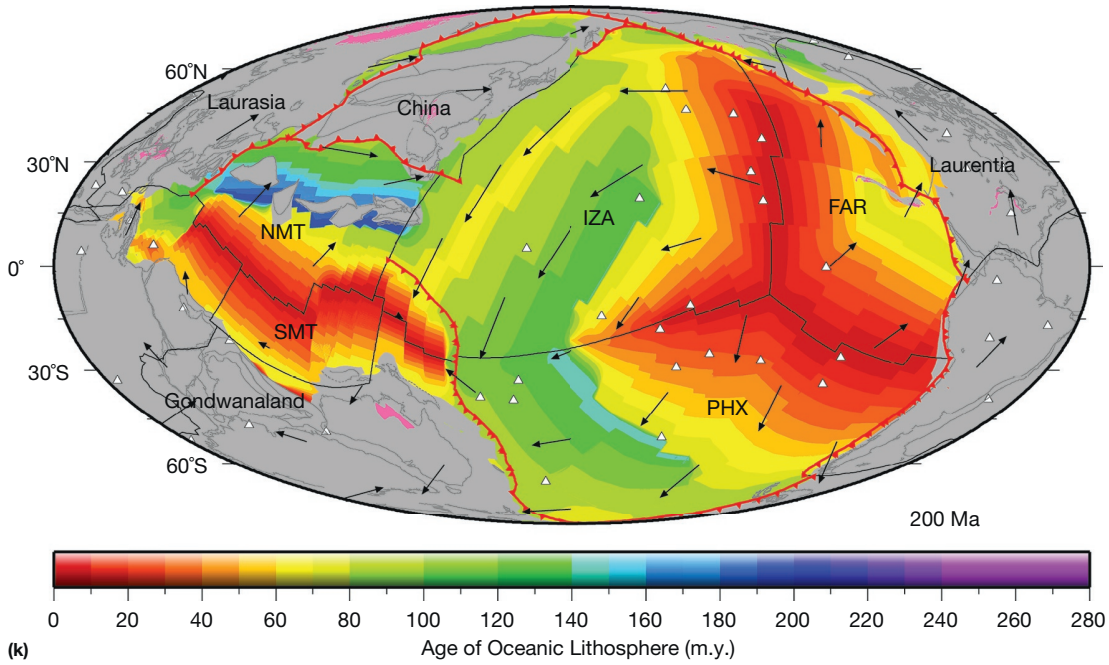

Figure 29 (a) Global plate reconstruction at selected periods. Base map shows the age–area distribution of oceanic lithosphere at the time of formation. Red lines denote subduction zones; black lines denote mid-ocean ridges and transform faults. Pink polygons indicate products of plume-related excessive volcanism, and white triangles are the present-day hot spot locations. Absolute plate velocity vectors are denoted as black arrows. (a) 200 Ma reconstruction: FAR, Farallon; IZA, Izanagi; NMT, North Meso-Tethys; PHX, Phoenix; SMT, South Meso-Tethys. (b) 180 Ma reconstruction: FAR, Farallon; FLK, Falkland; IZA, Izanagi; NMT, North Meso-Tethys; PAC, Pacific; PHX, Phoenix; SMT, South Meso-Tethys. (c) 160 Ma reconstruction: FAR, Farallon; FLK, Falkland; IZA, Izanagi; NMT, North Meso-Tethys; PAC, Pacific; PHX, Phoenix; SMT, South Meso-Tethys. (d) 140 Ma reconstruction: ALA, Alaska; COL, Colorado; FAR, Farallon; FLK, Falkland; IZA, Izanagi; JUN, Junction; NNT, North Neo-Tethys; PAC, Pacific; PAT, Patagonia; PAR, Parana; PHX, Phoenix. (e) 120 Ma reconstruction: ALA, Alaska; CAT, Catequil; CHA, Chasca; FAR, Farallon; GRN, Greenland; HIK, Hikurangi; IZA, Izanagi; JUN, Junction; MAN, Manihiki; NEA, Northeast Africa; NMT, North Meso-Tethys; NWA, Northwest Africa; PAC, Pacific; PHX, Phoenix; SAF, South Africa; SLB, South Loyalty; SMT, South Meso-Tethys. (f) 100 Ma reconstruction: ALA, Alaska; CAT, Catequil; CHA, Chasca; FAR, Farallon; GRN, Greenland; HIK, Hikurangi; IZA, Izanagi; JUN, Junction; MAN, Manihiki; NEA, Northeast Africa; NMT, North Meso-Tethys; NWA, Northwest Africa; PAC, Pacific; PHX, Phoenix; SAF, South Africa; SLB, South Loyalty; SMT, South Meso-Tethys. (g) 80 Ma reconstruction: AFR, Africa; FAR, Farallon; GRN, Greenland; IZA, Izanagi; JUN, Junction; LHR, Lord Howe Rise. (h) 60 Ma reconstruction: AFR, Africa; FAR, Farallon; GRN, Greenland; IZA, Izanagi; JUN, Junction; LHR, Lord Howe Rise; KUL, Kula; PAC, Pacific. (i) 40 Ma reconstruction: AFR, Africa; CAR, Caribbean; FAR, Farallon; GRN, Greenland; IBR, Iberia; JUN, Junction; NL, North Loyalty; PAC, Pacific; PS, Philippine Sea; SS, Solomon; VAN, Vancouver. (j) 20 Ma reconstruction: AFR, Africa; CAP, Capricorn; CAR, Caribbean; COC, Cocos; CS, Caroline; J, Juan de Fuca; JUN, Junction; NAZ, Nazca; NB, Norfolk; PAC, Pacific; PS, Philippine Sea; SCO, Scotia; SOM, Somalia; SS, Solomon. (k) Present-day reconstruction: AFR, Africa; CAP, Capricorn; CAR, Caribbean; COC, Cocos; J, Juan de Fuca; LB, Lau; NAZ, Nazca; NFB, North Fiji; PAC, Pacific; PS, Philippine Sea; R, Rivera; SCO, Scotia Sea; SOM, Somalia.

Howe Rise from about 100 to 50 Ma. However, recent work (Matthews et al., 2012) shows there is petrologic evidence for subduction in this region after 90 Ma, and there is clear seismological evidence of subducted slab material in the lower mantle underneath the Lord Howe Rise region that requires active subduction between the Pacific and the Lord Howe Rise after ~90–85 Ma. This argues for using the East–West Antarctica circuit despite its shortcomings.

The availability of paleolatitudes from the Louisville chain means two chains on the same plate now have considerable latitudinal constraints for their oldest sections. Combined with the time series of inter-hot spot distances (Wessel and Kroenke, 2009), there are now several types of data constraints available for APM models. Models of hot spot motion must broadly satisfy these independent datasets. In particular, the inter-hot spot distances can be computed given dated rock samples from several hot spot chains; such data are much more plentiful than the limited paleolatitude dataset that requires expensive oceanic drilling expedition that hopefully sample enough volcanic flow units to average out the paleosecular variation. Being independent datasets, additions of new chronology and paleolatitude measurements will be exceptionally valuable for future APM studies.

As more paleomagnetic data suggest changes in the latitudes of hot spots through time, approaches such as that of Doubrovine et al. (2012) will likely become refined over time. However, many challenges remain. For reconstructions that go back before 70 Ma, severe numerical artifacts tend to develop in mantle backward advection calculations (e.g., Conrad and Gurnis, 2003). Doubrovine et al. (2012) thus made the choice to limit the backward advection for their plumes to 70 Ma; for older times (i.e., up to 130 Ma), a constant flow field was assumed defined by the density structure reconstructed at 70 Ma. This necessary simplification creates additional uncertainty for the modeled hot spot motions. Further work will clearly be needed to refine global plate circuits and their effects

on global APM models, as well as improvements to the APM models themselves.

TPW is defined as the wholesale rotation of the Earth relative to its spin axis. TPW is believed to occur in response to changing mass distributions about the Earth's spin axis (e.g., Tsai and Stevenson, 2007) and has been called upon to explain tectonic and paleomagnetic puzzles in the Earth's past (e.g., Li et al., 2004). The possibility of TWP complicates the determination of global APM. For instance, in fitting their global APM model, Doubrovine et al. (2012) found evidence for significant amounts of TPW. In particular, they identified two nearly equal and antipodal rotations of the Earth relative to its spin axis for the 90–60 and 60–40 Ma intervals. Other workers have identified episodes of TPW around 100–110 Ma and several instances in the more distant past (e.g., Besse and Courtillot, 2002; Greff-Lefftz and Besse, 2012; Steinberger and Torsvik, 2008). Paleolatitude measurements from oceanic hot spot chains may contain components of TPW; hence, a key challenge of future work is to resolve the contributions from plume motions, TWP, and plate motions.

6.02.5 Driving Forces of Plate Tectonics

Even though it has been shown that surface tectonic plates can be self-consistently generated through 3-D mantle convection (Tackley, 1998), the relative importance of driving forces of the time-dependent plate geometries and velocities of plates is still controversial. The question of what drives plate motion is indeed regarded as one of the most important scientific problems yet to be solved (Maddox, 1998). Identifying the main set of forces is relatively straightforward, but resolving the relative importance of individual forces for driving plate breakup and motion more protracted. Ziegler (1993) argued for the dominance of basal shear traction for causing plate motion. Others argue that basal shear only plays a small role due to weak coupling between the lithosphere and asthenosphere (even though the magnitude and lateral variability of this coupling is still unknown). Forsyth and Uyeda (1975), Richardson (1992), and Carlson et al. (1983) argued that plate-boundary forces are the main driving mechanisms of plate motion. Exactly which boundary forces play the most important role, however, is still an area of hot debate. Forces acting along the boundaries of plates that presumably drive plate motions are mainly caused by the upwelling of hot, buoyant asthenosphere at the mid-ocean ridge and the subduction of cold, dense lithosphere at trenches.

6.02.5.1 Ridge Push

The ridge-push force is often regarded as the primary plate driving mechanism (Coblentz and Richardson, 1995; Meijer and Wortel, 1992; Richardson, 1992), although other authors regard it as secondary to other forces (Carlson et al., 1983; Forsyth and Uyeda, 1975). The ridge-push force originates from a distributed pressure gradient (i.e., a body force) that acts on the entire plate normal to the strike of a mid-ocean ridge. It arises from the isostatic sinking of the oceanic lithosphere away from the mid-ocean ridge as it cools and densifies (Wilson, 1993).

The contribution of this topographic force can be calculated in two ways (Richardson, 1992). Firstly, it can be calculated as a line force acting along the length of the ridge normal to the strike of the ridge. Secondly, it can be calculated as a pressure gradient integrated over a profile perpendicular to the strike of the mid-ocean ridge crossing an entire ridge flank. The second method provides a more accurate result. The ridge-push force F_{rp} can be calculated at a given location by the following equation based on a thermal boundary layer model (e.g., Turcotte and Schubert, 2002):

$$F_{rp} = g\rho_m\alpha_v(T_m - T_0)\left[1 + \frac{2}{\pi}\frac{\rho_m\alpha_v(T_m - T_0)}{(\rho_m - \rho_0)}\right]\kappa t$$

where $g = 10\ \mathrm{m\ s^{-2}}$, $\rho_m = 3300\ \mathrm{kg\ m^{-3}}$, $\rho_0 = 1000\ \mathrm{kg\ m^{-3}}$, $\kappa = 1\ \mathrm{mm^2}$, $(T_m - T_0) = 1200\ \mathrm{K}$, $\alpha_v = 3 \times 10^{-5}\ \mathrm{K^{-1}}$, and t is the age of the lithosphere.

If the plate model (McKenzie, 1967) is applied instead of a thermal boundary layer model, then it follows that that mainly oceanic crust younger than 80 Myr contributes to the ridge-push force as oceanic lithosphere older than this age does not cool considerably, resulting in the cessation of isostatic sinking of oceanic lithosphere older than 80 Myr.

Some authors have also found it advantageous to consider the ridge-push force as a torque acting on the plate. Richardson (1992) used the equation mentioned earlier, integrated over the plate for lithosphere younger than 80 Ma, to give

$$T_{rp} = \int^{A} r \times F_{rp}\, dA$$

where T_{rp} is the torque from the ridge-push force and A is the area of the plate younger than 80 Ma. Richardson (1992) demonstrated a good correlation between the azimuth of the ridge torque pole and the pole of absolute plate velocity. The T_{rp} has also been shown to correlate well with the direction of the first-order intraplate stress field of the Indo-Australian Plate (Coblentz et al., 1995).

6.02.5.2 Slab Pull

The slab-pull force originates from the negative buoyancy of the downgoing dense oceanic lithosphere at subduction zones and is proportional to the excess mass of the cold slab in relation to the mass of the warmer displaced mantle (Spence, 1987). This density contrast, and therefore energy contribution of the downgoing slab, can also be enhanced by the phase change from olivine to the more dense spinel, which occurs in the downgoing slab earlier than the surrounding mantle (Bott, 1982; Spence, 1987). Negatively buoyant slabs also induce mantle convection as they penetrate the mantle, in turn driving lithospheric plates through shear traction at the base of plates (Conrad and Lithgow-Bertelloni, 2004; Lithgow-Bertelloni and Richards, 1998). Because subduction induces mantle flow toward the downwelling material, these tractions cause nearby plates to move toward subduction zones (Conrad and Lithgow-Bertelloni, 2004; Lithgow-Bertelloni and Richards, 1998).

Energy transmitted to the plate from the downgoing slab must be proportional to the excess mass M_e of the plate (Carlson et al., 1983). The excess mass is given by

$$M_e = \frac{1}{2}(\rho_L - \rho_m)\frac{LE}{\sin\psi}$$

where ρ_L is the density of the lithosphere, ρ_m is the density of the mantle, L is the thickness of the lithosphere, E is the depth at which the excess density vanishes, and Ψ is the dip of the slab (Carlson et al., 1983). The force on the lithospheric plate F_{sp} can then be calculated using

$$F_{sp} = M_e g$$

where g is gravitational acceleration.

Forsyth and Uyeda (1975) regarded slab pull as the main constraint on the velocity of plates (**Figure 30**). They considered the downgoing slab as having a 'terminal velocity' and that the potential energy stored in the downgoing slab is an order of magnitude greater than any other force acting on the plate. The

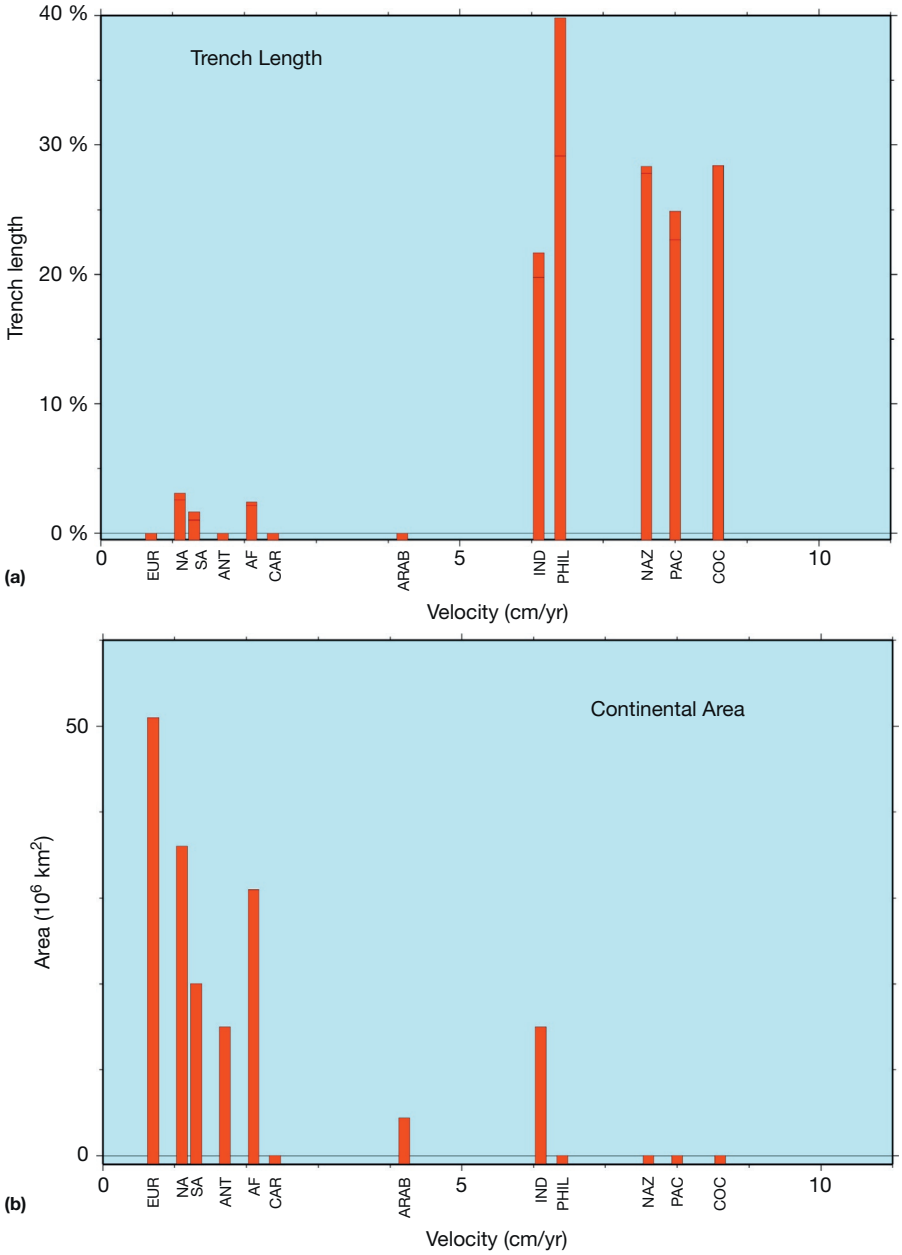

Figure 30 (a) Trench length as a percentage of plate circumference, plotted versus the plate velocity. There is a clear correlation between high velocities and high percentage of trench length, suggesting trench pull is one of the more significant plate driving forces. (b) Area of continental crust associated with a plate plotted versus plate velocity. It is seen that predominantly oceanic plates have significantly higher velocity than continental plates. Redrawn from Forsyth and Uyeda (1975).

exact magnitude of the energy contained in the downgoing slab has been disputed, with Spence (1987) suggesting it may only be three times the size of other forces acting on the plate. Carlson et al. (1983) suggested that the absolute plate speed is determined by the slab-pull force, as a function of the age of the oceanic lithosphere being subducted at trenches, with older subducted lithosphere resulting in higher absolute plate velocities.

The 'terminal velocity' of the plate, as discussed by Forsyth and Uyeda (1975), is due to high viscous drag forces acting on the downgoing slab that impede its entry into the mantle. Some authors have suggested that these viscous drag forces acting on the slab may actually be large enough to almost entirely balance out the negative buoyancy of the downgoing slab (Coblentz et al., 1995; Sandiford et al., 1995). In this case, the 'net force' experienced by the plate from the subducting slab may be of the same magnitude or less than other forces driving the plate. In contrast, Schellart's (2004) recent dynamic lab experiments suggest that the net slab-pull force may be up to twice as large as the ridge-push force, and Conrad and Lithgow-Bertelloni's models (2004) imply that slab suction and slab pull presently account for about 40% and 60% of the forces on plates, with ridge push globally playing a minor role.

6.02.5.3 Collisional Forces

Collisional forces do not act to drive the plate motions, but rather impede them. Collisional forces act along the boundary of plates and arise as a result of the frictional forces between the two colliding plates. At well-coupled subduction zones, there is a buildup of frictional strain energy between the subducting plate and the overriding plate. This energy is then released through earthquakes and crustal deformation. Where the collision of a continental landmass is also involved, loss of energy from plate momentum is converted into excess gravitational potential energy stored as thickened crust (Bott, 1982). For instance, in the case of the collision between India and Asia responsible for the Himalayan orogen, the amount of energy converted into crustal thickening is of the same order as the plate driving forces, as the velocity of the plate slowed upon collision (e.g., Copley et al., 2010; Sandiford et al., 1995).

6.02.5.4 Basal Shear Traction

The notion of shear forces acting at the base of the plates with the convecting mantle acting as a 'conveyor belt' driving the plates, while popular in the past, has fallen out of favor in preference to other plate driving mechanisms. While the relative importance of basal shear forces may be dominant under Pangaea-style megacontinents (Ziegler, 1993), they probably play only a minor role in the kinematics of dispersed plates (for discussion, see Wilson, 1993). Stoddard and Abbot (1996) argued that the crustal roots under cratons act like keels and penetrate a rapidly convecting mantle. This interaction with the rapidly convecting mantle then acts to drive the motion of the plate. However, given our lacking knowledge of the extent of coupling of the lithosphere to the mantle (Coblentz et al., 1995), it is difficult to quantify the relative importance of basal shear relative to other forces.

6.02.5.5 Trench Suction

Trench suction is regarded as a lifting pressure or suction on the upper surface of the downgoing plate caused by an asthenospheric corner flow that is induced by the motion of the descending plate. This force is balanced by the negative buoyancy of the descending lithospheric plate that acts to pull it vertically down by the motion of the descending plate. The balance of these two forces is thought to keep the plate at a finite descent angle (Stevenson and Turner, 1977).

6.02.5.6 Plume Push

Cande and Stegman (2011) extended the catalog of phenomena attributed to mantle plumes by suggesting that they are able to impart a substantial force on plates – a plume-push force – that can do more than just break up continents. Their hypothesis is that if a rising plume head impinges on the base of a tectonic plate long after supercontinent breakup and dispersal, then its pushing force may result in a substantial transient acceleration or deceleration of plates. The velocity of a plate being hit by a plume depends on how the plume-push force balances out with other forces acting on a given plate. Cande and Stegman (2011) developed their model by studying the effect of the Réunion plume, whose incipient head is thought to have reached the surface around 67 Ma, emplacing the Deccan flood basalts in India (Chenet et al., 2007). Using a careful analysis of marine geophysical data from the Indian Ocean, they noted several phenomena associated with this event: India sped up between 68 and 66 Myr ago and subsequently sustained APM speeds of 10–12 cm per year for about 15 million years, with peak speed reaching about 18 cm per year. Between 52 and 45 Myr ago, India's motion slowed down dramatically to less than 4 cm per year. In addition, Africa's motion slowed down while India sped up, only to return to its previous path and speed after India had decelerated (**Figure 31**).

6.02.5.7 What Drives Plate Tectonics?

A major debate concerns a 'top-down' versus mantle-driven mechanism for driving the organization of plates (Anderson, 2001). Abundant plume-driven continental breakup examples and hypotheses associated with magmatic provinces (Coffin and Eldholm, 1992; Dalziel et al., 2000; Ebinger and Sleep, 1998; Storey, 1995) emphasize mantle-driven tectonics. However, the good agreement between long-wavelength features of the intraplate stress field (Zoback, 1992) with the stress orientations predicted by ridge-push forces and large-scale APMs led to the view that plate motions and intraplate deformation result mainly from the balance between ridge-push and collisional forces, emphasizing a 'top-down' mechanism, but without a significant role for slab pull (Richardson, 1992). Alternatively, slab-pull forces have been advocated as the most important driving forces of current plate motions (Conrad and Lithgow-Bertelloni, 2002, 2004; Forsyth and Uyeda, 1975; Schellart, 2004) in a 'top-down' context.

Most analyses of plate driving forces and intraplate stresses are focused on the Earth's present dispersed plate geometry (e.g., Cloething, 1986; Richardson, 1992; Sandiford et al., 1995),

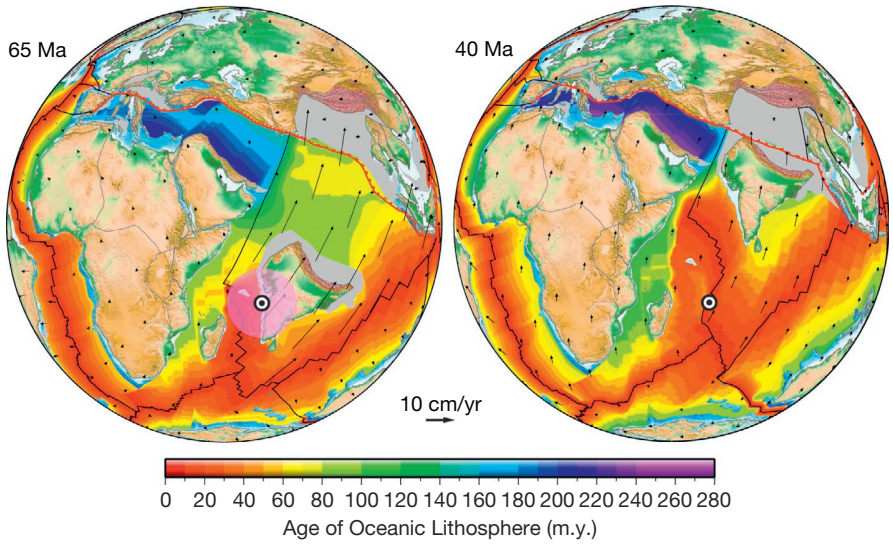

Figure 31 The Indian and African Plates at 65 and 40 Ma. Black arrows represent APMs, with the fast motion of India 65 Myr ago and the slow motion of Africa, corresponding to a time shortly after the Réunion plume head is thought to have arrived at the surface; plume head is hypothesized to have affected the plates' speeds. By 40 Ma, the influence of the plume had waned: The Indian Plate had slowed down considerably and the African Plate had resumed its former direction and speed. Rotated present-day topography is shown on the continents, and seafloor age is depicted in the ocean basins. The estimated extent of now-destroyed continental margins is represented by the gray areas; mid-ocean ridges and transform faults are shown as black lines; subduction zones are shown as a red line, with teeth on the overriding plate. (Plate reconstructions generated using the GPlates1.2 software, data, and rotations.)

where ridge push is a major contributor to plate motions; most continents are under gravity-controlled compression; and the most prominent intracontinental rift, the Afar Triangle in Africa, is driven by the excess gravitational potential produced by plume-driven uplift (Ebinger and Sleep, 1998). In contrast, the post-Devonian history of the Tethyan Ocean between Gondwanaland and Laurasia is characterized by a history of at least 12 continental blocks or plates of varying sizes that were rifted off the northern passive margin of Gondwanaland without much evidence for associated magmatism and accreted to Eurasia after crossing the Tethys (Audley-Charles et al., 1988; Metcalfe, 1999; Ricou, 1995). The absence of magmatism along the northeastern Gondwanaland passive margin during most of these continental breakup events precludes mantle upwelling as a dominating driving force and is difficult to understand if slab pull plays no significant role in driving continental breakup. Slab retreat was suggested by Collins (2003) as the main mechanism causing breakup of Pangaea, and based on a mantle convection model, Conrad and Lithgow-Bertelloni (2004) suggested that the importance slab pull has been increasing steadily through the Cenozoic because the mass and length of upper-mantle slabs have been increasing, causing subducting plates to double their speed relative to nonsubducting plates during this time period.

India's superfast motion has been puzzling. One model ascribed it to losing its continental roots due to mantle plume activity when Gondwanaland originally broke apart (Kumar et al., 2007). However, such an erosion and melting away of India's roots, thought to have occurred around 130 Ma, cannot be held responsible for the specific acceleration starting at 67 Ma. Moreover, some geodynamic models suggest that the maximum velocity that tectonic plates typically reach is 8 cm per year. The reason for this maximum speed is that plates are largely driven by the pull of slabs subducting in the mantle, especially upper-mantle slabs to which plates are attached (e.g., Goes et al., 2008; Schellart et al., 2007). The characteristic sinking velocity for upper-mantle slabs is about 7 cm per year with a maximum of 8 cm per year for the oldest, thickest, most negatively buoyant slabs (Goes et al., 2008). This work has been confirmed by sophisticated numerical models for the present-day plate motions (Stadler et al., 2010), which show a near-perfect agreement between observed plate motions and those predicted by driving plates with only upper-mantle slabs.

Therefore, geodynamic models raise the question how plates can achieve velocities in great excess of 8 cm per year. Cande and Stegman (2011) used their detailed kinematic models to make a conceptual argument that by adding a plume-push force, India can be sufficiently accelerated, while Africa is slowed down. This dichotomy is explained by considering the location of the Réunion plume relative to the two plates. In India's case, the plume-push force would act in unison with slab pull north of India, whereas in Africa's case, it would counteract slab pull, slowing the continent down. After exhaustion of the plume head and the waning of its presumed pushing force, Africa exhibits a speed-up synchronous with the slowdown of India.

Of course, this scenario is not without problems. One potential difficulty is that the Deccan Traps – emplaced as a direct consequence of the partial melts supplied by the Réunion plume head – were emplaced over a comparatively short period of time from 68 to 65 Ma (Chenet et al., 2007). The Indian Plate velocity anomaly, on the other hand, lasted for more than 15 Myr. Another potential problem comes from geodynamic modeling. Van Hinsbergen et al. (2011) recently

explored the magnitude of the plume-push force and concluded that while a plume head effect could account for an acceleration of India, it could only do so by a few cm per year, certainly not the 10 cm per year required to explain the Indian Plate velocities. Equivalently, their models indicate that a combination of reduced plume flux, reduced coupling with the plate and the plate moving away from the plume, can only account for a small portion of India's dramatic slowdown at 52 Ma. Whether the plume-push force model for India's superfast motion will stand the test of time remains to be seen.

6.02.6 Future Challenges

Perhaps, one of the key components to make significant progress in the analysis and testing of the hot spot hypothesis is the availability of samples from several hot spot chains. The study of APMs over hot spots remains a data-starved field, and it is to be expected that as more and better age data become available, particularly in key sections currently underrepresented and poorly constrained, they will play a major role in deciding among competing hypotheses. One of the particularly challenging tasks will be to develop an accepted approach that can be used to separate volcanism caused by hot spots from other volcanism unrelated to plume activity. A growing body of evidence suggests much surface volcanism can also occur as a consequence of extension. For instance, the Pacific Ocean has several linear volcanic ridges (e.g., Lynch, 1999) whose ages are not compatible with the hot spot paradigm and may be better explained in terms of transient extensional stresses during times of plate motion changes (Anderson et al., 1992; Sandwell et al., 1995; Wessel and Kroenke, 2007).

The field of relative plate motion studies has revealed much about the plate tectonic motions between oceanic plates. However, new discoveries are needed in areas where magnetic anomalies are scarce or of very low amplitude, such as in the Cretaceous quiet zone (e.g., Granot et al., 2012). It is possible that a combination of high-resolution magnetic profiling and multibeam bathymetric mapping of abyssal hill fabric can remedy this situation (e.g., Sandwell et al., 2002). Recent modeling improvements, such as Bayesian methods that can recover smooth plate motions in the presence of noisy finite rotations (Iaffeldano et al., 2012), are expected to take on a larger role in linking observed kinematics to mantle dynamics.

Over the last 10 years, new evidence has been gathered that seems to suggest that hot spots are far from being the stationary features originally envisioned. The best-documented case comes from the Emperor seamounts where drilling results have shown that the Emperor seamounts have paleolatitudes that are incompatible with formation over a hot spot at the current 19–20° latitude of the Hawaiian Island (Tarduno et al., 2003). More recently, paleolatitudes from the oldest section of the Louisville chain have become available (Koppers et al., 2012), showing a much more limited latitudinal motion. Modeling of APMs must allow for the possibility of such hot spot motion, as the techniques of O'Neill et al. (2005) and Wessel et al. (2006) both do. However, while hot spot motion paths predicted from mantle flow models (e.g., Doubrovine et al., 2012; Steinberger, 2000) are presently required, ideally, it should be possible to determine the optimal path of motion for hot spots from available geochronology, seamount chain geometry, and paleomagnetic data alone and then compare the results to the predictions of the flow models. Theoretical improvements along such lines seem pertinent to solving this problem.

Further advances in the mapping of seafloor morphology depend on better coverage of high-quality data. Given the size of the oceans, the pace of oceanic exploration, and the ever-increasing costs of ship fuel, it seems exceedingly unlikely that complete bathymetric coverage will be achieved in the next hundred years, despite the optimism in some quarters (Vogt and Jung, 2000). If this is true, more emphasis should be placed on obtaining the best possible data coverage using space-based techniques; for marine tectonic studies, this means collecting a new set of altimetry measurements capable of resolving much smaller wavelengths and amplitudes of the sea surface undulations from which the marine geoid is derived (Sandwell et al., 2002). From such data, the proven techniques of reconstructing the Earth's gravity field and from it undertaking bathymetric prediction will enable scientists to better classify seafloor fabric and complement the information inferred from traditional shipboard geophysical observations. Nevertheless, plate tectonic deciphering of seafloor formed during the Cretaceous Normal Superchron will require high-resolution imaging beyond what is attainable via satellite altimetry; hence, seagoing explorations will continue to be a key requirement to make progress in these difficult regions.

In order to advance our understanding of the coupling and feedbacks between deep Earth processes and plate kinematics, tools and workflows need to be established in which observations, plate kinematics through time, geodynamic modeling, and model/data visualization are seamlessly linked, based on open standards and open-source tools. With more and better data and the continued development of more sophisticated models that combine data and model outputs with powerful dynamic visualization, an additional need is the ability of scientists to better communicate and exchange information in well understood and suitable formats. The burgeoning field of geoinformatics is likely to enable key advances in all of the Earth sciences during the next decade. We are already seeing the results of this work with the release of user-friendly plate tectonic-specific software (Williams et al., 2012) that has the potential to elevate plate reconstructions from the purview of a few specialists to a common activity for everybody studying plate tectonics. For this transition to be successful, it is important that Earth scientists embrace the computational skills required to manage data and strive to communicate both data and results efficiently to the community.

Acknowledgments

This chapter was greatly improved by reviewer comments. We thank Christian Heine and Maria Seton for the help with **Figures 1–3** and **29**, respectively. This is SOEST contribution no. 9213.

References

Acton GD and Gordon RG (1994) Paleomagnetic tests of Pacific plate reconstructions and implications for motion between hotspots. *Science* 263: 1246–1254.
Anderson DL (2001) Top-down tectonics? *Science* 293: 2016–2018.
Anderson DL, Tanimoto T, and Zhang Y-S (1992) Plate tectonics and hotspots: The third dimension. *Science* 256: 1645–1651.

Andrews DL, Gordon RG, and Horner-Johnson BC (2006) Uncertainties in plate reconstructions relative to the hotspots; Pacific-hotspot rotations and uncertainties for the past 68 million years. *Geophysical Journal International* 166: 939–951.

Argus DF, Gordon RG, Heflin MB, et al. (2010) The angular velocities of the plates and the velocity of Earth's centre from space geodesy. *Geophysical Journal International* 180: 913–960.

Aslanian D, Géli L, and Olivet J-L (1998) Hotspotting called into question. *Nature* 396: 127.

Audley-Charles MB, Ballantyne PD, and Hall R (1988) Mesozoic–Cenozoic rift–drift sequence of Asian fragments from Gondwanaland. *Tectonophysics* 155: 317–330.

Baksi AK (1995) Petrogenesis and timing of volcanism in the Rajmahal flood basalt province, northeastern India. *Chemical Geology* 121: 73–90.

Baksi AK (1999) Reevaluation of plate motion models based on hotspot tracks in the Atlantic and Indian Oceans. *Journal of Geology* 107: 13–26.

Barrell J (1914) The strength of the Earth's crust, VIII, physical conditions controlling the nature of lithosphere and asthenosphere. *Journal of Geology* 22: 425–443.

Batiza R (1982) Abundances, distribution, and sizes of volcanoes in the Pacific Ocean and implications for the origin of non-hotspot volcanoes. *Earth and Planetary Science Letters* 60: 195–206.

Batiza R (2001) Seamounts and off-ridge volcanism. In: Steele J, Thorpe S, and Turekian K (eds.) *Encyclopedia of Ocean Sciences*. San Diego: Academic Press.

Bercovici D (1993) A simple model of plate generation from mantle flow. *Geophysical Journal International* 114: 635–650.

Bercovici D and Kelly A (1997) The non-linear initiation of diapirs and plume heads. *Physics of the Earth and Planetary Interiors* 101: 119–130.

Bercovici D and Mahoney J (1994) Double flood basalts and plume head separation at the 660-kilometer discontinuity. *Science* 266: 1367–1369.

Bergman EA and Solomon SC (1980) Oceanic intraplate earthquakes: Implications for local and regional intraplate stress. *Journal of Geophysical Research* 85: 5389–5410.

Besse J and Courtillot V (2002) Apparent and true polar wander and the geometry of the geomagnetic field over the last 200 Myr. *Journal of Geophysical Research* 107. http://dx.doi.org/10.1029/2000JB000050.

Bird P (2003) An updated digital model of plate boundaries. *Geochemistry, Geophysics, Geosystems* 4: 1027.

Bott MHP (1982) *The Interior of the Earth: Its Structure, Constitution and Evolution*. London: Arnold.

Boyden JA, Müller RD, Gurnis M, et al. (2011) Next-generation plate-tectonic reconstructions using GPlates. In: Keller GR and Baru C (eds.) *Geoinformatics: Cyberinfrastructure for the Solid Earth Sciences*. Cambridge: Cambridge University Press.

Bullard EC, Everett JE, and Smith AG (1965) Fit of continents around Atlantic. In: Blackett PMS, Bullard EC, and Runcorn SK (eds.) *A Symposium on Continental Drift, Roy. Soc. Lond*.

Burke KC and Wilson JT (1976) Hot spots on the Earth's surface. *Journal of Geophysical Research* 93: 7690–7708.

Campbell IH and Griffiths RW (1990) Implications of mantle plume structure for the evolution of flood basalts. *Earth and Planetary Science Letters* 99: 79–93.

Cande SC, Labrecque JL, and Haxby WF (1988) Plate kinematics of the south Atlantic: Chron C34 to present. *Journal of Geophysical Research* 93: 13479–13492.

Cande SC, Raymond CA, Stock J, and Haxby WF (1995) Geophysics of the Pitman fracture zone and Pacific–Antarctic plate motions during the Cenozoic. *Science* 270: 947–953.

Cande SC and Stegman DR (2011) Indian and African plate motions driven by the push force of the Réunion plume head. *Nature* 475: 47–52.

Cande SC, Stock JM, Müller RD, and Ishihara T (2000) Cenozoic motion between East and West Antarctica. *Nature* 404: 145–150.

Cao Q, Van Der Hilst R, De Hoop MV, and Shim S-H (2011) Seismic imaging of transition zone discontinuities suggests hot mantle west of Hawaii. *Science* 332: 1068–1071.

Carlson RL, Hilde TWC, and Uyeda S (1983) The driving mechanism of plate tectonics: Relation to age of lithosphere at trenches. *Geophysical Research Letters* 10: 297–300.

Cazenave A, Dominh K, Rabinowicz M, and Ceuleneer G (1988) Geoid and depth anomalies over ocean swells and troughs: Evidence of an increasing trend of the geoid to depth ratio with age of plate. *Journal of Geophysical Research* 93: 8064–8077.

Ceuleneer G, Rabinowicz M, Monnereau M, Cazenave A, and Rosemberg C (1988) Viscosity and thickness of the sub-lithospheric low-viscosity zone: Constraints from geoid and depth over oceanic swells. *Earth and Planetary Science Letters* 89: 84–102.

Chandler MT, Wessel P, Taylor B, Seton M, Kim S-S, and Hyeong K (2012) Reconstructing Ontong Java Nui: Implications for Pacific absolute plate motion, hotspot drift and true polar wander. *Earth and Planetary Science Letters* 331–332: 140–151.

Chang T (1987) On the statistical properties of estimated rotations. *Journal of Geophysical Research* 92: 6319–6329.

Chang T (1988) Estimating the relative rotation of two tectonic plates from boundary crossings. *Journal of the American Statistical Association* 83: 1178–1183.

Chang T, Stock J, and Molnar P (1990) The rotation group in plate tectonics and the representation of uncertainties of plate reconstructions. *Geophysical Journal International* 101: 649–661.

Chapple WM and Tullis TE (1977) Evaluation of the forces that drive the plates. *Journal of Geophysical Research* 82: 1967–1984.

Chenet AL, Quidelleur X, Fluteau F, Courtillot V, and Bajpai S (2007) ^{40}K–^{40}Ar dating of the Main Deccan large igneous province: Further evidence of KTB age and short duration. *Earth and Planetary Science Letters* 263: 1–15.

Chu D and Gordon RG (1999) Evidence for motion between Nubia and Somalia along the Southwest Indian Ridge. *Nature* 398: 64–67.

Clague D and Dalrymple GB (1989) The tectonic and geologic setting of the Hawaiian–Emperor volcanic chain. In: Winterer EL, Hussong DM, and Decker RW (eds.) *The Eastern Pacific Ocean and Hawaii*. Boulder, CO: Geological Society of America.

Cloething S (1986) Intraplate stresses: A new tectonic mechanism for fluctuations in sea level. *Geology* 14: 617–620.

Cloos M (1993) Lithospheric buoyancy and collisional orogenesis; subduction of oceanic plateaus, continental margins, island arcs, spreading ridges, and seamounts. *Geological Society of America Bulletin* 105: 715–737.

Clouard V and Bonneville A (2001) How many Pacific hotspots are fed by deep-mantle plumes? *Geology* 29: 695–698.

Clouard V and Bonneville A (2005) Ages of seamounts, islands, and plateaus on the Pacific plate. In: Foulger GR, Natland JH, Presnall DC, and Anderson DL (eds.) *Plates, Plumes, and Paradigms*. Boulder, CO: Geological Society of America.

Coblentz DD and Richardson RM (1995) Statistical trends in the intraplate stress field. *Journal of Geophysical Research* 100: 20245–20255.

Coblentz DD, Sandiford M, Richardson RM, Zhou S, and Hillis R (1995) The origins of the intraplate stress field in continental Australia. *Earth and Planetary Science Letters* 133: 299–309.

Coffin MF and Eldholm O (1992) Volcanism and continental breakup: A compilation of large igneous provinces. In: Storey BC (ed.) *Magmatism and the Causes of Continental Breakup*. London: Geological Society of London.

Coffin MF and Eldholm O (1993) Large igneous provinces. *Scientific American* 269: 42–49.

Coffin MF, Gahagan LM, and Lawver LA (1997) Present-day plate boundary digital data compilation. University of Texas Institute for Geophysics Technical Report.

Coffin MF, Prince MS, and Duncan RA (2002) Kerguelen hotspot magma output since 130 Ma. *Journal of Petrology* 43: 1121–1139.

Collette BJ, Slootweg AP, Verhoef J, and Roest WR (1984) Geophysical investigations of the floor of the Atlantic ocean between 10° and 38° N (kroonvlag-project). *Proceedings of the Royal Netherlands Academy of Sciences* 87: 1–76.

Collins WJ (2003) Slab pull, mantle convection, and Pangaean assembly and dispersal. *Earth and Planetary Science Letters* 205: 225–237.

Conrad CP and Gurnis M (2003) Seismic tomography, surface uplift, and the breakup of Gondwanaland: Integrating mantle convection backwards in time. *Geochemistry, Geophysics, Geosystems* 4: 1031.

Conrad CP and Lithgow-Bertelloni C (2002) How mantle slabs drive plate tectonics. *Science* 298: 207–209.

Conrad CP and Lithgow-Bertelloni C (2004) The temporal evolution of plate driving forces: Importance of "slab suction" versus "slab pull" during the Cenozoic. *Journal of Geophysical Research* 109: 1–14.

Copley A, Avouac J-P, and Royer JY (2010) India–Asia collision and the Cenozoic slowdown of the Indian plate: Implications for the forces driving plate motions. *Journal of Geophysical Research* 115. http://dx.doi.org/10.1029/2009JB006634.

Cox A and Hart RB (1986) *Plate Tectonics: How it Works*. Oxford, UK: Blackwell.

Craig CH and Sandwell DT (1988) Global distribution of seamounts from Seasat profiles. *Journal of Geophysical Research* 93: 10408–10420.

Crough ST (1983) Hotspot swells. *Annual Review of Earth and Planetary Sciences* 11: 165–193.

Dalziel IWD, Lawver LA, and Murphy JB (2000) Plumes, orogenesis, and supercontinental fragmentation. *Earth and Planetary Science Letters* 178: 1–11.

Das AK, Piper JDA, Bandyopadhyay G, and Mallik SB (1996) Polarity inversion in the Rajmahal lavas, north-east India: Trap emplacement near commencement of the cretaceous normal superchron. *Geophysical Journal International* 124: 427–432.

Davies GF (1992) Temporal variation of the Hawaiian plume flux. *Earth and Planetary Science Letters* 113: 277–286.

Demets C, Gordon RG, and Argus DF (2010) Geologically current plate motions. *Geophysical Journal International* 181: 1–80.

Detrick RS and Crough ST (1978) Island subsidence, hot spots, and lithospheric thinning. *Journal of Geophysical Research* 83: 1236–1244.

Dickinson WR (1998) Geomorphology and geodynamics of the Cook-Austral island-seamount chain in the south Pacific ocean: Implications for hotspots and plumes. *International Geology Review* 40: 1039–1075.

Dietz RS (1961) Evolution by spreading of the sea floor. *Nature* 190: 854.

Doubrovine PV, Steinberger B, and Torsvik TH (2012) Absolute plate motions in a reference frame defined by moving hot spots in the Pacific, Atlantic, and Indian oceans. *Journal of Geophysical Research* 117, B09101.

Douglas BC (1991) Global sea level rise. *Journal of Geophysical Research* 96: 6981–6992.

Duncan RA (1981) Hotspots in the Southern ocean – An absolute frame of reference for motion of the Gondwana continents. *Tectonophysics* 74: 29–42.

Duncan RA and Clague DA (1985) Pacific plate motion recorded by linear volcanic chains. In: Nairn AEM, Stehli FG, and Uyeda S (eds.) *The Ocean Basins and Margins*. New York: Plenum.

Ebinger CJ and Sleep NH (1998) Cenozoic magmatism throughout east Africa resulting from impact of a single plume. *Nature* 395: 788–791.

Engdahl ER, Van Der Hilst R, and Buland R (1998) Global teleseismic earthquake relocation with improved travel times and procedures for depth determination. *Bulletin of the Seismological Society of America* 88: 722–743.

Engebretson DC, Cox A, and Gordon RG (1985) Relative motions between oceanic and continental plates in the Pacific Ocean. *Special Paper, Geological Society of America* 206: 1–58.

Forsyth DW and Uyeda S (1975) On the relative importance of the driving forces of plate motion. *Geophysical Journal* 43: 163–200.

Fryer P (1996) Evolution of the Mariana convergent plate margin system. *Reviews of Geophysics* 34: 89–125.

Gaina C, Müller RD, Brown BJ, and Ishihara T (2003) Microcontinent formation around Australia. *Geological Society of America Special Paper* 372: 405–416.

Gaina C, Müller RD, Brown B, Ishihara T, and Ivanov S (2007) Breakup and early seafloor spreading between India and Antarctica. *Geophysical Journal International* http://dx.doi.org/10.1111/j.1365-246X.2007.03450.x.

Gardner JV, Dean WE, and Blakely RJ (1984) Shimada seamount: An example of recent mid-plate volcanism. *Geological Society of America Bulletin* 95: 855–862.

Goes S, Capitanio FA, and Morra G (2008) Evidence of lower-mantle slab penetration phases in plate motions. *Nature* 451: 981–984.

Golonka J (2007) Late Triassic and Early Jurassic palaeogeography of the world. *Palaeogeography, Palaeoclimatology, Palaeoecology* 244: 297–307.

Gordon RG (1998) The plate tectonic approximation: Plate nonrigidity, diffuse plate boundaries, and global plate reconstructions. *Annual Review of Earth and Planetary Sciences* 26: 615–642.

Gordon RC (2000) Diffuse oceanic plate boundaries: Strain rates, vertically averaged rheology, and comparisons with narrow plate boundaries and stable plate interiors. In: Richards MA, Gordon RC, and Van Der Hilst RD (eds.) *The History and Dynamics of Global Plate Motions*. Washington, DC: American Geophysical Union.

Granot R, Dyment J, and Gallet Y (2012) Geomagnetic field variability during the Cretaceous Normal Superchron. *Nature Geoscience* 5: 220–223.

Greff-Lefftz M and Besse J (2012) Paleo movement of continents since 300 Ma, mantle dynamics and large wander of the rotational pole. *Earth and Planetary Science Letters* 345–348: 151–158.

Gripp AE and Gordon RG (2002) Young tracks of hotspots and current plate velocities. *Geophysical Journal International* 150: 321–361.

Haase KM and Devey CW (1994) The petrology and geochemistry of Vesteris seamount Greenland basin – An intraplate alkaline volcano of non-plume origin. *Journal of Petrology* 35: 295–328.

Hager BH and O'Connell RJ (1981) A simple global model of plate dynamics and mantle convection. *Journal of Geophysical Research* 86: 4843–4867.

Hall CE, Gurnis M, Sdrolias M, Lavier LL, and Muller RD (2003) Catastrophic initiation of subduction following forced convergence across fracture zones. *Earth and Planetary Science Letters* 212: 15–30.

Hanna MS and Chang T (1990) On graphically representing the confidence region for an unknown rotation in three dimensions. *Computers & Geosciences* 16: 163–194.

Harada Y and Hamano Y (2000) Recent progress on the plate motion relative to hotspots. In: Richards MA, Gordon RG, and Hilst RDVD (eds.) *The History and Dynamics of Global Plate Motions*. *Geophysical Monograph*. Washington, DC: American Geophysical Union.

Harbert W and Cox A (1989) Late Neogene motion of the Pacific plate. *Journal of Geophysical Research* 94: 3052–3064.

Harris RN, Fisher AT, and Chapman DS (2004) Fluid flow through seamounts and implications for global mass fluxes. *Geology* 32: 725–728.

Haxby WF (1987) *Gravity Field of the World's Oceans*. Boulder, CO: National Geophysical Data Center, NOAA.

Haxby WF, Karner GD, Labrecque JL, and Weissel JK (1983) Digital images of combined oceanic and continental data sets and their use in tectonic studies. *Eos* 64: 995–1004.

Heezen BC and Tharp M (1961) *Physiographic Diagram of the South Atlantic, the Caribbean, the Scotia Sea, and the Eastern Margin of the South Pacific Ocean*. New York: Geological Society of America.

Heezen BC and Tharp M (1964) *Physiographic Diagram of the Indian Ocean, the Red Sea, the South China Sea, the Sulu Sea, and the Celebes Sea*. New York: Geological Society of America.

Heine C, Müller RD, and Gaina C (2004) Reconstructing the lost eastern Tethys ocean basin: Convergence history of the SE Asian margin and marine gateways. In: Clift PD (ed.) *Continent–Ocean Interactions Within East Asian Marginal Seas*. Washington, DC: American Geophysical Union.

Heirtzler JR, Dickson GO, Herron EM, Pitman WC III, and Le Pichon X (1968) Marine magnetic anomalies, geomagnetic field reversals, and motions of the ocean floor and continents. *Journal of Geophysical Research* 73: 2119–2136.

Hellinger SJ (1981) The uncertainties of finite rotations in plate tectonics. *Journal of Geophysical Research* 86: 9312–9318.

Hess HH (1946) Drowned ancient islands of the Pacific Basin. *American Journal of Science* 244: 772–791.

Hess HH (1962) History of ocean basins. *Geological Society of America Bulletin; Petrologic Studies: A Volume to Honour A.F. Buddington* 559–620.

Hillier JK and Watts AB (2007) Global distribution of seamounts from ship-track bathymetry data. *Geophysical Research Letters* 34(L13304). http://dx.doi.org/10.1029/2007GL029874.

Holmes A (1944) *Principles of Physical Geology*. Edinburgh: Thomas Nelson & Sons.

Hyndman RD and Hamilton TS (1993) Queen Charlotte area Cenozoic tectonics and volcanism and their association with relative plate motions along the northeastern Pacific margin. *Journal of Geophysical Research* 98: 14257–14277.

Iaffeldano G, Bodin T, and Sambridge M (2012) Reconstructing plate-motion changes in the presence of finite-rotations noise. *Nature Communications* 3: 1048.

Idnurm M (1985) Late Mesozoic and Cenozoic palaeomagnetism of Australia – II. Implications for geomagnetism and true polar wander. *Geophysical Journal of the Royal Astronomical Society* 83: 419–433.

Janney PE, Macdougall JD, Natland JH, and Lynch MA (2000) Geochemical evidence from the Pukapuka volcanic ridge system for a shallow enriched mantle domain beneath the South Pacific superswell. *Earth and Planetary Science Letters* 181: 47–60.

Jaroslow GE, Smith DK, and Tucholke BE (2000) Record of seamount production and off-axis evolution in the western North Atlantic Ocean, 25°25'–27°10'N. *Journal of Geophysical Research* 105: 2721–2736.

Jayne SR, St. Laurent LC, and Gille ST (2004) Connections between ocean bottom topography and Earth's climate. *Oceanography* 17: 65–74.

Jordan TH (1979) Mineralogies, densities, and seismic velocities of garnet lherzolites and their geophysical implications. In: Boyd FR and Meyer HOA (eds.) *The Mantle Sample: Inclusions in Kimberlites and Other Volcanics*. Washington, DC: American Geophysical Union.

Kim S-S and Wessel P (2011) New global seamount census from altimetry-derived gravity data. *Geophysical Journal International* 186: 615–631.

Kirkwood BH, Royer J-Y, Chang TC, and Gordon RG (1999) Statistical tools for estimating and combining finite rotations and their uncertainties. *Geophysical Journal International* 137: 408–428.

Klitgord K and Schouten H (1986) Plate kinematics of the central Atlantic. In: Vogt PR and Tucholke BE (eds.) *The Western North Atlantic Region, DNAG*. Boulder, CO: Geological Society of America.

Knesel KM, Cohen BE, Vasconcelos PM, and Thiede DS (2008) Rapid change in drift of the Australian plate records collision with Ontong Java plateau. *Nature* 454: 754–757.

Kogan MG and Steblov GM (2008) Current global plate kinematics from GPS (1995–2007) with the plate-consistent reference frame. *Journal of Geophysical Research* 113, B04416.

Kono M (1980) Paleomagnetism of DSDP Leg 55 basalts and implications for the tectonics of the Pacific plate. In: Jackson ED, Koizumi I, Kirkpatrick RJ, Avdeiko G, Clague D, Dalrymple GB, Karpoff A-M, Mckenzie J, Butt A, Ling HY, Takayama T, Greene HG, Morgan J, and Kono M (eds.) *Initial Reports DSDP*. Washington: US Government Printing Office.

Koppers AAP, Duncan RA, and Steinberger B (2004) Implications of a nonlinear $^{40}Ar/^{39}Ar$ age progression along the Louisville seamount trail for models of fixed and moving hot spots. *Geochemistry, Geophysics, Geosystems* 5. http://dx.doi.org/10.1029/2003GC000671.

Koppers AAP, Gowen MD, Colwell LE, et al. (2011a) New $^{40}Ar/^{39}Ar$ age progression for the Louisville hot spot trail and implications for inter-hot spot motion. *Geochemistry, Geophysics, Geosystems* 12. http://dx.doi.org/10.1029/2011GC003804.

Koppers AAP, Phipps Morgan J, Morgan JW, and Staudigel H (2001) Testing the fixed hotspot hypothesis using $^{40}Ar/^{39}Ar$ age progressions along seamount trails. *Earth and Planetary Science Letters* 185: 237–252.

Koppers AAP, Russell JA, Roberts J, et al. (2011b) Age systematics of two young en echelon Samoan volcanic trails. *Geochemistry, Geophysics, Geosystems* 12, Q07025.

Koppers AA and Staudigel H (2005) Asynchronous bends in Pacific seamount trails: A case for extensional volcanism? *Science* 307: 904–907.

Koppers AAP, Yamazaki T, Geldmacher J, et al. (2012) Limited latitudinal mantle plume motion for the Louisville hotspot. *Nature Geoscience* 5(12): 911–917.

Krijgsman W, Hilgen FJ, Raffi I, Sierro FJ, and Wilson DS (1999) Chronology, causes and progression of the Messinian salinity crises. *Nature* 400: 652–655.

Kroenke LW (1996) Plate tectonic development of the Western and Southwestern Pacific. In: Keast A and Miller SE (eds.) *The Origin and Evolution of Pacific Island Biotas*. Amsterdam: SPB Academic Publishing.

Kumar P, Yuan X, Kumar MR, Kind R, Li X, and Chadha R (2007) The rapid drift of the Indian tectonic plate. *Nature* 449: 894–897.

Kunze E and Llewellyn Smith SG (2004) The role of small-scale topography in turbulent mixing of the global ocean. *Oceanography* 17: 55–64.

Labails C, Olivet J-L, Aslanian D, and Roest WR (2010) An alternative early opening scenario for the Central Atlantic Ocean. *Earth and Planetary Science Letters* 297: 355–368.

Larson RL and Chase CG (1972) Late Mesozoic evolution of the western Pacific Ocean. *Geological Society of America Bulletin* 83: 3627–3644.

Le Pichon X (1968) Sea floor spreading and continental drift. *Journal of Geophysical Research* 73: 3661–3697.

Li ZX, Evans DAD, and Zhang S (2004) A 90° spin on Rodinia: Possible causal links between the Neoproterozoic supercontinent, superplume, true polar wander and low-latitude glaciation. *Earth and Planetary Science Letters* 220: 409–421.

Lithgow-Bertelloni C and Richards MA (1998) The dynamics of Cenozoic and Mesozoic plate motions. *Reviews of Geophysics* 36: 27–78.

Lonsdale P (1988) Geography and history of the Louisville hotspot chain in the southwest Pacific. *Journal of Geophysical Research* 93: 3078–3104.

Ludwig WJ and Houtz RE (1979) *Isopach Map of the Sediments in the Pacific Ocean Basin, Color Map with Text*. Tulsa, OK: American Association of Petroleum Geologist.

Lueck RG and Mudge TD (1997) Topographically induced mixing around a shallow seamount. *Science* 276: 1831–1833.

Lynch MA (1999) Linear ridge groups: Evidence for tensional cracking in the Pacific Plate. *Journal of Geophysical Research* 104: 29321–29333.

Maddox J (1998) *What Remains to be Discovered: Mapping the Secrets of the Universe, the Origins of Life, and the Future of the Human Race*. New York: Free Press.

Matias LM, Olivet J-L, Aslanian D, and Fidalgo L (2005) PLACA: A white box for plate reconstruction and best-fit pole determination. *Computers & Geosciences* 31: 437–452.

Matthews KJ, Müller RD, Wessel P, and Whittaker JM (2011) The tectonic fabric of the ocean basins. *Journal of Geophysical Research* 116(B12109): 1–28.

Matthews KJ, Seton M, Flament N, and Müller RD (2012) Late Cretaceous to present-day opening of the southwest Pacific constrained by numerical models and seismic tomography. In: *Eastern Australian Basins Symposium, IV*, pp. 105–119.

McDougall I (1971) Volcanic island chains and sea floor spreading. *Nature* 231: 141–144.

McDougall I (1979) Age of shield-building of Kauai and linear migration of volcanism in the Hawaiian island chain. *Earth and Planetary Science Letters* 46: 31–42.

McKenzie DP (1967) Some remarks on heat flow and gravity anomalies. *Journal of Geophysical Research* 72: 6261–6273.

McKenzie DP (1969) Speculations on the consequences and causes of plate motion. *Geophysical Journal* 18: 1–32.

Mckenzie DP and Parker RL (1967) The North Pacific: An example of tectonics on a sphere. *Nature* 216: 1276–1280.

Mckenzie DP, Roberts J, and Weiss N (1973) Numerical models of convection in the Earth's mantle. *Tectonophysics* 19: 89–103.

Mckenzie DP and Sclater JG (1971) The evolution of the Indian Ocean since the Late Cretaceous. *Geophysical Journal of the Royal Astronomical Society* 24: 437–528.

McNutt MK (1998) Superswells. *Reviews of Geophysics* 36: 211–244.

Mcnutt MK, Caress DW, Reynolds J, Jordahl KA, and Duncan RA (1997) Failure of plume theory to explain midplate volcanism in the southern Austral Islands. *Nature* 389: 479–482.

Meijer PT and Wortel M (1992) The dynamics of motion of the South American Plate. *Journal of Geophysical Research* 97: 11915–11931.

Menard HW (1964) *Marine Geology of the Pacific*. New York: McGraw-Hill.

Metcalfe I (1999) Gondwana dispersion and Asian accretion: An overview. In: Metcalfe I (ed.) *Gondwana Dispersion and Asian Accretion*. Rotterdam: A. A. Balkema.

Molnar P and Stock JM (1985) A method for bounding uncertainties in combined plate reconstructions. *Journal of Geophysical Research* 90: 12537–12544.

Molnar P and Stock J (1987) Relative motions of hotspots in the Pacific, Atlantic and Indian Oceans since Late Cretaceous time. *Nature* 327: 587–591.

Montelli R, Nolet G, Dahlen FA, Masters G, Engdahl ER, and Hung S-H (2004) Finite-frequency tomography reveals a variety of plumes in the mantle. *Science* 303: 338–343.

Morgan WJ (1968) Rises, trenches, great faults and crustal blocks. *Journal of Geophysical Research* 73: 1959–1982.

Morgan WJ (1971) Convection plumes in the lower mantle. *Nature* 230: 43–44.

Morgan WJ (1972) Plate motions and deep mantle convection. *Geological Society of America Memoirs* 132: 7–22.

Morgan WJ (1978) Rodriguez, Darwin, Amsterdam, . . ., a second type of hotspot island. *Journal of Geophysical Research* 83: 5355–5360.

Mueller S and Phillips RJ (1991) On the initiation of subduction. *Journal of Geophysical Research* 96: 651–665.

Müller RD and Roest WR (1992) Fracture zones in the north Atlantic from combined Geosat and Seasat data. *Journal of Geophysical Research* 97: 3337–3350.

Müller RD, Roest WR, and Royer JY (1998) Asymmetric sea-floor spreading caused by ridge–plume interactions. *Nature* 396: 455–459.

Müller RD, Royer JY, Cande SC, Roest WR, and Maschenkov S (1999) New constraints on Carribean plate tectonic evolution. In: Mann P (ed.) *Caribbean Basins*. Amsterdam: Elsevier.

Müller RD, Royer J-Y, and Lawver LA (1993) Revised plate motions relative to the hotspots from combined Atlantic and Indian Ocean hotspot tracks. *Geology* 21: 275–278.

Müller RD, Royer J-Y, and Lawver LA (1994) Revised plate motions relative to the hotspots from combined Atlantic and Indian Ocean hotspot tracks: Reply. *Geology* 22: 277–278.

Müller RD, Sandwell DT, Tucholke BE, Sclater JG, and Shaw PR (1991) Depth to basement and geoid expression of the Kane fracture zone: A comparison. *Marine Geophysical Research* 12: 105–129.

Müller RD, Sdrolias M, Gaina C, and Roest WR (2008) Age, spreading rates, and spreading asymmetry of the world's ocean crust. *Geochemistry, Geophysics, Geosystems* 9. http://dx.doi.org/10.1029/2007GC001743.

Nakanishi M, Tamaki K, and Kobayashi K (1992) A new Mesozoic isochron chart of the northwestern Pacific Ocean: Paleomagnetic and tectonic implications. *Geophysical Research Letters* 19: 693–696.

Nataf H-C (2000) Seismic imaging of mantle plumes. *Annual Review of Earth and Planetary Sciences* 28: 391–417.

O'Connor JM and Le Roex AP (1992) South Atlantic hot spot-plume systems: 1. Distribution of volcanism in time and space. *Earth and Planetary Science Letters* 113: 343–364.

Olson P (1990) Hot spots, swells and mantle plumes. In: Ryan MP (ed.) *Magma Transport and Storage*. New York: John Wiley.

O'Neill C, Muller D, and Steinberger B (2003) Geodynamic implications of moving Indian Ocean hotspots. *Earth and Planetary Science Letters* 215: 151–168.

O'Neill C, Müller D, and Steinberger B (2005) On the uncertainties in hot spot reconstructions and the significance of moving hot spot reference frames. *Geochemistry, Geophysics, Geosystems* 6, Q04003.

Phipps Morgan J, Morgan WJ, and Price E (1995) Hotspot melting generates both hotspot volcanism and a hotspot swell? *Journal of Geophysical Research* 100: 8045–8062.

Pollitz F (1986) Pliocene change in Pacific-plate motion. *Nature* 320: 738–741.

Prevot M, Mattern F, Camps P, and Daignieres M (2002) Evidence for a 20° tilting of the Earth's rotation axis 100 million years ago. *Earth and Planetary Science Letters* 179: 517–528.

Price JP and Clague DA (2002) How old is the Hawaiian biota? Geology and phylogeny suggest recent divergence. *Proceedings of the Royal Society of London* 269: 2429–2435.

Qin X, Müller RD, Cannon J, et al. (2012) The GPlates geological information model and markup language. *Geoscientific Instrumentation, Methods and Data Systems* 2: 163.

Rao GVSP and Rao JM (1996) Palaeomagnetism of the Rajmahal traps of India: Implication to the reversal in the cretaceous normal superchron. *Journal of Geomagnetism and Geoelectricity* 48: 993–1000.

Raymond CA, Stock JM, and Cande SE (2000) Fast paleogene motion of the Pacific hotspots from revised global plate circuit constraints. In: Richards MA, Gordon RG, and Van Der Hilst RD (eds.) *The History and Dynamics of Global Plate Motions*. Washington, DC: American Geophysical Union.

Ribe NM and Christensen UR (1999) The dynamical origin of Hawaiian volcanism. *Earth and Planetary Science Letters* 171: 517–531.

Richards MA, Duncan RA, and Courtillot V (1989) Flood basalts and hot spot tracks: Plume heads and tails. *Science* 246: 103–107.

Richardson RM (1992) Ridge forces, absolute plate motions, and the intraplate stress field. *Journal of Geophysical Research* 97: 11739–11748.

Ricou L-E (1995) The plate tectonic history of the past Tethys ocean. In: Nairn AEM (ed.) *The Ocean Basins and Their Margins*. New York: Plenum Press.

Roest W (1987) Seafloor spreading pattern of the north Atlantic between 10° and 40° N. PhD. Utrecht, Netherlands.

Roest WR, Dañobeitia JJ, Verhoef J, and Collette BJ (1992) Magnetic anomalies in the Canary Basin and the Mesozoic evolution of the central North Atlantic. *Marine Geophysical Research* 14: 1–24.

Rogers AD (1994) The biology of seamounts. *Advances in Marine Biology* 30: 305–350.

Royer J-Y and Chang T (1991) Evidence for relative motions between the Indian and Australian plates during the last 20 m.y. from plate tectonic reconstructions: Implications for the deformation of the Indo-Australian plate. *Journal of Geophysical Research* 96: 11779–11802.

Royer J-Y and Gordon RG (1997) The motion and boundary between the Capricorn and Australian plates. *Science* 277: 1268–1274.

Royer J-Y, Gordon RG, Demets C, and Vogt PR (1997) New limits on the motion between India and Australia since chron 5 (11 Ma) and implications for lithospheric deformation in the equatorial Indian Ocean. *Geophysical Journal International* 129: 41–74.

Sager WW and Keating B (1984) Paleomagnetism of Line Islands seamounts: Evidence for late Cretaceous and early Tertiary volcanism. *Journal of Geophysical Research* 89: 11135–11151.

Sager WW, Lamarche AJ, and Kopp C (2005) Paleomagnetic modeling of seamounts near the Hawaiian–Emperor bend. *Tectonophysics* 405: 121–140.

Sandiford M, Coblentz DD, and Richardson RM (1995) Ridge torques and continental collision in the Indian–Australian plate. *Geology* 23: 653–656.

Sandwell D, Gille ST, and Smith WHF (2002) *Bathymetry from Space: Oceanography, Geophysics, and Climate*. Bethesda, MD: Geoscience Professional Services.

Sandwell DT and Smith WHF (1997) Marine gravity anomaly from Geosat and ERS-1 satellite altimetry. *Journal of Geophysical Research* 102: 10039–10054.

Sandwell DT, Winterer EL, Mammerickx J, et al. (1995) Evidence for diffuse extension of the Pacific plate from Pukapuka ridges and cross-grain gravity lineations. *Journal of Geophysical Research* 100: 15087–15099.

Schellart WP (2004) Quantifying the net slab pull force as a driving mechanism for plate tectonics. *Geophysical Research Letters* 31. http://dx.doi.org/10.01029/02004GL019528.

Schellart WP, Freeman J, Stegman DR, Moresi L, and May D (2007) Evolution and diversity of subduction zones controlled by slab width. *Nature* 446: 308–311.

Sclater JG, Anderson RN, and Bell ML (1971) Elevation of ridges and evolution of the central Eastern Pacific. *Journal of Geophysical Research* 76: 7888–7915.

Sclater JG and Francheteau J (1970) The implications of terrestrial heat flow observations on current tectonic and geochemical models of the crust and upper mantle. *Geophysical Journal* 20: 509–542.

Seton M, Müller RD, Zahirovic S, et al. (2012) Global continental and ocean basin reconstructions since 200 Ma. *Earth Science Reviews* 113: 212–270.

Sharp WD and Clague DA (2006) 50-Ma initiation of Hawaii–Emperor bend records major change in Pacific plate motion. *Science* 313: 1281–1284.

Shaw PR and Cande SC (1990) High-resolution inversion for South Atlantic plate kinematics using joint altimeter and magnetic anomaly data. *Journal of Geophysical Research* 95: 2625–2644.

Sleep NH (1990) Hotspots and mantle plumes: Some phenomenology. *Journal of Geophysical Research* 95: 6715–6736.

Smith DK and Cann JR (1990) Hundreds of small volcanoes on the median valley floor of the Mid-Atlantic Ridge at 24–30°N. *Nature* 348: 152–155.

Smith WHF and Sandwell DT (1997) Global sea floor topography from satellite altimetry and ship depth soundings. *Science* 277: 1956–1962.

Spence W (1987) Slab pull and the seismotectonics of subducting lithosphere. *Reviews of Geophysics* 25: 55–69.

Stadler G, Gurnis M, Burstedde C, Wilcox LC, Alisic L, and Ghattas O (2010) The dynamics of plate tectonics and mantle flow: From local to global scales. *Science* 329: 1033–1038.

Stampfli GM and Borel GD (2002) A plate tectonic model for the Paleozoic and Mesozoic constrained by dynamic plate boundaries and restored synthetic oceanic isochrons. *Earth and Planetary Science Letters* 196: 17–33.

Stein S (1979) Intraplate seismicity on bathymetric features: The 1968 Emperor Trough earthquake. *Journal of Geophysical Research* 84: 4763–4768.

Steinberger B (2000) Plumes in a convecting mantle: Models and observations for individual hotspots. *Journal of Geophysical Research* 105: 11127–11152.

Steinberger BM and O'Connell RJ (1997) Changes of the Earth's rotation axis owing to advection of mantle density heterogeneities. *Nature* 387: 169–173.

Steinberger B and O'Connell RJ (1998) Advection of plumes in mantle flow: Implications for hot spot motion, mantle viscosity and plume distributions. *Geophysical Journal International* 132: 412–434.

Steinberger B, Sutherland R, and O'Connell RJ (2004) Prediction of Emperor–Hawaii seamount locations from a revised model of global plate motion and mantle flow. *Nature* 430: 167–173.

Steinberger B and Torsvik TH (2008) Absolute plate motions and true polar wander in the absence of hotspot tracks. *Nature* 452: 620–624.

Stevenson DJ and Turner JS (1977) Angle of subduction. *Nature* 270: 334–336.

Stock JM and Molnar P (1983) Some geometrical aspects of uncertainties in combined plate reconstructions. *Geology* 11: 697–701.

Stoddard PR and Abbot D (1996) Influence of the tectosphere upon plate motion. *Journal of Geophysical Research* 101: 5425–5433.

Storey BC (1995) The role of mantle plumes in continental breakup: Case histories from Gondwanaland. *Nature* 377: 301–308.

Sykes LR (1978) Intraplate seismicity, reactivation of preexisting zones of weakness, alkaline magmatism, and other tectonism postdating continental fragmentation. *Reviews of Geophysics* 16: 621–688.

Tackley PJ (1998) Self-consistent generation of tectonic plates in three-dimensional mantle convection. *Earth and Planetary Science Letters* 157: 9–22.

Tarduno JA, Bunge H-P, Sleep NH, and Hansen U (2009) The bent Hawaiian–Emperor hotspot track: Inheriting the mantle wind. *Science* 324: 50–53.

Tarduno JA and Cottrell RD (1997) Paleomagnetic evidence for motion of the Hawaiian hotspot during formation of the Emperor seamounts. *Earth and Planetary Science Letters* 153: 171–180.

Tarduno JA, Duncan RA, Scholl DW, et al. (2003) The Emperor Seamounts: Southward motion of the Hawaiian Hotspot plume in Earth's mantle. *Science* 301: 1064–1069.

Taylor B (2006) The single largest oceanic plateau: Ontong Java–Manihiki–Hikurangi. *Earth and Planetary Science Letters* 241: 372–380.

Torsvik T, Müller RD, Van Der Voo R, Steinberger B, and Gaina C (2008) Global plate motion frames: Toward a unified model. *Reviews of Geophysics* 46. http://dx.doi.org/10.1029/2007RG000227.

Torsvik TH, Van Der Voo R, and Redfield TF (2002) Relative hotspot motions versus True Polar Wander. *Earth and Planetary Science Letters* 202: 185–200.

Tsai VC and Stevenson DJ (2007) Theoretical constraints on true polar wander. *Journal of Geophysical Research* 112. http://dx.doi.org/10.1029/2005JB003923.

Turcotte DL and Schubert G (2002) *Geodynamics*. Cambridge, UK: Cambridge University Press.

Turner DL and Jarrard RD (1982) K–Ar dating of the Cook-Austral island chain: A test of the hot-spot hypothesis. *Journal of Volcanology and Geothermal Research* 12: 187–220.

Turner DL, Jarrard RD, and Forbes RB (1980) Geochronology and origin of the Pratt-Welker seamount chain, Gulf of Alaska: A new pole of rotation for the Pacific plate. *Journal of Geophysical Research* 85: 6547–6556.

Tushingham AM and Peltier WR (1992) Validation of the ICE-3G model of Würm-Wisconsin deglaciation using a global data base of relative sea level histories. *Journal of Geophysical Research* 97: 3285–3304.

Van Der Voo R, Spakman W, and Bijwaard H (1999) Mesozoic subducted slabs under Siberia. *Nature* 397: 246–249.

Van Fossen MC and Kent DV (1992) Paleomagnetism of 122 Ma plutons in New England and the Mid-Cretaceous paleomagnetic field in North America: True polar wander or large-scale differential mantle motion? *Journal of Geophysical Research* 97: 19651–19661.

Van Hinsbergen DJJ, Steinberger B, Doubrovine PV, and Gassmöller R (2011) Acceleration and deceleration of India–Asia convergence since the Cretaceous: Roles of mantle plumes and continental collision. *Journal of Geophysical Research* 116, B06101.

van Wyckhouse R (1973) *SYNBAPS*. Stennis Space Center, MS: U.S. Natl. Oceanogr. Office.

Vidal V and Bonneville A (2004) Variations of the Hawaiian hot spot activity revealed by variations in the magma production rate. *Journal of Geophysical Research* 109. http://dx.doi.org/10.1029/2003JB002559.

Viso RF, Larson RL, and Pockalny RA (2005) Tectonic evolution of the Pacific–Phoenix–Farallon triple junction in the South Pacific Ocean. *Earth and Planetary Science Letters* 233: 179.

Vogt PR and Jung W-Y (2000) GOMap: A matchless resolution to start the new millennium. *Eos, Transactions of the American Geophysical Union* 81: 254–258.

Watts AB and Ten Brink US (1989) Crustal structure, flexure, and subsidence history of the Hawaiian Islands. *Journal of Geophysical Research* 94: 10473–10500.

Wessel P (1993) Observational constraints on models of the Hawaiian hot spot swell. *Journal of Geophysical Research* 98: 16095–16104.

Wessel P (2001) Global distribution of seamounts inferred from gridded Geosat/ERS-1 altimetry. *Journal of Geophysical Research* 106: 19431–19441.

Wessel P (2008) Hotspotting: Principles and properties of a plate tectonic Hough transform. *Geochemistry, Geophysics, Geosystems* 9. http://dx.doi.org/10.1029/2008GC002058.
Wessel P, Harada Y, and Kroenke LW (2006) Towards a self-consistent, high-resolution absolute plate motion model for the Pacific. *Geochemistry, Geophysics, Geosystems* 7: Q03L12.
Wessel P and Kroenke LW (1997) A geometric technique for relocating hotspots and refining absolute plate motions. *Nature* 387: 365–369.
Wessel P and Kroenke LW (1998a) Factors influencing the locations of hot spots determined by the hot-spotting technique. *Geophysical Research Letters* 25: 555–558.
Wessel P and Kroenke LW (1998b) The geometric relationship between hot spots and seamounts: Implications for Pacific hot spots. *Earth and Planetary Science Letters* 158: 1–18.
Wessel P and Kroenke LW (1998c) Hotspotting called into question—Reply. *Nature* 396: 127–128.
Wessel P and Kroenke LW (2000) Ontong Java plateau and Late Neogene changes in Pacific plate motion. *Journal of Geophysical Research* 105: 28255–28277.
Wessel P and Kroenke LW (2007) Reconciling Late Neogene Pacific absolute and relative plate motion changes. *Geochemistry, Geophysics, Geosystems* 8. http://dx.doi.org/10.1029/2007GC001636.
Wessel P and Kroenke LW (2008) Pacific absolute plate motions since 145 Ma: An assessment of the fixed hotspot hypothesis. *Journal of Geophysical Research* 113. http://dx.doi.org/10.1029/2007JB005499.
Wessel P and Kroenke LW (2009) Observations of geometry and ages constrain relative motion of Hawaii and Louisville plumes. *Earth and Planetary Science Letters* 284: 467–472.
Wessel P and Lyons S (1997) Distribution of large Pacific seamounts from Geosat/ERS-1: Implications for the history of intraplate volcanism. *Journal of Geophysical Research* 102: 22459–22476.
Wessel P, Sandwell DT, and Kim S-S (2010) The global seamount census. *Oceanography* 23: 24–33.
White SM, Macdonald KC, Scheirer DS, and Cormier M-H (1998) Distribution of isolated semounts on the flanks of the East Pacific Rise, 15.3°S–20°S. *Journal of Geophysical Research* 103: 30371–30384.
Williams SE, Müller RD, Landgrebe TCW, and Whittaker JM (2012) An open-source software environment for visualizing and refining plate tectonic reconstructions using high-resolution geological and geophysical data sets. *GSA Today* 22: 4–9.
Wilson JT (1963) A possible origin of the Hawaiian islands. *Canadian Journal of Physics* 41: 863–870.
Wilson JT (1965) A new class of faults and their bearing on continental drift. *Nature* 207: 343–347.
Wilson M (1993) Plate-moving mechanisms – Constraints and controversies. *Journal of the Geological Society* 150: 923–926.
Wolfe CJ, Bjarnason IT, Vandecar JC, and Solomon SC (1997) Seismic structure of the Iceland mantle plume. *Nature* 385: 245–247.
Wolfe CJ, Solomon SC, Laske G, et al. (2009) Mantle shear-wave velocity structure beneath the Hawaiian Hot Spot. *Science* 326: 1388–1390.
Yan CY and Kroenke LW (1993) A plate tectonic reconstruction of the southwest Pacific, 0–100 Ma. *Proceedings of the Ocean Drilling Program. Scientific Results* 130: 697–709.
Zatman S, Gordon RG, and Mutnuri K (2005) Dynamics of diffuse oceanic plate boundaries: Insensitivity to rheology. *Geophysical Journal International* 162: 239–248.
Zatman S, Gordon RG, and Richards MA (2001) Analytic models for the dynamics of diffuse oceanic plate boundaries. *Geophysical Journal International* 145: 145–156.
Ziegler P (1993) Plate-moving mechanisms: Their relative importance. *Journal of the Geological Society (London)* 150: 927–940.
Zoback ML (1992) First- and second-order patterns of stress in the lithosphere: The world stress map project. *Journal of Geophysical Research* 97: 11703–11728.